

**Effect of air, peroxides and diabetes on antioxidant enzyme
localization in red blood cells**

Zornitsa Stoyanova

A Thesis

In the Department

of

Chemistry and Biochemistry

Presented in Partial Fulfillment of the Requirements
for the Degree of Master of Science (Chemistry) at
Concordia University
Montreal, Quebec, Canada

August 2013

© Zornitsa Stoyanova, 2013

CONCORDIA UNIVERSITY

School of Graduate Studies

This is to certify that the thesis prepared

By: Zornitsa Stoyanova

Entitled: Effect of air, peroxides and diabetes on antioxidant enzyme localization in red blood cells

and submitted in partial fulfillment of the requirements for the degree of

Master of Science (Chemistry)

complies with the regulations of the University and meets the accepted standards with respect to originality and quality.

Signed by the final Examining Committee:

_____	Chair
Dr. Christine Dewolf	
_____	Examiner
Dr. Heidi Muchall	
_____	Examiner
Dr. Andreas Bergdahl	
_____	Examiner
Dr. Alisa Piekny	
_____	Supervisor
Dr. Ann English	

Approved by _____
Chair of Department or Graduate Program Director

Sep 6th 2013 _____
Dean of Faculty

ABSTRACT

Effect of air, peroxides and diabetes on antioxidant enzyme localization in red blood cells

Zornitsa Stoyanova

Red blood cells (RBCs) circulate through the lung and capillaries during their 120-day life span, transporting oxygen and carbon dioxide. They are exposed continuously to reactive oxygen species (ROS) derived from hemoglobin autoxidation. Protection of the RBC membrane from ROS is critical since on oxidation the cell loses its ability to deform in narrow capillaries. We investigated by Western blotting and confocal microscopy membrane recruitment of the key antioxidant enzymes, CuZn-superoxide dismutase (CuZnSOD), catalase, peroxiredoxin-2 (Prx2) and glutathione peroxidase-1 (Gpx1).

Prolonged air exposure of human RBCs, which likely increases their $O_2^{\bullet-}$ levels, resulted in less membrane-associated CuZnSOD but more membrane-associated catalase and Gpx1. Prx2 membrane levels remained unchanged.

Challenge with H_2O_2 or cumene hydroperoxide recruited Gpx1 to the membrane to metabolize lipid peroxides. Localization of catalase, which is always present at the membrane, remained unchanged but membrane-associated Prx2 decreased after peroxide treatment.

We also investigated membrane recruitment of the antioxidant enzymes in diabetic vs control rat RBCs. Notably, CuZnSOD increased at the RBC membrane in control animals at 2 versus 4 weeks. We attributed this to the observed increase in PTP1B activity, suggesting that CuZnSOD membrane localization is regulated by

phosphorylation of the cytoplasmic domain of Band-3 (CDB3). Catalase decreased at RBC membranes of 4-week diabetic rats whereas Prx2 levels increased. Gpx1 membrane levels did not change in diabetic RBCs suggesting that its membrane binding sites are always saturated to protect against lipid oxidation. Our results provide evidence that CuZnSOD, catalase, Prx2 and Gpx1 respond to damaging ROS in RBCs.

Acknowledgements

I would like to express my gratitude to my colleagues who shared their knowledge and contributed to the successful completion of my MSc degree.

I would like to thank my supervisor, Dr Ann M. English, for the opportunity to join her outstanding research team. In the past two years, I have realized that greater synergy is achieved by a diverse group of individuals working together. I acquired solid knowledge of basic and advanced biochemical techniques and principles. I learned how to apply this knowledge to results obtained in the laboratory and to critically analyze and present scientific information. Dr English has a dedication to research and her invaluable guidance has prepared me for a successful career in science.

I would like to thank my research committee members, Dr Heidi Muchall, Dr Andreas Bergdahl, Dr Alisa Piekny and Dr William Zerges for their time and constructive feedback.

I would like to express my gratitude to my group members for demonstrating professionalism and for sharing valuable skills and knowledge. It has been an honour to be a member of this diverse team and I was also energized in this dynamic learning environment. Thank you, Mr Marc Ouellet, Dr Maria Shadrina, Mr Dorival Martins, Ms Samaneh Dastpeyman, Mr Vinod Parmar, Ms Andrea Clarke, and Ms Meena Kathiresan for your consistent support and for a very enjoyable laboratory experience.

Finally, I would like to thank my family and friends for their support throughout the years, and particularly to my very special friend Marika Dochia for her precious listening skills and encouragement.

Dedication

To my father Mr Nancho Stoyanov and my mother Ms Svetlana Stoyanova

*Mom and Dad, thank you for giving me life, for teaching me right from wrong,
and for providing a loving home.*

*You have taught me to pursue my goals with passion, to be independent, to
respect and be respected.*

I hope to make a difference in the scientific community and change lives.

Thank you for your relentless support!

Table of contents

List of Figures.....	x
List of Schemes	xiii
List of Tables	xiv
List of Abbreviations	xv
Chapter 1: Introduction	1
1.1 Organization and function of red blood cells.....	1
1.2 Band-3 as major organizer of the RBC membrane.....	2
1.3 ROS and oxidative stress in RBCs	5
1.4 Nonenzymatic antioxidant defence systems in RBCs	12
1.5 Enzymatic antioxidant defence systems in RBCs	13
1.6 Copper, zinc-superoxide dismutase (CuZnSOD)	15
1.6.1 Properties of human CuZnSOD (SOD 1).....	15
1.6.2 Superoxide dismutase (SOD) activity of CuZnSOD	17
1.7 Catalase	17
1.7.1 Properties of human catalase	18
1.7.2 H ₂ O ₂ decomposition by catalase.....	20
1.8 Peroxiredoxin-2 (Prx2).....	21
1.8.1 Properties of mammalian peroxiredoxins	21
1.8.2 Antioxidant role of RBC Prx2	22
1.9 Structure of Glutathione peroxidases (Gpx)	23
1.9.1 Antioxidant role of RBC Gpx1	25
1.10 Outline and scope of thesis	27
Chapter 2: Materials and Methods	29
2.1 Materials.....	29
2.2 Antibodies used for Western blotting of isolated membranes from human and rat RBCs.....	29

2.3	Antibodies used for confocal microscopy of fixed and stained human RBCs	30
2.4	Methods	30
2.2.1	Quantitation of membrane-associated proteins by Western blotting	30
2.2.1.1	Human blood collection and washing of RBCs	30
2.2.1.2	Prolonged exposure to air of human RBCs	31
2.2.1.3	Human RBC exposure to H ₂ O ₂ and cumene hydroperoxide (CHP)	31
2.2.1.4	Isolation of membranes from human RBCs	32
2.2.1.5	Rat blood collection and washing of rat RBCs	33
2.2.1.6	Isolation of membranes from rat RBCs	34
2.2.1.7	SDS-PAGE and Western blotting of membrane-associated proteins from human and rat RBCs.....	34
2.2.1.8	Densitometry of membrane-associated proteins from human and rat RBCs	36
2.2.1.9	Coomassie staining of PVDF as loading control	37
2.2.1.10	Standard plot preparation	37
2.2.2	Localization of proteins in fixed human RBCs by confocal microscopy	38
2.2.2.1	Preparation of human RBCs	38
2.2.2.2	Fixing and permeabilization of human RBCs	39
2.2.2.3	Staining of human RBCs for CuZnSOD, catalase, Gpx1 and Prx2	40
2.2.2.4	Confocal microscopy of fixed human RBCs	41
Chapter 3: Characterizing controls for immunoblotting, immunofluorescence and hemolysis		43
3.1	Standard plot preparation of the detection of CuZnSOD, catalase, Prx2 and Gpx1	43
3.2	Linear range for CuZnSOD, Prx2, catalase and Gpx1 analysis by Western blotting	44
3.3	Sum of Coomassie bands as a loading control in Western blot analysis	48
3.4	Confocal controls for CDB3 and Hb localization in human RBCs	49
3.5	Prx2 visualization in fixed human RBCs	51
3.6	Determination of most appropriate hemolysis method	52
Appendix 3.1		63
Appendix 3.2		65
Chapter 4: Effects of prolonged air exposure on membrane localization of CuZnSOD, catalase, Prx2 and Gpx1 in human RBCs		67
4.1	Introduction	67

4.2	Results	68
4.2.1.	CuZnSOD localization after air exposure	71
4.2.2.	Catalase localization after air exposure.....	71
4.2.3.	Prx2 localization after air exposure	72
4.2.4.	Gpx1 localization after air exposure.....	73
4.3	Discussion	74
Appendix 4.....		77
Chapter 5 Membrane localization of CuZnSOD, catalase, Prx2 and Gpx1 in human RBCs on exposure to H ₂ O ₂ and CHP		81
5.1	Introduction.....	81
5.2	Results	82
5.2.1.	CuZnSOD localization after peroxide treatment	82
5.2.2.	Catalase localization after peroxide treatment.....	82
5.2.3.	Prx2 localization after peroxide treatment	84
5.2.4.	Gpx1 localization after peroxide treatment.....	85
5.3	Discussion	85
Appendix 5.....		89
Chapter 6: Membrane localization of RBC antioxidant proteins in a diabetic rat model..		92
6.1	Introduction.....	92
6.2	Results	93
6.2.1.	CuZnSOD localization in diabetic RBCs.....	93
6.2.2.	Catalase localization in diabetic RBCs	94
6.2.3.	Prx2 localization in diabetic RBCs.....	95
6.2.4.	Gpx1 localization in diabetic RBCs	95
6.3	Discussion	98
Appendix 6.....		101
Chapter 7: Overall discussion and conclusions		110
Chapter 8: Future studies		113
References.....		115

List of Figures

Fig 1.1 Top and cross sectional view of a red blood cell	1
Fig 1.2 Two types of multiprotein complexes at the RBC membrane, Band-3 and 4.1R complexes	3
Fig 1.3 Formation of ROS and RBC oxidative damage	8
Fig 1.4 Crystal structure of human SOD1 homodimer	15
Fig 1.5 Oxidized and reduced metal-binding sites of bovine CuZnSOD	16
Fig 1.6 Structure of human catalase	19
Fig 1.7 Active-site channel of human catalase	20
Fig 1.8 Mechanism of H ₂ O ₂ decomposition by Prx2	23
Fig 1.9 Structure of GSH-dependent Gpx1	25
Fig 1.10 Mechanism of catalysis by Gpx1	27
Fig 2.1 Structure of cumene hydroperoxide (CHP)	32
Fig 2.2 Structure of streptozotocin (STZ)	33
Fig 2.3 Densitometry measurements	36
Fig 2.4 Structure of acrolein	39
Fig 2.5 Excitation (blue) and emission (red) spectra of Cy2 and FITC dyes	42
Fig 3.1 Determination of the linear region in Western blots of CuZnSOD, catalase, Prx2 and Gpx1 in human RBC membranes	45
Fig 3.2 Standard plots of CuZnSOD, catalase, Prx2 and Gpx1 in isolated membranes from human RBCs	46
Fig 3.3 Four CuZnSOD, catalase, Prx2 and Gpx1 controls to be loaded	

on each gel for Western blotting	47
Fig 3.4 Plot of summed band intensities vs total protein per lane	48
Fig 3.5 Confocal immunofluorescence and corresponding bright field images of Hb and CDB3 in fixed intact human RBCs	50
Fig 3.6 Confocal immunofluorescence and corresponding bright field images of Prx2 in fixed intact human RBCs	52
Fig 3.7 Hb content of membrane fractions from human RBCs varies with the phosphate concentration in the hemolysis buffer but not after NEM addition	57
Fig 3.8 Western blot of Prx2 from a <u>non-reducing</u> SDS- PAGE (no β -mercaptoethanol) of membrane fractions of human RBCs lysed in 10 mM phosphate \pm 30 min incubation or 40 mM phosphate \pm 100 mM NEM	58
Fig 3.9 Effect of hemolysis method on CuZnSOD, catalase, and Prx2 membrane localization	61
Fig 4.1 Western blots of CuZnSOD, catalase, Prx2 and Gpx1 in membrane fractions isolated from human RBC following air exposure for 0 min (control), 30 min and 60 min	69
Fig 4.2 Relative amounts of CuZnSOD, catalase, Prx2 and Gpx1 in membrane fractions isolated from human RBC following air exposure for 0 min, 30 min and 60 min	70
Fig 4.3 Confocal immunofluorescence and corresponding bright field images of CuZnSOD, catalase, and Gpx1 in fixed intact	

human RBCs	75
Fig 5.1 Western blots of CuZnSOD, catalase, Prx2 and Gpx1 in membranes isolated from human RBCs treated with H ₂ O ₂ or cumene hydroperoxide (CHP)	85
Fig 5.2 Relative amounts of CuZnSOD, catalase, Gpx1 and Prx2 in membranes isolated from human RBCs treated with H ₂ O ₂ or cumene hydroperoxide (CHP)	84
Fig 5.3 Confocal immunofluorescence images of CuZnSOD, catalase, and Gpx1 in fixed intact human RBCs under H ₂ O ₂ flux	87
Fig 6.1 Western blots for CuZnSOD, catalase Prx2 and Gpx1 in isolated membranes from rat RBCs	96
Fig 6.2 Densitometry of CuZnSOD, catalase, Prx2 and Gpx1 bands in Western blots from control and STZ-treated rat RBCs after removal of outliers	97
Fig 6.3 Comparison of PTP1B activity in membrane fractions from diabetic and normal rat RBCs	98

List of Schemes

Scheme 1.1 CuZnSOD-catalyzed dismutation of $O_2^{\bullet-}$ to O_2 and H_2O_2	17
Scheme 1.2 Two-step mechanism of H_2O_2 decomposition by catalase	21
Scheme 2.1 Reaction of acrolein with proteins	40

List of Tables

Table 1.1 Summary of properties for CuZnSOD in human RBCs	13
Table 1.2 Summary of properties of the three major peroxide-metabolizing enzymes in human RBCs, catalase, Prx2 and Gpx1	14
Table 3.1 Summary of linear regions and optimum protein loaded for CuZnSOD, catalase, Prx2 and Gpx1 as determined from standard plots in Fig 3.2 and detected by Western blotting	47
Table 3.2 Total protein controls for Western blotting	47
Table 5.1 Localization of catalase, Gpx1 and CuZnSOD in human RBCs after a steady-state generation of H ₂ O ₂	86

List of Abbreviations

CDB3	Cytoplasmic domain of Band-3
CHP	Cumene hydroperoxide
CpdI	Compound I
CuZnSOD	CuZn-superoxide dismutase
DeoxyHb	Deoxyhemoglobin
GAPDH	Glyceraldehyde 3-phosphate dehydrogenase
Gpx1	Glutathione peroxidase-1
G-PBS	Glucose phosphate buffered saline
GSH	γ -glutamylcysteinylglycine or glutathione
Hb	Hemoglobin
HRP	Horseradish peroxidase
Ht	Hematocrit
H ₂ O ₂	Hydrogen peroxide
MetHb	Methemoglobin
MDA	Malondialdehyde
NEM	N-ethylmaleimide
OxyHb	Oxyhemoglobin
PBS	Phosphate buffered saline
PFK	Phosphofructokinase
PMSF	Phenylmethylsulfonyl fluoride
Prx2	Peroxiredoxin-2

PSS	Physiological saline solution
PTPase	Phosphotyrosine phosphatase
p-NPP	p-nitrophenyl phosphate
RBC	Red blood cell
ROS	Reactive oxygen species
STZ	Streptozotocin

Chapter 1: Introduction

1.1 Organization and function of red blood cells

Blood is composed of cells and plasma. The most abundant cells in blood are red blood cells (RBCs, also called erythrocytes), which contain a high concentration of the heme protein hemoglobin (Hb). Hb reversibly binds O_2 and greatly increases O_2 solubility in blood.

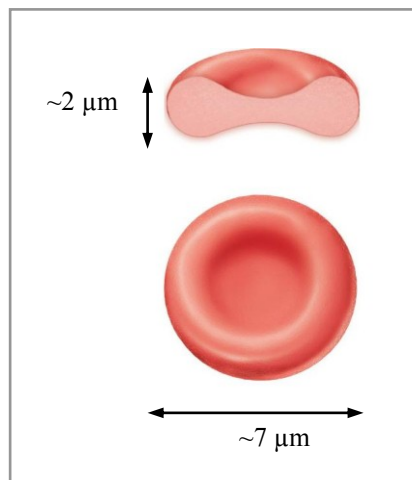


Fig 1.1 Top and cross sectional view of a red blood cell. RBC has a biconcave disk shape and is $\sim 2 \mu\text{m}$ thick with $\sim 7 \mu\text{m}$ diameter. Adapted from http://www.easynotecards.com/print_cards/2967: accessed Mar 5, 2013

Human RBCs are produced in the bone marrow. As the RBCs emerge from the bone marrow to enter the blood, they lose their nuclei, ribosomes, and mitochondria and therefore all capacity for cell division, protein synthesis, and mitochondrial-based oxidative reactions (1, 2). The anucleated mature human RBC is one of the most specialized cells in the body. Human RBCs are small biconcave discs with high surface-to-volume ratio (Fig 1.1) related to their main function of O_2 transport to tissues and CO_2

transport from tissues to the lungs (1). Approximately 25×10^{12} RBCs course through the human circulatory system. They travel through microcapillaries (1-2 μm in diameter) and must undergo extensive deformation and resist fragmentation, which is essential for function and survival (3-7). Membrane rigidity is an important factor in reducing cell deformability (8) and maintenance of deformability aids in the exit of mature RBCs from the bone marrow (9). RBCs cannot divide or maintain their structure for very long and have an average lifespan of 120 days (10).

Plasma constitutes $\sim 55\%$ of whole blood and acts as a buffer to maintain human arterial blood pH at 7.35-7.45 while RBCs occupy $\sim 45\%$ of whole blood. White blood cells (WBCs or leukocytes) and platelets, occupy $\sim 1\%$ of whole blood. They participate in the immune response and blood clotting, respectively (1).

1.2 Band-3 as major organizer of the RBC membrane

The RBC plasma membrane consists of a lipid bilayer composed of $\sim 50\%$ protein, $\sim 40\%$ lipid and $\sim 10\%$ carbohydrate (11) and has a complex organization. It acts as a physical barrier, yet it readily passes ions, nutrients and information between the cytoplasm and the extracellular environment. Many transmembrane and cytosolic proteins are associated with the abundant anion channel protein Band-3, forming a metabolon (12). Two types of Band-3 containing multiprotein complexes at the membrane have been defined as shown in Fig 1.2. On the left side, tetrameric Band-3 is attached to spectrin via ankyrin, which is referred to as the Band-3 complex. On the right side of Fig 1.2, dimeric Band-3 interacts with protein 4.1 to form what is known as 4.1R

complex (13). It has been speculated that the RBC membrane is composed of repeating units of these Band-3 and 4.1R complexes (14).

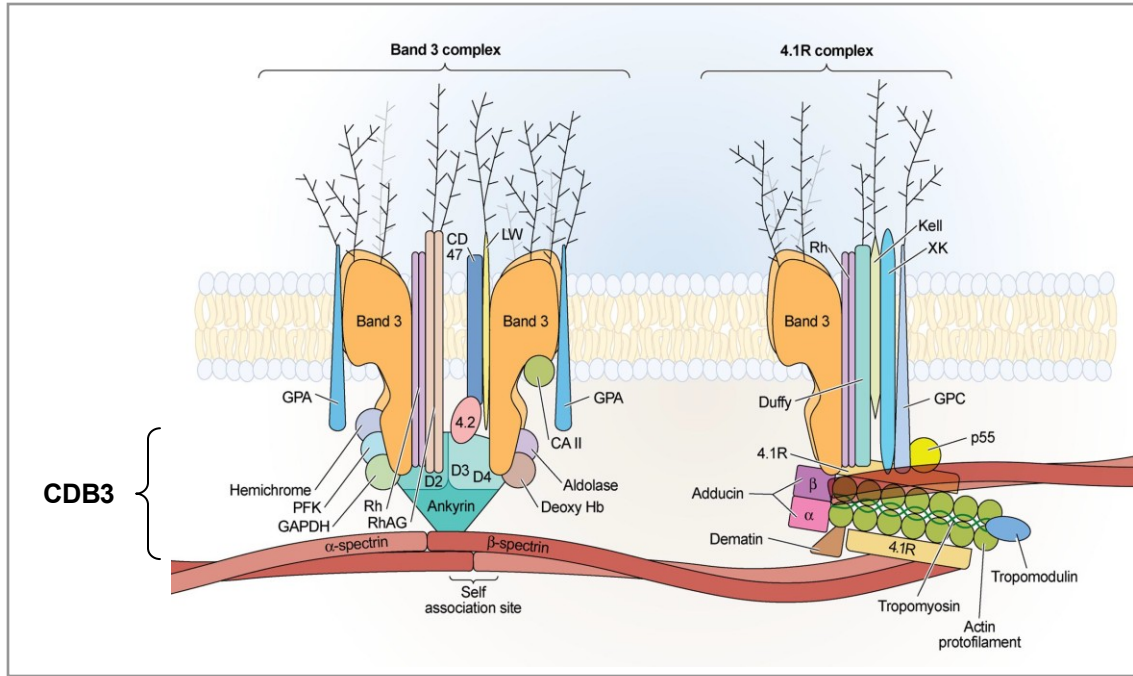


Fig 1.2 Two types of multiprotein complexes at the RBC membrane, Band-3 and 4.1R complexes (modified from (15)). (Left) Band-3 complex: the N-terminal cytoplasmic domain of Band-3 (CDB3) contains binding sites for many proteins including deoxyHb, hemichromes and the glycolytic enzymes - aldolase, phosphofruktokinase (PFK), and glyceraldehyde 3-phosphate dehydrogenase (GAPDH). Note that carbonic anhydrase II (CAII) binds to the short C-terminus of Band-3. (Right) 4.1R protein complex. (15).

Band-3 constitutes the most abundant polypeptide in the RBC membrane, comprising 25% of the total membrane protein. Band-3 can be divided into two independent structural domains. The 55 kD membrane-spanning domain is thought to traverse the bilayer twelve times and serves to catalyze the exchange of anions (mainly Cl^- for HCO_3^- across the membrane during gas transport in the blood (16). The membrane-spanning domain may also mediate removal of senescent RBCs from

circulation (17-19), and it has been shown to carry a number of common blood group antigens (20). The external domain of Band-3 contains many attached sugars (20).

The 41 kDa N-terminal cytosolic domain of Band-3 (CDB3) from human RBCs was crystallized and characterized by Zhang et al. in 2000 (21). The first 54 residues at the N-terminus and the last 23 residues at the C-terminus at CDB3 were not resolved (21). Physical studies of CDB3 have shown a remarkable flexibility of this region (22, 23). The first 54 residues form a strongly anionic region, containing 20 acidic residues, no basic residues and a blocked N-terminal methionine (24, 25). This region is also involved in peripheral protein interactions and contains a critical Tyr8 residue which is the main site of phosphorylation by protein kinases in the N-terminus of Band-3 (26). Included among the protein binding partners of ligands of CDB3 are Hb (35, 36), hemichromes (37), the protein tyrosine kinase (p72syk) (38), ankyrin (27), protein 4.2 (28, 29), protein 4.1 (30, 31), GAPDH (32), PFK (33), and aldolase (34). Interestingly, oxidation of Cys β 93 on the β -chain of Hb has been proposed as a specific and sensitive marker for oxidative stress during storage (39), but the effect of Cys β 93 oxidation on CDB3 binding affinity has not been reported. Note that CAII binds to the short cytosolic C-terminal domain of Band-3 and not to CDB3. It was reported that *in vitro* phosphorylation of the human purified CDB3 by a protein-tyrosine kinase (p40) results in the inhibition of binding of aldolase, GAPDH, PFK, and Hb, suggesting that CDB3 might be involved in regulation of glycolysis (40). Importantly, each of these Band-3 interactions has nontrivial consequences for the structure and function of the cell, ranging from control of cell flexibility and shape (41), to regulation of glucose metabolism (42), ion transport (43), and cell lifespan (19).

1.3 ROS and oxidative stress in RBCs

Molecular oxygen is beneficial and harmful to living systems. Partially reduced forms of O_2 are damaging and are collectively termed reactive oxygen species (ROS) (44). ROS include the superoxide radical anion ($O_2^{\bullet-}$), the hydroxyl radical (OH^{\bullet}) and hydrogen peroxide (H_2O_2).

During its lifetime, a RBC passes through the human circulation $\sim 75,000$ times (45) and reversibly binds O_2 on each cycle (Fig 1.3, Panel A). As a result of their main physiological role, RBCs are subjected to constant oxidative stress. Moreover, the RBCs ($\sim 7 \mu m$ in diameter) need to withstand turbulent flow, and must be deformable to pass through capillary beds with 1-2 μm in diameter (46). In most cells, mitochondria are major sources of endogenous ROS (47). Despite their lack of mitochondria, RBCs continuously produce ROS because these cells possess high O_2 and heme concentrations (48). Various factors lead to generation of ROS such as $O_2^{\bullet-}$, H_2O_2 , and OH^{\bullet} in RBCs (49). Some exogenous sources of ROS in the blood are the phagocytic cells, neutrophils and macrophages (50).

The main source of ROS in erythrocytes is the O_2 carrier protein Hb. This protein has two forms (oxyHb and deoxyHb) and undergoes autoxidation. Since the intracellular concentration of oxyHb is ~ 5 mM, even a small rate of autoxidation can produce substantial levels of $O_2^{\bullet-}$ with a concomitant formation of metHb (Fig 1.3, Panel B). The steady-state concentration of $O_2^{\bullet-}$ inside RBCs is ~ 10 pM (51). MetHb formation results in the loss of the most important task of RBCs (52) because metHb cannot bind and transport O_2 . During autoxidation an electron is lost from the heme Fe^{II} to give Fe^{III} . Spontaneously generated $O_2^{\bullet-}$ or $O_2^{\bullet-}$ arises due to the effect of an exogenous source

such as certain drugs (53) and is capable of attacking the RBC membrane directly and causing structural alterations in lipids and proteins (54). Furthermore, dismutation of $O_2^{\bullet-}$ readily generates a second ROS, H_2O_2 (Equation 1.1) (53).



Superoxide crosses membranes via transmembrane anion channels such as Band-3, but its uncharged dismutation product, H_2O_2 (Equation 1.1), crosses membranes by passive diffusion (55) or via aquaporin (56). Human RBCs have a limited ability to synthesize new proteins to replace damaged ones (57). However, RBCs have strong antioxidant defences and H_2O_2 is not particularly damaging to the membrane and molecules within RBCs. Exported H_2O_2 could be harmful to the extracellular milieu because the plasma possesses few antioxidant defences (55). Thus, not only could oxidative stress harm the RBC itself, but the exit of large quantities of H_2O_2 from the RBC could damage other components in the circulatory system (58).

The harmful effects of ROS causing potential biological damage are collectively termed oxidative stress. Oxidative stress results from ROS overproduction or a weakening of the antioxidant defence system. The most obvious oxidative damage is the formation of Heinz bodies. Heinz bodies are composed of denatured Hb and some membrane proteins, including Band-3. Although Heinz bodies may form by oxidation of internal sulfhydryl groups in Hb (59), hemichrome formation seems more important (37) in Heinz body formation. Reversible hemichromes, such as Hb hydroxide and bishistidine ferrihemochrome, are formed from metHb (Fig 1.3, Panel C). As the name indicates, the reversible hemichromes can be converted back to methemoglobin, and,

eventually, to reduced Hb. If irreversible hemichromes (bishistidine ferrihemochrome or a mercaptide derivative) are formed, Hb denaturation cannot be stopped, and Hb aggregates to form hemichromes (60). Hemichromes have an increased affinity for CD3 and bind to it (37). The resulting Band-3-hemichrome complex promotes the aggregation of additional molecules to form a cluster that can be recognized microscopically as Heinz bodies. Because it is an integral protein and spans the lipid bilayer, this also results in Band-3 clustering on the outside of the RBC membrane, which creates a recognition site for auto-antibodies (17). Auto-antibodies against Band-3 clusters likely play a key role in recognizing senescent erythrocytes (61) since RBCs with attached auto-antibodies are trapped and degraded by macrophages in the spleen and liver. Heinz bodies can also be removed from RBCs by the spleen, and the repaired cells remain in circulation (62), a phenomenon known as splenic “pitting”.

Also, progressive hemichrome formation, oxidation and phosphorylation of Band-3 have been observed in RBCs under oxidative stress, while in control RBCs Band-3 oxidation and phosphorylation are transient and no hemichrome formation is observed. Hemichromes bind to Band-3 and promote the clustering of phosphorylated Band-3 (63).

In Fig 1.3, Panel D, $O_2^{\bullet-}$ generated in the production of metHb is converted into H_2O_2 by CuZn-superoxide dismutase (CuZnSOD). Hydroxyl radicals are produced with H_2O_2 and ferrous iron from denatured metHb products functioning as Fenton reagents (64).

ROS can cause lipid peroxidation when OH^\bullet attacks polyunsaturated fatty acids within the membrane (54) as shown in Fig 1.3, Panel E. Hydroxyl radicals in the membrane attack unsaturated lipids to form lipid radicals (CH^\bullet), then combine with

molecular oxygen to form lipid peroxy radicals (HCOO^\bullet), which in turn attack unsaturated lipid to complete the cycle. Lipid peroxidation leads to altered phospholipid fluidity, loss of membrane integrity and loss of cellular homeostasis (48). Also, malondialdehyde (MDA), a highly reactive bifunctional molecule, is an end product

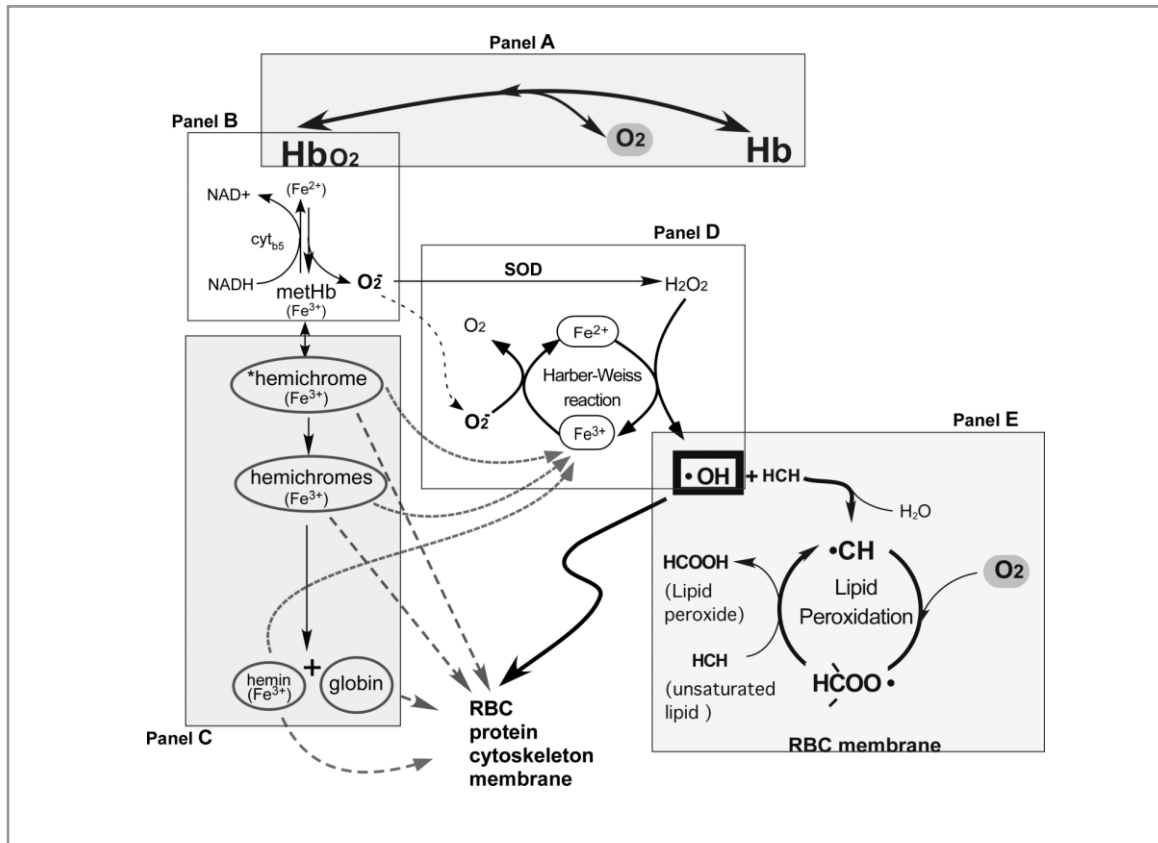


Fig 1.3 Formation of ROS and RBC oxidative damage (taken from Yoshida et al. (64)). **Panel A:** Normal function of Hb-reversible binding of O_2 to reduced (ferrous) heme in Hb. **Panel B:** Auto-oxidation of oxyHb to methemoglobin (metHb; ferric) with production of superoxide anion. In a steady-state, 1-2% of Hb exists as metHb in the circulation. **Panel C:** MetHb denatures first to 'reversible hemichromes', in which conformational distortions are minor and can still be reversed. Reversible hemichromes further denature to 'irreversible hemichromes', which subsequently dissociate to globins and heme. **Panel D:** The Haber-Weiss reaction produces hydroxyl radicals. **Panel E:** Lipid peroxidation cycle.

within cells of membrane lipid peroxidation (52) and has been shown to bind to proteins. This may result in the impairment of membrane-related functions that could ultimately diminish survival. MDA accumulation can affect Band-3 function as well as the function of its associated enzymes, such as GAPDH and PFK (49). It might also be involved in recruiting certain enzymes to the RBC membrane, such as glutathione peroxidase-1 (Gpx1), as discussed later.

ROS not only react with lipids but also with membrane and cytosolic proteins, resulting in cellular damage. ROS alter proteins by modifying amino acids such as sulfhydryl groups on Band-3 and calcium ATP-ase (Ca-ATPase). Dimer formation and tetramer formation is important for the proper function of Band-3 as this protein exists primarily as a mixture of dimers and tetramers in its membrane environment (65, 66). CDB3 has two oxidizable Cys residues, Cys201 and Cys317, which form an inter-subunit disulfide bond upon treatment with an oxidizing agent (21). Formation of this S-S bond is critical for dimerization, tetramerization (67) and the proper function of CDB3. Therefore, it is important to prevent ROS accumulation to maintain proper function of CDB3 and control Band-3 clustering.

Among other membrane proteins that are possible targets for oxidants, Ca-ATPase is also essential for RBC survival. Ca-ATPase contains one or more reactive sulfhydryl groups that are susceptible to oxidation with resultant loss of enzyme activity. Because this enzyme is critical in maintaining the very steep gradient between extracellular and intracellular calcium, loss of activity is associated with decreased deformability and premature destruction of RBCs (68).

Like RBC membrane proteins, cytosolic proteins, such as Hb, are also susceptible to oxidation. Oxidative modifications in oxyHb as a result of H₂O₂ exposure have been proposed to act as selective signals for proteolysis in RBCs (69). In addition to the modification of Hb by H₂O₂, peroxidation may result in Hb crosslinking to membrane proteins, such as spectrin and Band-3, and also the aggregation of Band-3 (70, 71) as discussed in Fig 1.3, Panel C. Snyder et al. demonstrated that H₂O₂ induces complex formation between spectrin and Hb as well as altered phospholipid organization, RBC shape, membrane deformability, and cell surface characteristics (72). The formation of crosslinked spectrin and Hb causes the RBC membrane to become more rigid, less deformable and less adaptable (72). Thus, protection of the RBC membrane is essential to prevent hemolysis which increases in cells with rigid membranes (73). Loss of membrane flexibility has profound implications because the survival of many other cells depends upon the proper functioning of RBCs.

When blood is stored under blood bank conditions, RBCs slowly lose their ability to survive following transfusion (74). Although preservation of adenosine 5'-triphosphate (ATP) levels lengthen storage time, the ATP concentration is not the major determinant of proper RBC function. Erythrocyte membrane function seems to be abnormal in stored blood. The *in vitro* ability of spectrin to bind to actin in the presence of membrane protein 4.1 decreases during blood storage. The membrane changes that occur in stored RBCs are partially reversed by dithiothreitol, suggesting sulfhydryl oxidation. Erythrocytes also lose phospholipids during storage, and that loss correlates with Hb leakage.

Current blood storage practices are known to cause oxidative damage to RBCs, known as "storage lesion" that may alter their biological function, including delivery of

O₂ to cells (75). In clinical settings, blood is stored in air-permeable bags for 42 days (76) at 4 °C but deformation of the RBC membrane due to oxidation occurs after only five days of ambient air exposure (77). Accumulation of oxidized Hb and the formation of crosslinks between Hb and membrane proteins were recently demonstrated in RBCs subjected to prolonged hypothermic storage at 4 °C (78). Another study demonstrated the progressive linkage of catalase and Prx2 to RBC membranes together with non-reducible membrane crosslinking of Hb after blood storage for 28 days (79). Thus, growing evidence indicates the involvement of oxidized Hb and protein re-localization in degenerative processes pertaining to blood storage and draws interest to the fields of transfusion medicine and blood banking.

Diabetes also causes oxidative stress in RBCs (80). Diabetes results in decreased RBC membrane fluidity and loss of flexibility, due to the *in vivo* glycation of proteins as well as to changes in lipid composition (81). Glycated proteins include Hb and the membrane proteins, ankyrin, actin, and spectrin (82). This modification of Hb and membrane proteins by glucose is non-enzymatic and depends on blood glucose levels as well as erythrocyte age (82). The glycation of Hb increases its oxygen affinity and makes it more susceptible to oxidation (83).

In humans, oxidative stress is involved in many pathological conditions, including atherosclerosis, hypertension, Parkinson's disease, nephropathy, inflammatory arthritis and diabetes (84).

1.4 Nonenzymatic antioxidant defence systems in RBCs

The antioxidant system in human RBCs consists of non-enzymatic and enzymatic pathways. The non-enzymatic defences inside RBCs can be divided into lipophilic (vitamin E, vitamin A, ubiquinone, melatonin) and water-soluble compounds (vitamin C, glutathione, uric acid). Three antioxidant vitamins A, C, E provide defence against oxidative damage as chain-breaking antioxidants. Vitamin C reduces $O_2^{\bullet-}$ and $HCOO^{\bullet}$, radicals and participates in the recycling of vitamin E (48, 85). Vitamin C has been shown to play a protective role against peroxidation of RBC membrane lipids and vitamin E by t-butylhydroperoxide (tert-B-OOH), preserving lipids by up to 92% (86). Vitamin E is the most widely distributed antioxidant in nature. When vitamin E donates an electron to a lipid peroxy radical, it is converted to free radical stabilized by resonance structure (87). Vitamin C and E work together to inhibit lipid peroxidation reactions in plasma lipoproteins and membranes. Vitamin A is a potent free radical scavenger (48) and addition of vitamin A *in vitro* to erythrocyte membranes has been shown to decrease lipid peroxide production.

GSH (γ -glutamylcysteinylglycine, or glutathione) is the most important nonenzymatic, peptidic regulator of intracellular redox homeostasis. GSH is the major antioxidant in RBCs since it prevents disulfide formation in important structural proteins such as spectrin, which leads to increased membrane stiffness (88). GSH not only supports antioxidant defence, but is also an important sulfhydryl buffer, maintaining –SH groups in Hb and enzymes in the reduced state (48).

GSH is present at high levels (~5 mM) in RBCs. It protects against oxidative damage by directly interacting with H_2O_2 and organic peroxides, or as a substrate of

detoxification enzymes like Gpx. Importantly, GSH plays an essential role in maintaining a constant redox environment inside the RBC that is critical for the function of cellular proteins. GSH exists either in reduced GSH or oxidized GSSG forms and participates in redox reactions by the reversible oxidation of its active thiol. Inside cells GSH is predominantly present in the reduced form (89). Maintenance of high GSH-to-GSSG ratio is important in RBCs as it protects against oxidative stress.

1.5 Enzymatic antioxidant defence systems in RBCs

In addition to non-enzymatic defences, RBCs also rely on abundant antioxidant enzymes including CuZnSOD, catalase, Prx2 and Gpx1. CuZnSOD rapidly dismutates $O_2^{\bullet-}$ to H_2O_2 (Table 1.1), which is a substrate for catalase, Prx2 or Gpx1. The latter three enzymes react rapidly with H_2O_2 , organic hydroperoxides or lipid peroxides (Table 1.2) and whether they carry out nonredundant functions is a matter of considerable debate. Catalase degrades H_2O_2 without consuming cellular reducing equivalents (NADPH), which is an energy efficient way of removing H_2O_2 . In addition to catalase, Prx2 and Gpx1, RBCs contain glutaredoxin and glutathione S-transferase, which can act as peroxidases themselves, but at much slower rates (90).

Table 1.1 Summary of properties for CuZnSOD in human RBCs

Substrate	$O_2^{\bullet-}$
k_2^*	$2 \times 10^9 \text{ M}^{-1} \text{ s}^{-1}$
K_m	0.0029 mM
k_{cat}	$1.7 \times 10^4 \text{ s}^{-1}$
MW monomer / # amino acids monomer	16 kDa / 153 aa
Copies per RBC / Concentration	2.7×10^5 copies / 1.8 – 10 μM

Table 1.2 Summary of properties of the three major peroxide-metabolizing enzymes in human RBCs, catalase, Prx2 and Gpx1

RBC Enzyme	Catalase	Prx2	Gpx1
Substrates	H ₂ O ₂	H ₂ O ₂ , ROOH	H ₂ O ₂ , ROOH, lipid peroxides
k₂^a	10 ⁷ M ⁻¹ s ⁻¹	k _{H₂O₂/tert-B-OOH} = 2.2 × 10 ⁶ - 7.0 × 10 ⁷ M ⁻¹ s ⁻¹	k _{tert-B-OOH} = 4.2 × 10 ⁶ M ⁻¹ s ⁻¹ k _{H₂O₂} = 4.1 × 10 ⁶ M ⁻¹ s ⁻¹ k _{L-OOH} = 4.0 × 10 ⁶ M ⁻¹ s ⁻¹
K_m	25 mM	<0.001 mM (for H ₂ O ₂)	0.24 mM (for H ₂ O ₂)
k_{cat}	2.25 × 10 ⁷ s ⁻¹	4.0 × 10 ⁷ s ⁻¹ (for H ₂ O ₂)	4.1 × 10 ⁷ s ⁻¹ (for H ₂ O ₂) 4.1 × 10 ⁶ s ⁻¹ (for tert-B-OOH)
MW monomer / # amino acids monomer	60 kDa / 527 aa	22 kDa / 198 aa	23 kDa / 203 aa
Copies per RBC / Concentration	1.4 × 10 ⁵ copies / 2.3 μM	14 × 10 ⁶ copies / 240 μM	4 × 10 ⁵ copies / 6.7 μM
Reducing substrate	H ₂ O ₂	Thioredoxin	GSH

^a k₂ = bimolecular rate constant for reduction/oxidation of enzyme by the substrate L-OOH, linoleic acid hydroperoxide; tert-B-OOH, tert-butyl hydroperoxide

The altered activities of these antioxidant enzymatic systems have been documented during oxidative stress conditions, making them reliable markers of oxidative stress. Ample experimental reports exist in support of the elevation of oxidative stress during redox imbalance leading to the development of a number of pathological changes in RBCs (88). A significant decrease in the activities of enzymatic antioxidant defence system has also been reported in diabetic patients (89).

1.6 Copper, zinc-superoxide dismutase (CuZnSOD)

The SOD family of enzymes is comprised of three major classes based on the metal cofactor. The first class contains Cu and Zn at the active site, the second class contains Fe or Mn, and the third class contains Ni. Three forms of SOD are present in humans: SOD1 is found in cytosol (Cu and Zn at active site), SOD2 is found in the mitochondrion (Mn at active site) and SOD3 is extracellular (Cu and Zn at active site). The best known function of SOD is the protection of cells from ROS, particularly $O_2^{\bullet-}$ (Equation 1.1).

1.6.1 Properties of human CuZnSOD (SOD 1)

Human RBCs contain only CuZnSOD (SOD1) which is a 32 kDa homodimer with one Cu- and one Zn-binding site per 153-residue subunit (Fig 1.4). The distance between the two active sites in the homodimer is over 30 Å. Each monomer is essentially a β -barrel with two functional loops, called the electrostatic and zinc loops, which encase the metal-binding region. This region of CuZnSOD is fully contained within each subunit and the Cu and Zn are in close enough proximity to share an imidazolate ligand, His63 (Fig 1.5). The two subunits are held together primarily by hydrophobic interactions and an intrasubunit disulfide bond as shown in red in Fig 1.4.

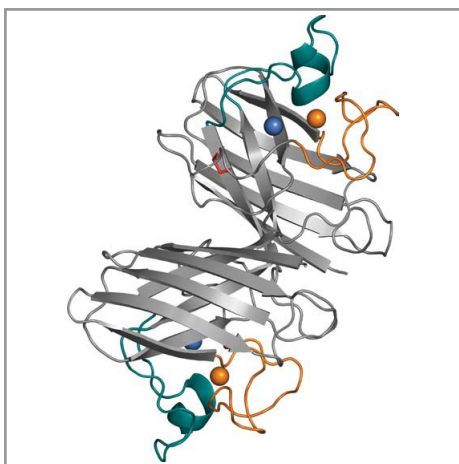


Fig 1.4 Crystal structure of human SOD1 homodimer (PDB ID: 2C9S) (adapted from (90)). Copper and zinc ions are shown as blue and orange spheres, respectively. The zinc loop is depicted in orange and the electrostatic loop in teal and the intrasubunit disulfide bond is shown in red.

The Cu and Zn ions have catalytic and structural roles respectively in CuZnSOD. In the oxidized cupric (Cu^{II}) form of the enzyme, the copper is bound to four His residues, His63, His46, His48, and His120, and a water molecule (Fig 1.5). In the reduced cuprous (Cu^{I}) form of the enzyme, the copper undergoes a 1.3 Å shift in position, moving away from the bridging His63 and releasing the water ligand, thereby switching from an irregular five-coordinate geometry to a nearly trigonal planar three-coordinate configuration. At the same time, the bridging imidazolate of His63 becomes protonated and binds exclusively to the zinc ion, which remains tetrahedrally-coordinated (91) (Fig 1.5).

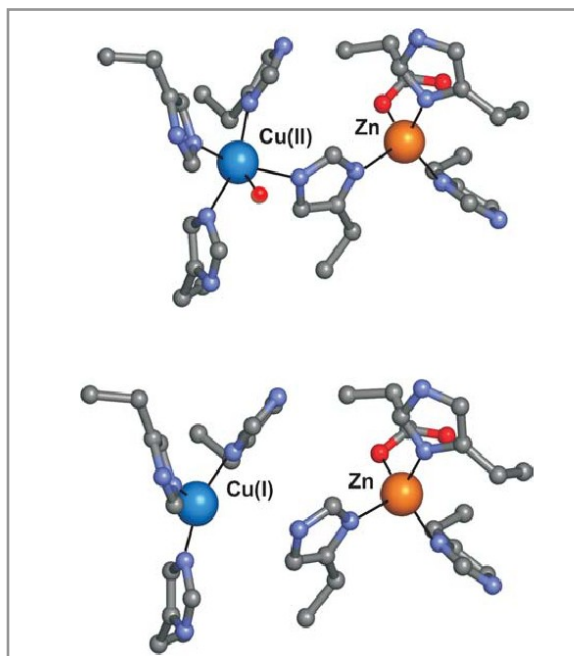
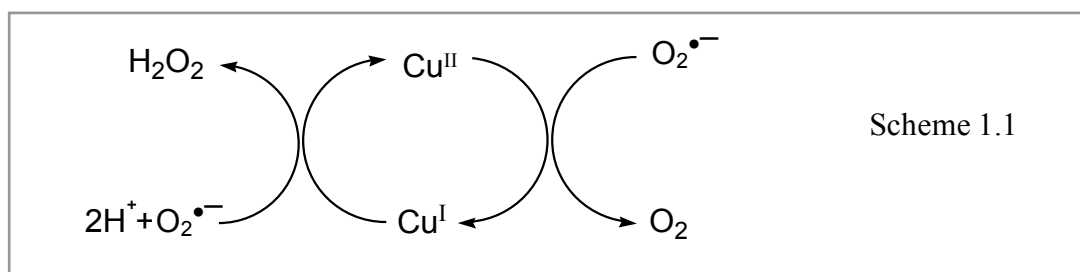


Fig 1.5 Oxidized and reduced metal-binding sites of bovine CuZnSOD (SOD1) (taken from ref (90)). The oxidized enzyme (top, from PDB ID: ICBJ) possesses an intact imidazolate bridge between Cu^{II} and Zn^{II} . Cu^{II} is five-coordinate and is bound to four His and one water molecule. In the reduced (bottom, from PDB ID: IQ0E) the imidazolate bond is broken between the bridging His63 and Cu^{I} , which is bound to three His side chains only.

1.6.2 Superoxide dismutase (SOD) activity of CuZnSOD

RBCs are well protected against ROS by CuZnSOD, which is abundant (1.8 – 10 μM) and efficiently scavenges $\text{O}_2^{\bullet-}$ (Table 1.1). In nucleated cells, CuZnSOD synthesis is induced by $\text{O}_2^{\bullet-}$ and also its activity is increased in the presence of $\text{O}_2^{\bullet-}$ with activation of regulatory genes (49). CuZnSOD is very stable and its activity is pH-independent in the range of 5.0 to 9.5 (90).

A two-step dismutation of $\text{O}_2^{\bullet-}$ to O_2 and H_2O_2 (84) (Equation 1.2) occurs at the active-site copper of CuZnSOD. First, one molecule of $\text{O}_2^{\bullet-}$ reduces Cu^{II} to form O_2 and then a second molecule of $\text{O}_2^{\bullet-}$ reoxidizes Cu^{I} to form H_2O_2 . The enzyme's catalytic cycle is described as a ping-pong mechanism (92) (Scheme 1.1). Under non-saturating conditions, the rate-limiting step in the dismutation is the diffusion of $\text{O}_2^{\bullet-}$ to the active-site cavity. Based on the estimated diffusion rates of $\text{O}_2^{\bullet-}$ and CuZnSOD, the catalytic rate constant of $2 \times 10^9 \text{ M}^{-1} \text{ s}^{-1}$ corresponds to that of a diffusion-controlled reaction (93).



1.7 Catalase

Catalase catalyzes the decomposition of H_2O_2 to water and oxygen and is found in most aerobic organisms. It was first reported in 1811 in living tissue as the molecule responsible for H_2O_2 breakdown (94) and was given the name 'catalase' in 1900 (95). In

1969, the amino acid sequence of bovine liver catalase was determined (96), and by 2004 over 300 catalase sequences were available (97).

Catalases can be organized into four main groups (98). The first group is most widespread and includes monofunctional, heme-containing enzymes, which are subdivided based on subunit size (>75 kDa or <60 kDa) (97). The second group is comprised of bifunctional, heme-containing catalase-peroxidases. Third group is nonheme or Mn-containing catalases. The fourth group includes miscellaneous proteins with minor catalatic activities.

1.7.1 Properties of human catalase

Human catalase, a homotetramer of 60-kDa subunits (Fig 1.6A), belongs to the group of monofunctional catalases. Each subunit contains an active-site heme (ferriprotoporphyin IX) and requires a NADPH cofactor. One NADPH molecule binds per monomer to a pocket located ~ 19 Å from the heme (99). Two dimers assemble to form the tetramer, which is roughly square with overall dimensions of 100 Å \times 100 Å \times 70 Å (Fig 1.6B) (99). Tetramerization forces the threading arms from the arm-exchanged dimer to cover the hemes in the other dimer. Tetramerization is likely critical for sequestering the hemes allowing the enzyme to complete its reaction cycle rather than the generation of OH^\bullet from exposed hemes (99).

The heme is at the bottom of a 25-Å channel extending from the enzyme's surface. A 3-Å-wide hydrophobic constriction, lined by the side chains of Val74, Val116, Phe153, Phe154, and Trp186 (Fig 1.7), is located directly above the heme. Thus, only H_2O or other small molecules can reach the heme. Throughout the catalase structure, H_2O

fills packing defects in each subunit, and between subunits within the tetramer. At either end of the hydrophobic constriction, well-ordered H₂O molecules form hydrogen bonds to the protein, which promotes selection of H₂O₂ (99). This is known as ‘molecular ruler recognition’ mechanism for H₂O₂.

Human catalase is a very stable enzyme and works at an optimum physiological temperature of 37 °C (100). When the solution pH falls outside the range of 3.5-11, the heme dissociates from the active site and catalase loses its enzymatic activity (101). Catalase exhibits strong absorbance in the Soret region ($\epsilon_{405 \text{ nm}} = 3.24 \times 10^5 \text{ M}^{-1} \text{ cm}^{-1}$) (94) and possesses one of the highest known enzymatic rates with a turnover number of $2.25 \times 10^7 \text{ s}^{-1}$ for H₂O₂ (59) at its pH optimum of ~7.0 (101).

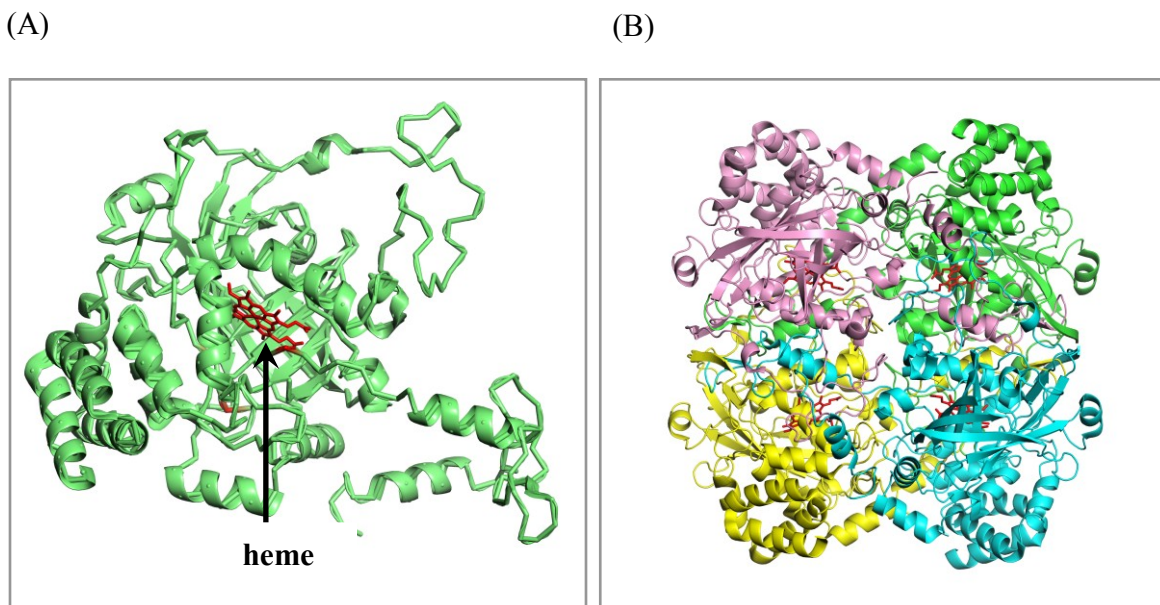


Fig 1.6 Structure of human catalase (pdbID: 1QQW). (A) Stereo view of an individual subunit with active-site heme in red. (B) Stereo view of the catalase tetramer. Note that formation tetramer formation buries the hemes from the solvent. Tetramerization forces the threading arms from an arm-exchanged dimer to cover the hemes in the other dimer. This figure was created using PyMol (DeLano Scientific).

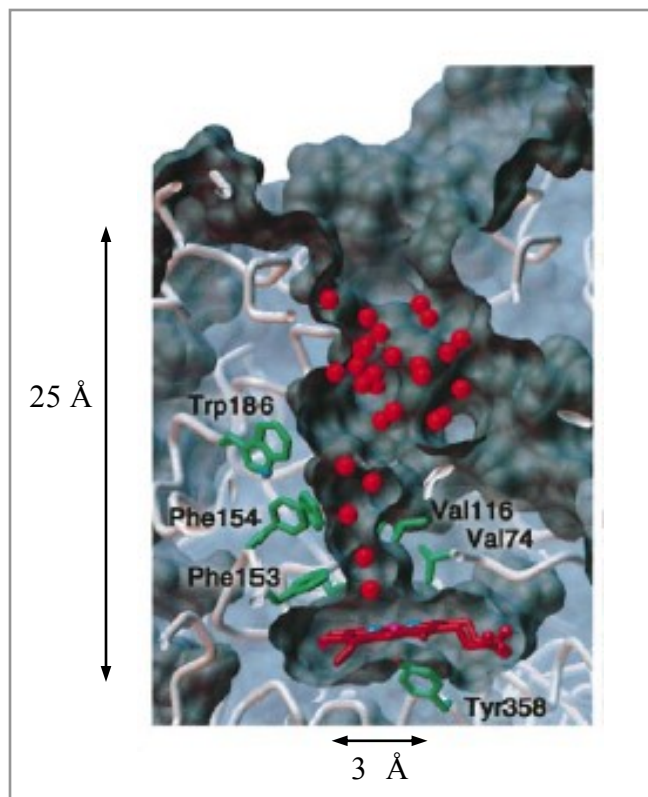


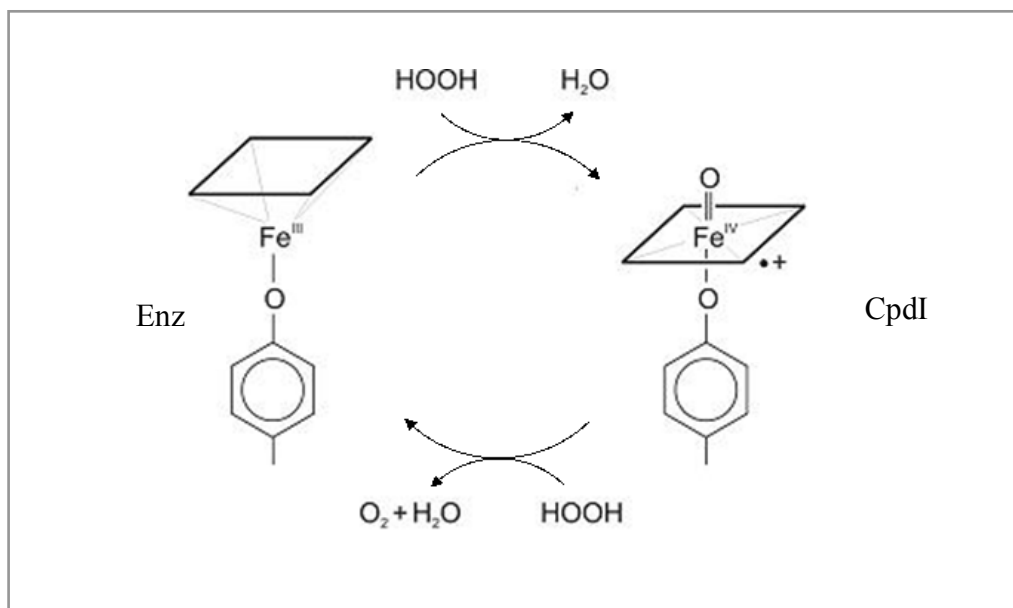
Fig 1.7 Active-site channel of human catalase (taken from ref (99)). A 25-Å channel leads from the enzyme's surface to the heme active site and forms a hydrophobic constriction 3-Å wide immediately above the heme. Side chains making up the hydrophobic channel and the proximal Tyr358 ligand are displayed in green. The backbone is shown in white, water in red, and the heme in dark red.

1.7.2 H₂O₂ decomposition by catalase

Catalase catalyses the dismutation $2\text{H}_2\text{O}_2 \rightarrow 2\text{H}_2\text{O} + \text{O}_2$ (Scheme 1.2) and removes H₂O₂ from RBCs, protecting them from oxidative stress. The first step involves oxidation by H₂O₂ of the heme iron to form compound I (Cpd I), an oxyferryl group with a cationic porphyrin radical. In the second step, reduction of Cpd I regenerates the resting-state enzyme (Enz) by reacting with another H₂O₂ molecule (99).

In RBCs, catalase functions alongside other systems including Gpx1 and Prx2 to prevent oxidation of Hb by H₂O₂. Moreover, the amount of metHb generated in RBCs by

exposing them to H_2O_2 has been found to be inversely proportional to their catalase content (101), suggesting that catalase is a critical enzyme in the defence against oxidative damage and inactivation of Hb in RBCs (99).



Scheme 1.2 Two-step mechanism of H_2O_2 decomposition by catalase. The first step involves oxidation of the heme iron by H_2O_2 to form compound I (Cpd I). In the second step, Cpd I is reduced back to the resting enzyme (Enz) (99).

1.8 Peroxiredoxin-2 (Prx2)

1.8.1 Properties of mammalian peroxiredoxins

The peroxiredoxins (Prxs) constitute a family of homodimeric peroxidases that reduce H_2O_2 and alkyl hydroperoxides to water and alcohol, respectively. They rely on a conserved cysteine residue to catalyze peroxide reduction. There are six known mammalian isoforms (Prx1-6), classified as typical 2-Cys, atypical 2-Cys, or 1-Cys Prxs

based on the mechanism and number of Cys residues involved in catalysis (102). It has been suggested that overoxidation of the active-site Cys to sulfinic (-SO₂H) or sulfonic acid (-SO₃H) allows intracellular accumulation of H₂O₂, which can then function as a signal transducer for various pathways, also known as the *floodgate hypothesis* (103, 104).

1.8.2 Antioxidant role of RBC Prx2

All six isoforms except Prx3 exist in human RBCs (105). Prx2 is the third most abundant RBC protein after Hb and carbonic anhydrase (106) and has previously been called calpromotin for its ability to regulate calcium-activated potassium efflux (107). For a long time, it was considered that catalase and glutathione peroxidase-1 (Gpx1) constitute the erythrocyte's defence against H₂O₂, and there has been continuous debate about which of these is the more significant in H₂O₂ metabolism (108-113). Recently, it was found that modeling peroxide metabolism in Gpx-deficient erythrocytes required the inclusion of Prx2 to fit the data (58). It has also been shown that circadian oscillation of Prx2 oxidation occurs in human RBCs (105). Prx2 is able to protect Hb from exogenous oxidation (114) and is thought to remove peroxides at the RBC membrane (115).

When Prx2 (a typical 2-Cys Prx) reacts with peroxide, the peroxidatic cysteine (S_P) at the active site on one subunit is oxidized to a sulfenic acid (-S_POH) (Fig 1.8). A second conserved cysteine at the C-terminal end of the other subunit (the resolving cysteine, S_R) then reacts with the sulfenic acid to form a disulfide bridge. Reduction of the disulfide by thioredoxin (Trx) regenerates Prx2 and completes the cycle. Trx is in turn regenerated by thioredoxin reductase (TrxR), with reducing equivalents derived from NADPH (116).

RBCs are notable among other cells because they are highly resistant to Prx2 overoxidation to sulfinic acid ($-S_pO_2H$) (117). Also, low TrxR activity has been reported in RBCs (117) and has been speculated that Prx2 accumulates as a dimer. In its dimeric form, Prx2 has been proposed to act as a chaperone for Hb or as a regulator of Ca^{2+} -activated K^+ transport (117). This is in contrast to other mammalian Prxs, which are overoxidized to $-S_pO_2H$ or sulfonic acid ($-S_pO_3H$) by high levels of peroxide (118). Overoxidation to S_pO_2H is reversed by sulfiredoxin (Srx) (119).

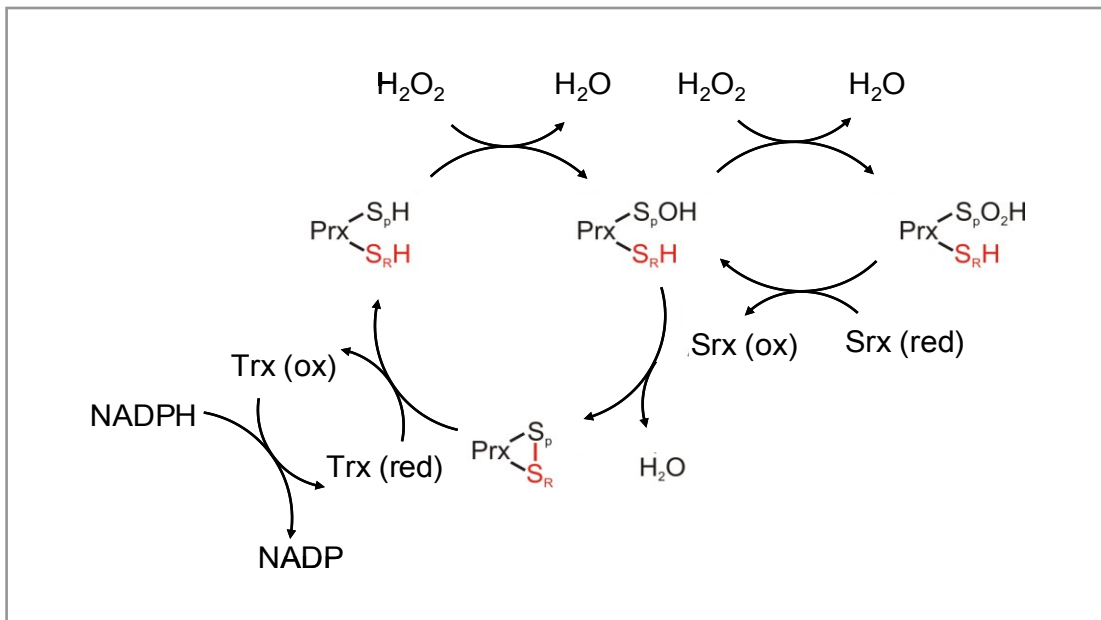


Fig 1.8 Mechanism of H₂O₂ decomposition by Prx2 (modified from ref (120)). One of two active sites within a functional dimer is shown. S_p and S_R (red) designate the sulfur atoms of the peroxidatic and resolving cysteines, respectively. Note that S_p and S_R come from different subunits within the dimer.

1.9 Structure of Glutathione peroxidases (Gpx)

The term Gpx was introduced by Mills in 1957. He discovered peroxidase activity with H₂O₂ in enzyme preparations from human RBCs (121) and Gpx was suggested to

protect RBCs against hemolysis by oxidation. Bovine Gpx1 was identified as the first selenoprotein to be discovered (122). Of the numerous mammalian Gpx isoforms only four or five have a selenocysteine (Sec) at the active site, and the rest possess a Cys residue (123). In 1992, Rocher et al. showed that a selenocysteine to cysteine substitution significantly reduces Gpx activity and that a serine mutant is completely inactive (124). Furthermore, among the numerous Gpx isoforms that have been identified in all domains of life, non-mammalian Gpxs usually have a Cys at the active site (125). The various Gpx isoforms use either Trx or GSH as reducing substrate (126).

Gpx1, the most abundant of the four mammalian types, is found in the cytosol of nearly all mammalian cells including RBCs. In all species, Gpx1 is a homotetramer with four spherical subunits, each with an active-site Sec in a depression near the surface (127). Gpx1 or cytosolic Gpx rapidly metabolizes H₂O₂ and organic peroxides, including cholesterol and lipid peroxides (128). The reducing substrate for Gpx1 is GSH. Gpx2, a cytosolic gastrointestinal tetrameric enzyme, has ~65% amino acid sequence identity (129) and similar substrate specificity to Gpx1 (130). Gpx3 is an extracellular tetrameric glycoprotein (131) with ~50% homology to human Gpx1 (132). It has activity against phospholipid hydroperoxides, suggesting a role in the protection of RBC membrane extracellularly (133). Gpx4 is a monomer and has a high preference for phospholipid hydroperoxides (134).

Several important structural features of Gpx1 are shown in Fig 1.9. Helix α 2 contributes to the monomer–monomer contact site in crystallized homotetrameric Gpx1 (127). Moreover, the α 2 helix often contains a cysteine residue and is termed the Cys block (135), because it is mechanistically relevant for Trx-dependent Gpx-isoforms, such

as yeast Gpx2 (136). The active-site Sec residue is found at the N-terminal end of helix α_1 . Another Cys residue in a FPCN-motif at the end of strand β_2 is highly conserved among all Gpx classes but its role remains unclear (137). The oligomerization loop covers a part of the active site and mediates the contact between two dimers in crystallized homotetrameric bovine Gpx1 (127).

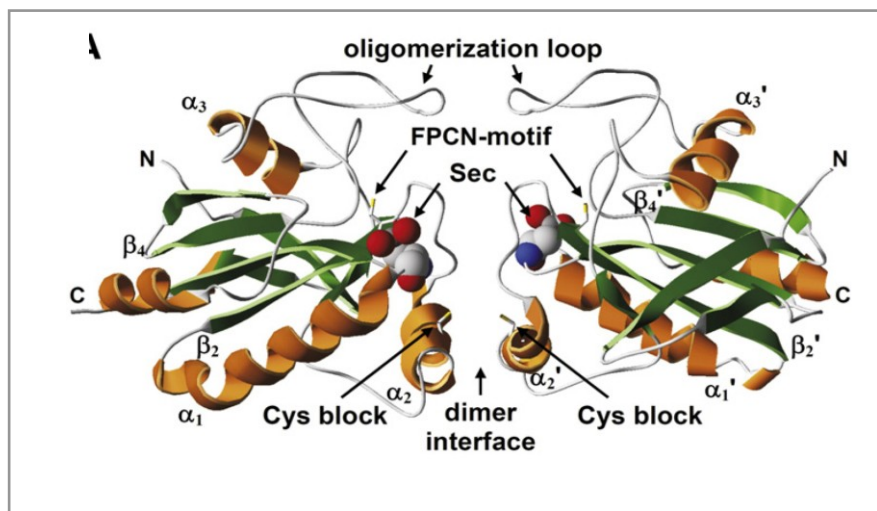


Fig 1.9 Structure of GSH-dependent Gpx1 (taken from ref (126)). View along the 2-fold axis of two subunits of homotetrameric Gpx1. Two subunits interacting with the so called oligomerization loops are omitted. The selenocysteine (Sec) residue is highlighted and further structural elements are labelled.

1.9.1 Antioxidant role of RBC Gpx1

Gpx1 is the only Gpx isoform present inside RBCs (138). The physiological role of Gpx1 in RBCs is difficult to evaluate because Prx2 and catalase also decompose H_2O_2 in RBCs. Although Gpx1 shares its substrate, H_2O_2 , with catalase and Prx2, Gpx1 can also react with lipid and other organic hydroperoxides.

Gpx1 has been suggested to be a minor antioxidant in RBCs since the RBCs of mice lacking Gpx1 appear normal unless stressed with lipid hydroperoxide. The primary

physiologic substrate of Gpx1 in mouse RBCs may be lipid hydroperoxide rather than H_2O_2 (139, 140). Humans deficient in RBC Gpx1 activity demonstrate hemolysis (141), suggesting that Gpx1 might be more important in human than mouse RBCs. Lipid oxidation is low in normal RBCs because the $\text{O}_2^{\bullet-}$ and H_2O_2 produced as a result of Hb autoxidation are removed efficiently by CuZnSOD and Prx2, respectively. However, in diseased states such as Sickle cell disease, the rate of Hb autoxidation is increased, the activity of CuZnSOD and Gpx1 is decreased (142, 143), and Prx2 is partially inactivated as a result of overoxidation to $-\text{SO}_2\text{H}$ (143), all of which may promote lipid peroxidation.

Kinetic measurements revealed that Gpx1 acts via a ping-pong mechanism (144). There is no ternary complex between Gpx1, the hydroperoxide and GSH, and the reaction can be subdivided to an oxidation half-reaction and reduction half-reaction. During the oxidation half-reaction, the active-site Sec is deprotonated to a selenolate (E-Se^- , $\text{pK}_a = 5.47$) (145) and acts as a nucleophile. Its activation depends on the side chains of three proximal residues Gln, Trp and Asn, whose precise role remains unclear (123). After the highly reactive anionic nucleophile is formed (Fig 1.10), the substrate (H_2O_2 , ROOH or lipid hydroperoxide) is irreversibly turned over. Based on the high reactivity of the active-site Sec, it was suggested that no real binding site for the hydroperoxide substrate exists, explaining the rather low substrate specificity (123). The oxidative half-reaction ends with the release of H_2O or alcohol (ROH), depending on the substrate (Fig 1.10). A conformational change has been proposed to occur at the end of this step to position the active site in the correct orientation.

During the reduction half-reaction after formation of the unstable selenenic (E-SeOH) or sulfenic acid, the first GSH molecule enters the active site and is turned over

yielding a water molecule as the second product (Fig 1.10). Since Gpx1 is highly specific for GSH (123), there has to be a defined GSH-binding site. However, a structure of a GSH-Gpx1 complex has not been solved to date. A second GSH molecule binds to Gpx1, yielding GSSG as the third product (Fig 1.10). It is not well understood which GSH molecule occupies which surface area during the catalytic mechanism.

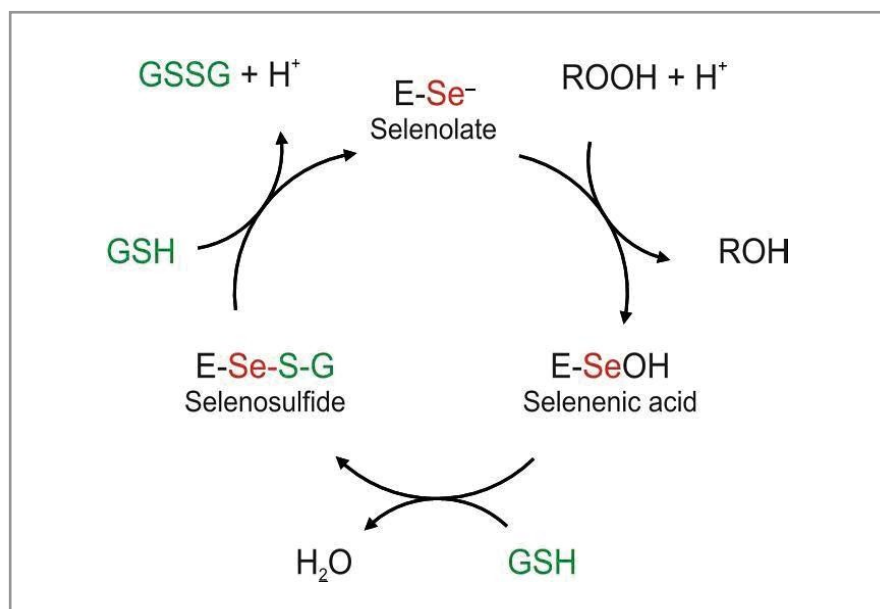


Fig 1.10 Mechanism of catalysis by Gpx1 (modified from (127)). During the oxidation half-reaction of Gpx1, the selenolate form of the enzyme (E-Se⁻) reacts with peroxides (ROOH) to give the selenenic acid (E-SeOH), which is trapped by a GSH molecule to form E-Se-S-G (first reduction half-reaction). During the second reduction half-reaction, the E-Se-S-G is reduced back to E-Se⁻ by another GSH molecule and GSSG is released as a by-product (146).

1.10 Outline and scope of thesis

The antioxidant enzymes, CuZnSOD, catalase, Prx2 and Gpx1 are critical for protection of the RBC membrane against ROS and maintaining cell viability and thus

protection against pathological conditions. Since enzyme localization often determines its function, understanding the properties and specific roles of these four RBC enzymes is essential. Thus, cell fractionation, quantitative Western blotting and immunofluorescence are used here to determine localization of CuZnSOD, catalase, Prx2 and Gpx1 in human RBCs.

This chapter provides background on RBCs and the harmful effects of ROS on RBCs. Also, an overview of nonenzymatic and enzymatic antioxidant defences in RBCs is presented, followed by a more detailed description of the properties and function of CuZnSOD, catalase, Prx2 and Gpx1.

Chapter 2 describes the two main techniques and the materials used in this study. The first technique involves fractionation of RBCs into cytosolic and membrane fractions followed by isolation and quantitation of RBC membrane-associated proteins by Western blotting. The second technique described is the preparation, fixation, membrane permeabilization by detergent addition and staining of RBCs for their visualization by confocal microscopy. The treatment of the RBC by different agents, such as prolonged air, H₂O₂, and CHP is also outlined in detail.

Standard plot preparation for each antioxidant protein, loading controls, and confocal controls are discussed in Chapter 3. Results for the membrane localization of CuZnSOD, catalase, Prx2 and Gpx1 in RBCs exposed to air for 30 or 60 min and H₂O₂ or CHP are discussed in Chapter 4 and 5, respectively. Chapter 6 provides the results for membrane localization of RBC proteins from diabetic rat RBCs.

Final conclusions and future studies are discussed in Chapter 7 and 8.

Chapter 2: Materials and Methods

2.1 Materials

Tris-HCl and Tris base were purchased from MP Biomedicals, Canada. Ultrapure potassium phosphate (K_2HPO_4 , monobasic) was from Anachemia, Canada. Glycine, sodium dodecyl sulphate (SDS), tetramethylethylenediamine (TEMED), ammonium persulphate (APS) and glycerol were from Bioshop, Canada. Proteins were denatured by 2-mercaptoethanol from Schwarz/Mann Biotech, USA. Bromophenol blue, Tween-20, butan-1-ol, methanol (HPLC grade), SuperSignal West Pico Chemiluminescent Substrate (ECL kit # 34077) were from Fisher Scientific, Canada. Acrylamide/Bis (29:1) was from BioBasic, Canada. Phosphate-buffered saline (PBS) tablets (one tablet was dissolved in 200 mL of deionized water to give 137 mM NaCl, 2.7 mM KCl, 8.1 mM K_2HPO_4 , 1.5 mM KH_2PO_4 at pH 7.4), potassium phosphate (K_2HPO_4 , dibasic), Triton-X, fish skin gelatin, sodium azide, polylysine, acrolein were from Sigma, USA. Glucose was from EMD Millipore, USA. Aqua-mount was from Lerner Laboratories, USA. All the chemicals were analytical grade. Novex MiniCell transfer system was from Invitrogen, Canada. The hemocytometer was purchased from Hausser Scientific, USA.

2.2 Antibodies used for Western blotting of isolated membranes from human and rat RBCs

The primary antibodies used were rabbit polyclonal anti-human CuZnSOD (#SOD-100) at 1:1000 dilution from Stressgen, USA. Sheep polyclonal anti-human catalase (#ab8954, 1:1000 dilution), sheep polyclonal anti-Gpx1 (cat #ab8850, 1:1000 dilution) and rabbit polyclonal anti-human Prx2 (cat #ab15572, 1:10000 dilution) were

from Abcam, United Kingdom. Secondary antibodies used were HRP-conjugated goat polyclonal anti-rabbit (cat #1706615, 1:3000 dilution) from Biorad and HRP-conjugated donkey polyclonal anti-sheep (cat #ab6900, 1:3000 dilution) also from Abcam, United Kingdom.

2.3 Antibodies used for confocal microscopy of fixed and stained human RBCs

Rabbit polyclonal anti-human CuZnSOD (#SOD-100) was from Stressgen, USA. Mouse monoclonal anti-human CDB3 (ab11012), rabbit polyclonal anti-human peroxiredoxin-2 (Prx2, ab15572, IgG fraction), sheep polyclonal anti-human hemoglobin (Hb, ab35306, IgG fraction), sheep polyclonal anti-human catalase (ab8954, IgG fraction), and sheep polyclonal anti-human glutathione peroxidase-1 (Gpx1, ab8850, IgG fraction) were from Abcam, United Kingdom. Cy2-(711-226-152) conjugated donkey anti-rabbit, FITC-(713-096-147) conjugated donkey anti-sheep and Cy2-(715-226-150) conjugated donkey anti-mouse were from Jackson ImmunoResearch, Canada. All the secondary antibodies were supplied as affinity purified.

2.4 Methods

2.2.1 Quantitation of membrane-associated proteins by Western blotting

2.2.1.1 Human blood collection and washing of RBCs

All procedures involving the collection of human blood samples from healthy female volunteers 25-35 years old were approved by Concordia's Human Research Ethics Committee. All blood donors provided their informed consent. Blood was drawn

with the use of a tourniquet into heparin-coated BD Vacutainer tubes (Fisher Scientific) from the antecubital area of the arm and gently mixed by reversing the vial several times. Heparin has been established as an appropriate coagulant with minimal effects on RBC properties (147). The collected blood was maintained at 4 °C in a sealed vial and processed within 1 h. About 18 mL whole human blood was centrifuged at 1800 xg (4400 rpm, MicroMax RF Centrifuge, Thermo IEC) for 6 min at 4 °C. After removal of the upper layer (plasma and buffy coat) by pipette, the RBC pellet was washed three times in isotonic glucose-PBS (G-PBS) (137 mM NaCl, 2.7 mM KCl, 8.1 mM K₂HPO₄, 1.5 mM KH₂PO₄, pH 7.4 containing 5 mM D-glucose). At the end of this step, about 9 mL of washed RBCs were obtained. G-PBS was added to adjust the number of washed RBCs to 3x10⁸ cells/mL with a hemocytometer.

2.2.1.2 Prolonged exposure to air of human RBCs

Washed RBCs (500 µL at 3x10⁸ cells/mL) were exposed to air for 30 or 60 min at 37 °C in 500 µL Eppendorf tubes. All tubes were filled to the top and gently stirred during incubation. Control samples were not exposed to air and the RBCs were lysed immediately following washing. To prevent unwanted disulfide-induced dimer formation during handling of Prx2, 15 min incubations at 37 °C with NEM (N-ethylmaleimide), an alkylating agent at 100 mM final concentration, was performed prior to RBC hemolysis (117).

2.2.1.3 Human RBC exposure to H₂O₂ and cumene hydroperoxide (CHP)

Washed intact human RBCs (500 µL at 3x10⁸ cells/mL) were treated with a 5-µL bolus of 5 mM H₂O₂ or CHP to give 50 µM final concentration of H₂O₂ or CHP. G-PBS

(5 μL) was added to control samples. CHP is not a substrate for catalase. The experiment was carried out in 500 μL Eppendorf tubes which were closed and gently stirred during incubation at 37 $^{\circ}\text{C}$ for 30 min ($\sim 100\%$ Ht).

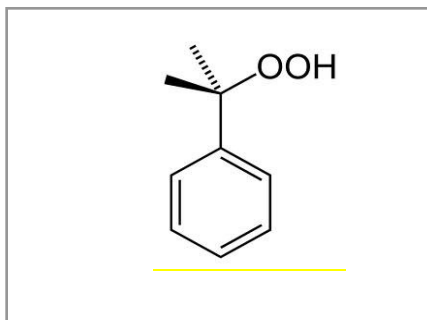


Fig 2.1 Structure of cumene hydroperoxide (CHP)

2.2.1.4 Isolation of membranes from human RBCs

Following treatment and NEM alkylation, human RBCs were quickly transferred to 25-mL centrifuge tubes and lysed by 1:15 dilution into 40 mM hypotonic sodium phosphate buffer with 0.1 mM PMSF (phenylmethylsulfonyl fluoride), a serine protease inhibitor, pH 7.4 at room temperature. The hypotonicity of this buffer, the pH and dilution were carefully chosen as detailed in Section 3.6 and have been documented as optimal for localization of RBC membrane-associated proteins and membrane-bound Hb (148). The hemolysates were immediately centrifuged at 30,000 $\times g$ (14,800 rpm) in Beckman J2-HS centrifuge (JA-17 rotor) at 4 $^{\circ}\text{C}$ and membrane fractions were isolated and resuspended in 100 μL of hemolysis buffer (40 mM sodium phosphate, pH 7.4, 0.1 mM PMSF).

2.2.1.5 Rat blood collection and washing of rat RBCs

This study was performed in collaboration with Dr Andreas Bergdahl and the rats used in this study were handled by his laboratory in accordance with the guidelines of the Canadian Council of Animal Care (approved by the Concordia University Animal Care Committee). In this study, 65 mg streptozotocin (STZ)/kg body weight was injected once into the tail vein of five Wistar male rats of the same age and weight (3 months old, ~500 grams). Saline solution was injected into the tail vein of 5 control animals. Blood glucose was monitored and the STZ-treated animals had >15 mM blood glucose at 48 h after injection vs <5 mM for the control animals. Animals were euthanized by CO₂ asphyxiation and the bloods, collected by cardiac puncture at 2 weeks and 4 weeks after injection, were provided to our group.

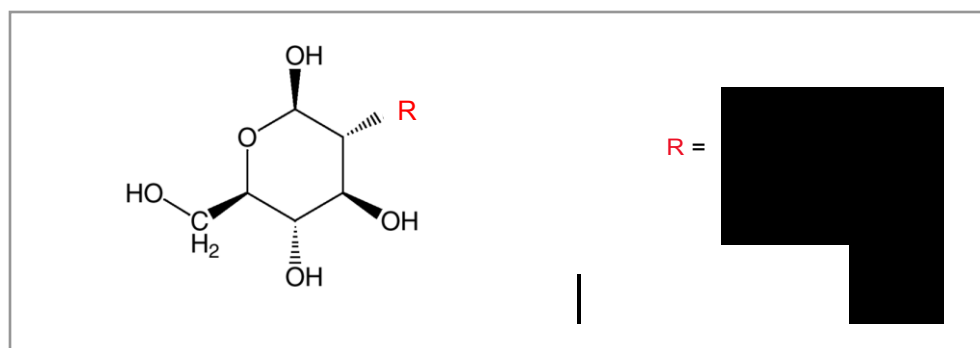


Fig 2.2 Structure of streptozotocin (STZ)

Following collection, the rat blood was donated to our laboratory and maintained at 4 °C in a sealed vial and processed within 1 h. Whole blood was centrifuged at 1000 xg (3300 rpm, MicroMax RF Centrifuge, Thermo IEC) for 2 min at 4 °C. After removal of the upper layer (plasma and buffy coat) by pipette, the RBC pellet was washed two times in isotonic physiological saline solution (PSS, 21 mM Tris base, 7.8 mM NaCl, 0.25 mM

KCl, 0.1 mM CaCl₂, 2.5 μM MgCl₂, 0.1 mM NaH₂PO₄, 0.5 mM HEPES, 7.5 μM BSA, 5 mM D-glucose). PSS buffer was used to wash the rat RBCs instead of G-PBS because G-PBS lysed the rat RBCs. PSS has been established as an appropriate buffer for washing of rat RBCs (149-151). The number of washed RBCs was counted with a hemocytometer and adjusted to 4x10⁸ cells/mL.

2.2.1.6 Isolation of membranes from rat RBCs

Washed rat RBCs were lysed by a 15-fold dilution into lysis buffer (10 mM hypotonic sodium phosphate buffer, pH 7.4, 0.1 mM EDTA, 1x cocktail inhibitor) at room temperature. The hemolysates were incubated on ice for 30 min and centrifuged at 21,000 xg (12,400 rpm) on Beckman J2-HS with a JA-17 rotor at 4 °C. To obtain Hb-free solubilized membranes (“white ghosts”), the pelleted membranes were washed three times with the lysis buffer. The non-ionic detergent, Triton-X at a final concentration of 0.5% was added to the ~100 μL pelleted membrane to solubilize the proteins in a final volume of 300 μL. For example, to obtain a final volume of 300 μL of solubilized membrane in 0.5% Triton-X, 105 μL of pelleted membrane and 30 μL of 5% Triton-X were added to 165 μL of lysis buffer.

2.2.1.7 SDS-PAGE and Western blotting of membrane-associated proteins from human and rat RBCs

The following protocol was used for Western blotting and visualization of proteins from both human and rat RBCs. The total protein concentration of membrane fractions prepared as described in Section 2.2.1.4 and Section 2.2.1.6 was determined by the Bradford method. SDS-PAGE (sodium dodecyl sulfate polyacrylamide gel

electrophoresis) was used to separate proteins in isolated membrane fractions according to size. Following the addition of 10% w/v SDS, proteins were briefly heated to near boiling in the presence of the reducing agent, β -mercaptoethanol, to further denature the proteins by reducing disulfide linkages and to interrupt quaternary complexes. This is known as reducing SDS-PAGE, and was used in our investigation (Fig 3.1, Fig 3.3, Fig 3.9, Fig 4.1, Fig 5.1, Fig 6.1). Non-reducing SDS-PAGE (no boiling and no β -mercaptoethanol) was used for the investigation of effects of NEM on Prx2 oligomerization state (Fig 3.8).

Loading buffer (5x, 10% w/v SDS, 10 mM β -mercaptoethanol, 20% v/v glycerol, 0.2 M Tris-HCl, pH 6.8, 0.05% bromophenol blue) was added to the samples. A 1-mm thick resolving gel (12%) and stacking gel (6%) were prepared and 30-35 μ g total protein were loaded per lane. A Nu-Page Novex Transfer System (from Invitrogen) was assembled and running buffer 1x (3.03 g/L Tris base, 1 g/L SDS, and 14.4 g/L glycine) was used to separate the proteins at 150 V (Hofer SX250 Power Supply). Transfer buffer (3.03 g/L Tris base, 14.4 g/L glycine and 20% methanol) was used to transfer the proteins from the gel to the PVDF membrane (100 mA, 2 h). After transfer, the PVDF membranes were immunoblotted with the appropriate antibodies as described in Section 2.2. Membranes were blocked for 2 h with 5% milk in Tris-buffered saline (TBST; 137 mM NaCl, 20 mM Tris, 0.1% Tween-20), incubated with the primary and secondary antibodies in 1% milk in TBST. Antibody incubations for 2 h at 25 °C were performed except when probing with sheep polyclonal anti-human Gpx1 which was incubated overnight at 4 °C for optimum signal detection. The primary antibodies recognize the human antigens (Section 2.2.2.3) but also cross-reacted with antigens in rat RBCs.

2.2.1.8 Densitometry of membrane-associated proteins from human and rat RBCs

The proteins were visualized by chemiluminescence using AlphaImager densitometer (Alpha Innotech Corporation, USA) using Fluorchem FC2 software, Version 3.0. Densitometry, or image quantification, was performed for each protein antigen to establish the linear range of the chemiluminescence signal (152). Densitometry integrates the pixel values over each band to give an integral value for the intensity of the band (Fig 2.3).

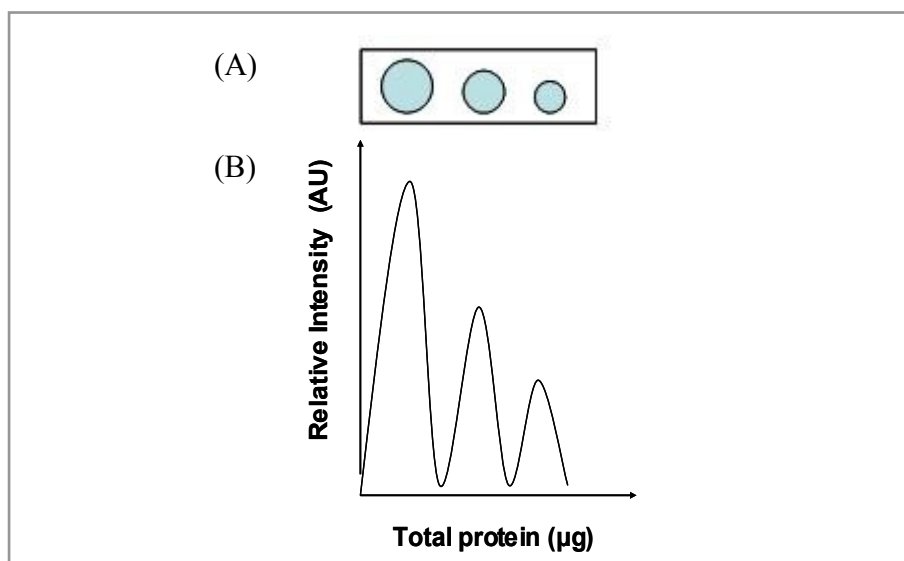


Fig 2.3 Densitometry measurements. (A) Various amounts of a membrane protein detected by Western blotting using antibodies as described in Section 2.2.1.7. (B) The densitometer passes a beam of light through the PVDF membrane and measures the absorbance of light by the sample bands such as those in Panel A. An intense band produces an intense absorbance peak because most light is absorbed whereas a weak band produces a small absorbance peak because most light passes through the sample (153).

The instrument passes a beam of light through the PVDF membrane and measures the absorbance of light by the sample. If the band is intense, most of the light is absorbed (large peak in absorbance). If the band is weak, most of the light passes through and the densitometer displays a small absorbance peak (153).

2.2.1.9 Coomassie staining of PVDF as loading control

Staining with Coomassie dye of the entire PVDF membrane was used as loading control according to procedure of Welinder et al. (154). PVDF membranes were rinsed briefly with H₂O after visualization by chemiluminescence and immersed in 0.1% Coomassie R-250 in methanol/H₂O (1:1) for 1 min, and destained for 20 min in acetic acid/ethanol/H₂O (1:5:4). The PVDF membranes were then washed briefly with H₂O, air-dried and scanned in a flatbed scanner (UMAX Powerlook III) at 600 dpi. The densities of all bands in each lane on the scanned image were summed using the AlphaImager densitometer. The background was established from the areas between the bands and subtracted from each band.

2.2.1.10 Standard plot preparation

The semi-quantitative Western blot, or immunoblot, allows quantitation of specific protein antigens by antibodies in biological samples after preparation of a standard plot for each protein (152). The unknown samples of interest are compared to the standard plot. After the membranes were isolated from RBCs, the total protein concentration was determined and equal amounts of total protein were loaded onto an SDS-PAGE to separate proteins according to molecular weight. Proteins were transferred (blotted) to a

PVDF membrane for subsequent antibody detection of antigen(s) found on the target proteins.

It is critical to avoid oversaturation of the ECL signal (152) as this would prevent accurate determination of the relative quantities of membrane-associated. The concentrations at which signal saturation occurs varies for each protein antigen and antibody. Therefore, the linear range of total protein loaded on a gel must be determined for each analyte. For example, the total protein per lane was 3-100 μg for CuZnSOD and 1-100 μg for catalase, Prx2 and Gpx1. To correct for errors due to inhomogeneities in blot transfer and to normalize for gel loading, the Welinder method (Section 2.2.1.9) was used with modifications for loading control (154).

2.2.2 Localization of proteins in fixed human RBCs by confocal microscopy

2.2.2.1 Preparation of human RBCs

Whole human blood collected as described in Section 2.2.2.1, was transferred to 2.0-mL Eppendorf tubes and centrifuged at 1000 $\times g$ for 6 min at room temperature. After removal of the upper layer (plasma and buffy coat) by pipette, the RBC pellet was washed three times in G-PBS and resuspended in this buffer at 10% hematocrit (Ht) where Ht is the percent by volume of RBCs in whole blood. Cells were examined using a light microscope with a 40x objective (Model M11-45659 Wild Heerbrugg, Switzerland) to ensure the RBCs retained their biconcave shape and had undergone lysis before fixing and staining.

2.2.2.2 Fixing and permeabilization of human RBCs

Cell fixation preserves cell structures and protects against subsequent treatments such as rinsing, permeabilizing and staining. Fixation is a necessary step in immunohistochemistry before visualization (155). Acrolein (Fig 2.4) is an aldehyde used for fixation because it reacts with protein side chains, including Cys, His, and Lys as shown in Scheme 2.1 (156). Crosslinking may interfere with antibody access to epitopes on target proteins. Furthermore, aggressive fixation has been shown to alter spatial relationships of macromolecules (157). Thus, to characterize the localization of antioxidant proteins in RBCs under physiologically relevant conditions, we used a method developed for RBCs by Low and coworkers (157) to rapidly fix freshly isolated human RBCs. To crosslink proteins side chains, a 50- μ L aliquot of cells at 10% Ht was centrifuged at 1000 xg (3300 rpm, MicroMax RF Centrifuge, Thermo IEC) for 5 min at room temperature. The RBC pellet was resuspended in 1 mL of 0.5% acrolein in PBS, gently mixed for 5 min at room temperature, centrifuged at 650 xg (2145 rpm) for 1 min and the supernatant was removed. The RBC pellet was rinsed 3x with rinsing buffer (PBS containing 0.1 M glycine) to remove excess acrolein, which reacts with the free amino group of glycine. Cells were then permeabilized in 1 mL rinsing buffer plus 0.1% Triton-X for 5 min, rinsed three times in rinsing buffer and further incubated in rinsing buffer at room temperature for 30 min to ensure complete neutralization of unreacted acrolein.

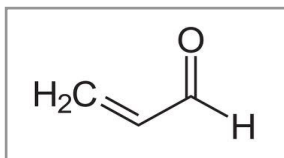
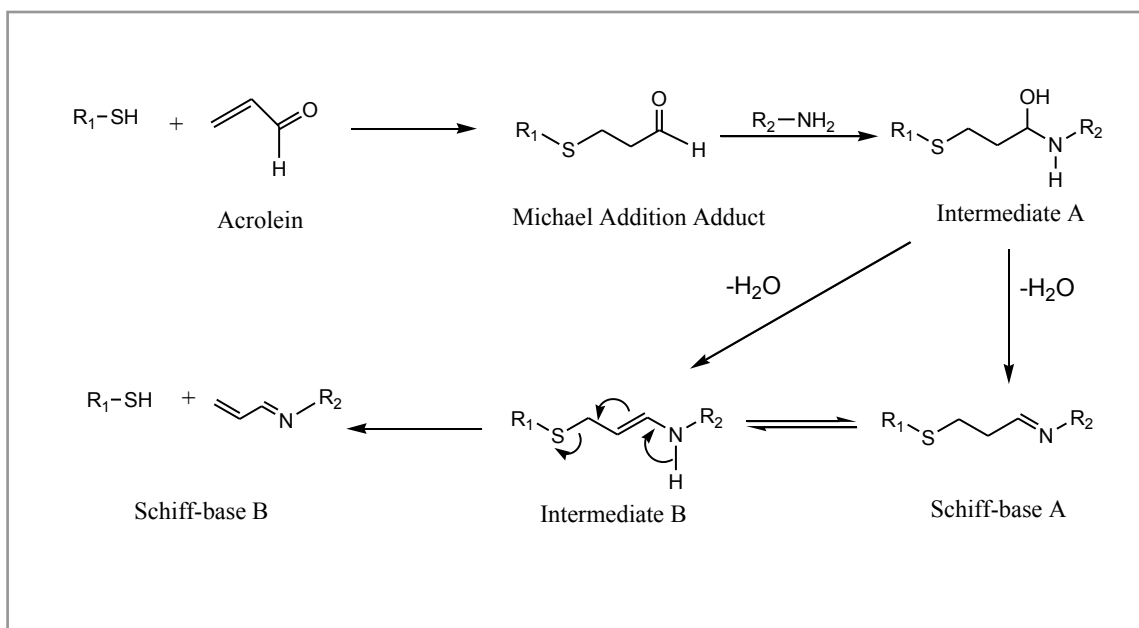


Fig 2.4 Structure of acrolein



Scheme 2.1 Reaction of acrolein with proteins (adapted from ref (158))

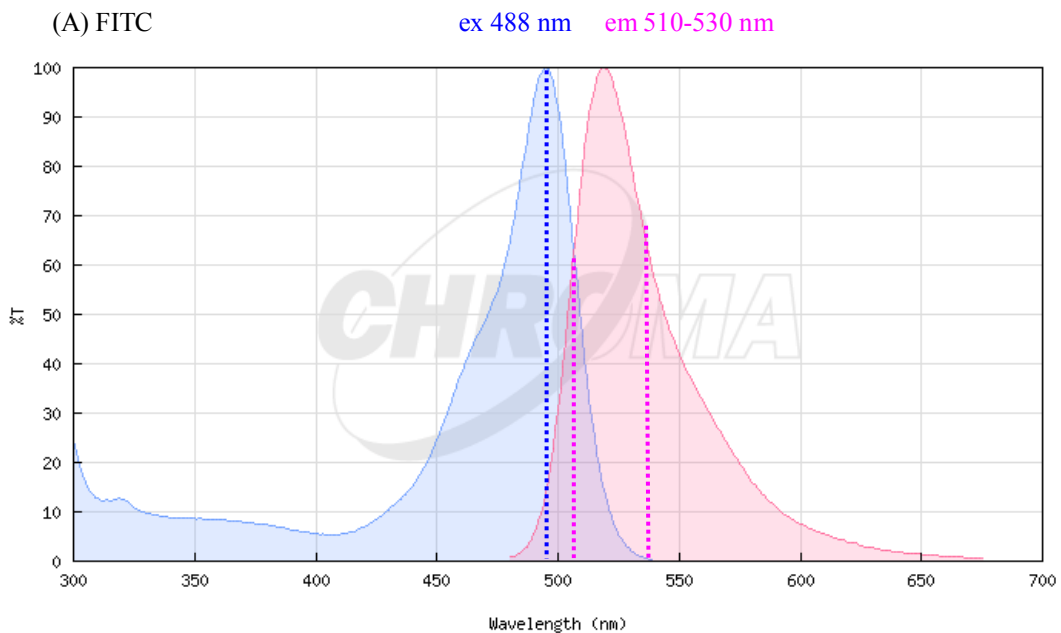
2.2.2.3 Staining of human RBCs for CuZnSOD, catalase, Gpx1 and Prx2

Fixed, permeabilized RBCs were next processed for immunofluorescence microscopy. After incubation in rinsing buffer for 30 min, the RBCs were pelleted by centrifugation at 650 xg for 1 min. To prevent nonspecific antibody binding, the pellet was resuspended (5% Ht) and incubated in blocking buffer (PBS containing 0.05 mM glycine, 0.2% fish skin gelatin, and 0.05% sodium azide) for 60 min. Staining of the fixed, permeabilized RBCs at 5% Ht was performed by incubating with the primary antibody at 1% dilution in blocking buffer overnight at 4 °C with gentle shaking. The RBCs were rinsed 3x in rinsing buffer, and incubated with secondary antibodies in blocking buffer with gentle shaking at room temperature for 2-3 h. After labelling, the RBCs were rinsed 2x in rinsing buffer and 1x in PBS, and resuspended in PBS. A 5- μ L

aliquot of labelled RBCs was added to a glass slide coated with 10% polylysine and mounted using Aqua-Mount (Lerner Laboratories, USA).

2.2.2.4 Confocal microscopy of fixed human RBCs

Stained, fixed RBCs were visualized using the 63X/1.32 optical objective on a Leica TCS SP1I laser confocal microscope at The Centre for Microscopy at Concordia (CMAC). The dyes, Cy2 and FITC, in the stained RBCs were excited with the 488/514 nm blue Argon laser. An emission filter was selected to ensure that the fluorescence from the samples did not include any laser light (Fig 2.5). The diameter of the detection pinhole was 1 Airy unit, which produced the best signal-to-noise ratio. The laser light power was set to 100% on the Leica TCS SP2.



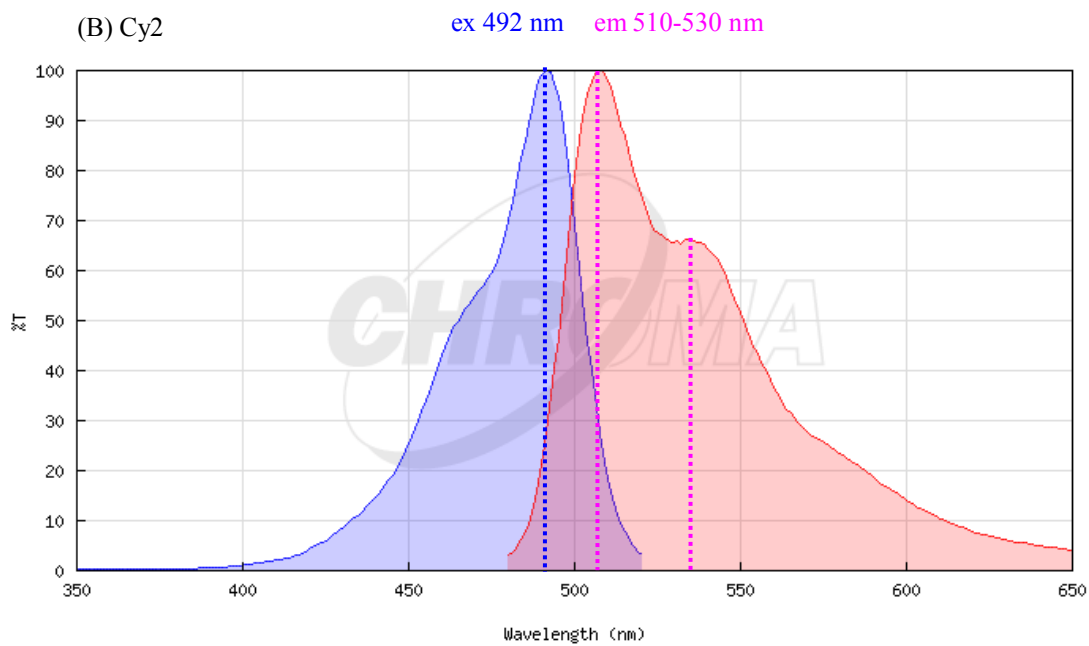


Fig 2.5 Excitation (blue) and emission (red) spectra of FITC and Cy2 dyes. In each panel, the excitation wavelength is marked by a dashed blue line, and the range of emission wavelengths detected by the confocal microscope is bracketed by the dashed pink lines. The excitation wavelength and the detected emission range were (A) 488 nm and 500-530 nm for FITC, and (B) 492 nm and 510-530 nm for Cy2. Modified from www.chroma.com/spectra-viewer?fluorochromes=631|644&showDetails=1: accessed Jun 5, 2013

Chapter 3: Characterizing controls for immunoblotting, immunofluorescence and hemolysis

3.1 Standard plot preparation of the detection of CuZnSOD, catalase, Prx2 and Gpx1

Standard plot preparation is a necessary step to determine the relative amounts of the proteins at the RBC membrane by semi-quantitative Western blotting. Standard plots were prepared for CuZnSOD, catalase, Prx2 and Gpx1 as described in Section 2.2.1.10. Samples containing different amounts of total protein from isolated membranes were tested (Fig 3.1). Quantification was performed in the linear range of the plot, avoiding concentrations at signal saturation where the curve levels off (Fig 3.2) Also, four standards from the linear region of a standard curve were chosen as controls and loaded on all subsequent gels (Fig 3.3).

Images were visualized using an enhanced luminol-based chemiluminescent substrate (ECL, Supersignal West Pico Chemiluminescent Substrate Kit, cat #34080, Thermo Scientific) for detection of horseradish peroxidase (HRP) activity from secondary antibodies on immunoblots (152). The ECL Western blotting detects picograms (pg) of antigen. The ECL kit contains Stable Peroxide Solution and the Luminol/Enhancer Solution and equal volumes of each were mixed. Following transfer, the proteins were visualized as described in Section 2.2.1.8 by submerging the PVDF membranes in equal parts Stable Peroxide Solution and Luminol/Enhancer Solution (0.1

mL per cm² of membrane). Saturation of images was minimized by avoiding overloading the SDS-PAGE gel and by using recommended antibody concentrations.

3.2 Linear range for CuZnSOD, Prx2, catalase and Gpx1 analysis by Western blotting

The standard plot for CuZnSOD is shown in Fig 3.2A based on the corresponding Western blot in Fig 3.1A. Linearity is maintained up to ~75 µg total protein for CuZnSOD and it was determined that 35 µg total protein is the optimum amount to load on each gel for CuZnSOD. This amount allows increases or decreases in the chemiluminescence signal to be detected if the amount of membrane-associated CuZnSOD is lower or higher than expected.

The standard plots for catalase, Prx2 and Gpx1 are shown in Fig 3.2B, C, D based on corresponding Western blots in Fig 3.1B, C, D. The plots shown in Fig 3.2 are biphasic, with two linear regions (shown by the red and blue lines in Fig 3.2). Ideally, the first more steep linear region should be used for standard curve preparation (red line, Fig 3.2) with a signal linear to ~12.5 µg total protein for catalase, Prx2 and Gpx1. Analogously to the standard plot for CuZnSOD, ideally ~6 µg, should be loaded per lane for catalase, Prx2 and Gpx1. However, the chemiluminescence signal would be rather low at these concentrations (Fig 3.1B, C, D) and should there be more than a 2-fold decrease in the signal upon treatment, no band would be observed. This was circumvented by choosing the second linear region (with smaller slope) at higher total protein concentrations seen in Fig 3.2B, C, D enclosed by the dotted lines. This was previously demonstrated as a good compromise between signal strength and linearity

(152). It was determined that 30 μg total protein was the optimum amount to be loaded on each gel for each condition tested for catalase, Prx2 and Gpx1. The linear regions and total protein amounts loaded per gel are summarized in Table 3.1.

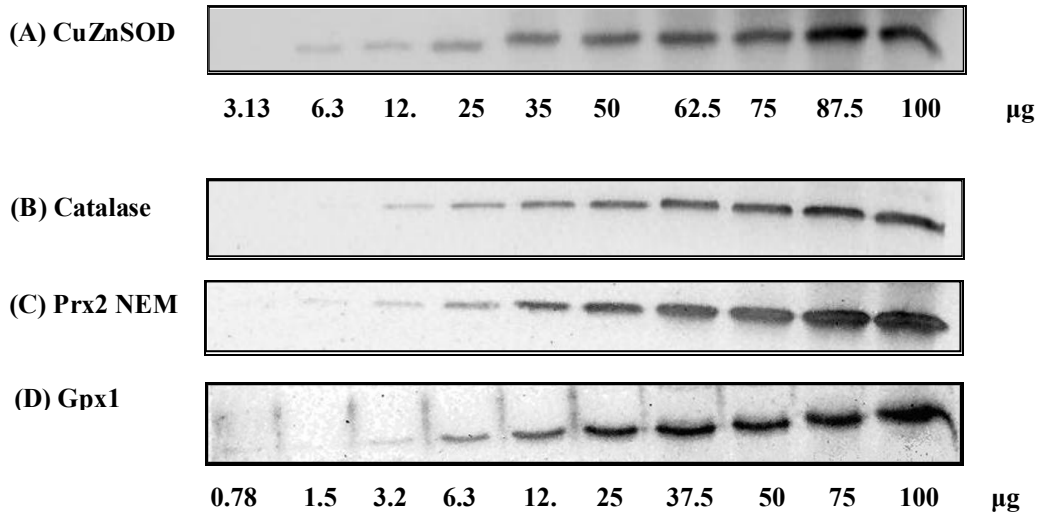


Fig 3.1 Determination of the linear region in ⁵Western blots of CuZnSOD, catalase, Prx2 and Gpx1 in human RBC membranes. RBCs were washed and lysed in 40 mM hypotonic sodium phosphate buffer (1:15 dilution) containing 0.1 mM PMSF, pH 7.4 at room temperature as described in Section 2.2.1.1 and 2.2.1.4. Prx2 sample was treated with 100 mM NEM for 15 min. Hemolysates were immediately centrifuged at 30,000 xg (14,800 rpm) on Beckman J2-HS centrifuge at 4 °C and membrane fractions were isolated and resuspended in 100 μL of hemolysis buffer (40 mM sodium phosphate, pH 7.4) containing 0.1 mM PMSF. Proteins from the isolated membranes were separated by a reducing SDS-PAGE and Western blotted as described in Section 2.2.1.7. (A) CuZnSOD in isolated RBC membranes were blotted and probed with rabbit polyclonal anti-CuZnSOD (Stressgen SOD-100), 1:1000 dilution, 1.5 h. (B) Catalase in isolated RBC membranes blotted and probed with sheep polyclonal anti-catalase (Abcam, ab8954), 1:1000 dilution, 1.5 h. (C) Prx2 in isolated RBC membranes blotted and probed with rabbit polyclonal anti-Prx2 (Abcam, ab15572), 1:10 000 dilution, 1.5 h. (D) Gpx1 in isolated RBC membranes blotted and probed with sheep polyclonal anti-Gpx1 (Abcam, ab8850), 1:7000 dilution, overnight incubation. The secondary antibody used for catalase and Gpx1 was donkey anti-sheep (HRP-conjugated, Abcam, ab6900), at a 1:5000 dilution, 1.5 h. The secondary antibody used for CuZnSOD and Prx2 was goat anti-rabbit (HRP-conjugated, Biorad, 1706615), also at a 1:5000 dilution. The PVDF membranes were incubated with the antibodies for 1.5 h. Exposure time for development of the ECL signal was 3 min for CuZnSOD and 1 min for catalase, Prx2 and Gpx1.

From the ten point-standard plots, four total protein concentrations were selected to be loaded on each subsequent Western blot (Table 3.2). Representative Western blots of selected controls are shown in Fig 3.3 and good linearity is observed between the total amount of protein loaded and the chemiluminescence signal strength.

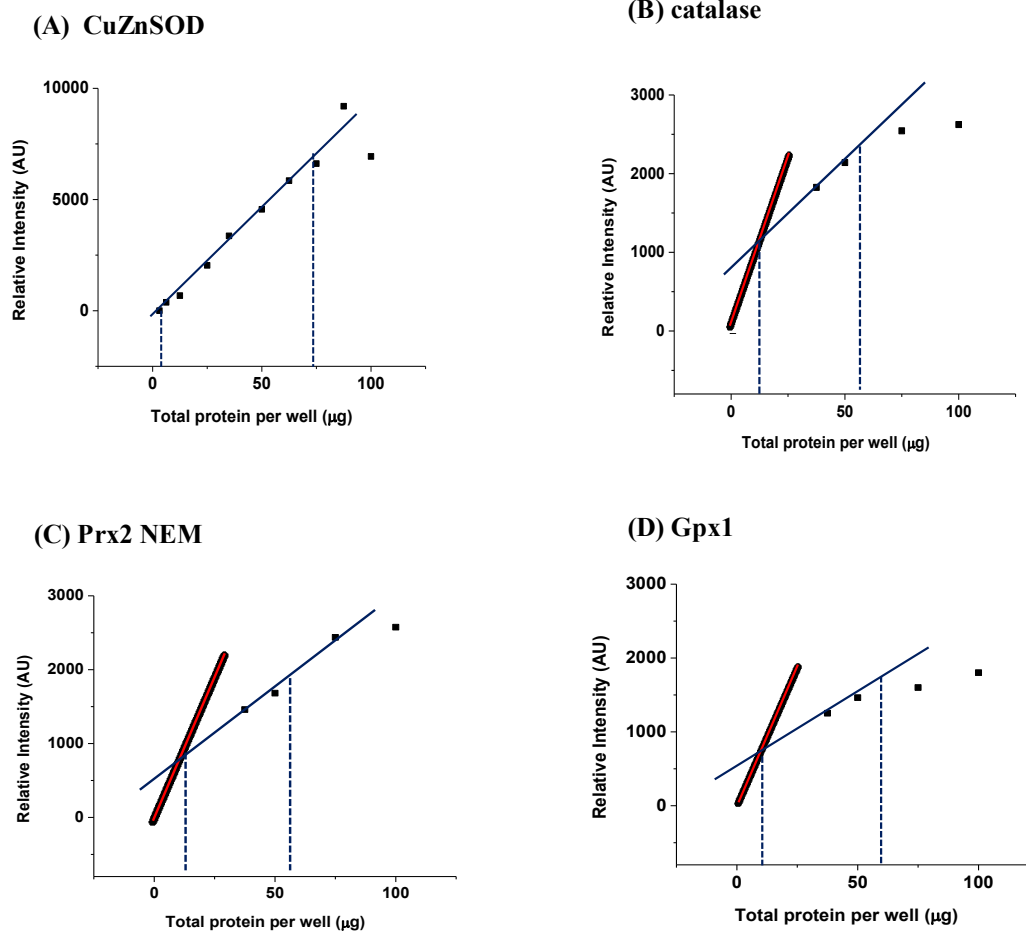


Fig 3.2 Standard plots of CuZnSOD, catalase, Prx2 and Gpx1 in isolated membranes from human RBCs. (A) CuZnSOD (B) Catalase (C) Prx2 (D) Gpx1. Densitometry was performed on the Western blots shown in Fig 3.1 by using FluorChem FC2 imaging software and the background was subtracted. Western blots were visualized by chemiluminescence by ECL.

Table 3.1: Summary of linear regions and optimum protein loaded for CuZnSOD, catalase, Prx2 and Gpx1 as determined from standard plots in Fig 3.2 and detected by Western blotting.

Antioxidant protein	a) Linear region	b) Optimum total protein per gel lane
CuZnSOD	3 - 75 μg	35 μg
catalase	12 - 60 μg	30 μg
Prx2 NEM	12 - 60 μg	30 μg
Gpx1	12 - 60 μg	30 μg

a) Determined from standard plots in Fig 3.2

b) Determined for subsequent Western blots

Table 3.2: Total protein controls for Western blotting

Antioxidant protein	a) Four-point standard plot
CuZnSOD	25, 37.5, 50, 75 μg
catalase	12.5, 25, 37.5, 60 μg
Prx2 NEM	10, 25, 40, 60 μg
Gpx1	10, 25, 40, 60 μg

a) These total protein concentrations were selected as controls for representative Western blots shown in Fig 3.3 below.

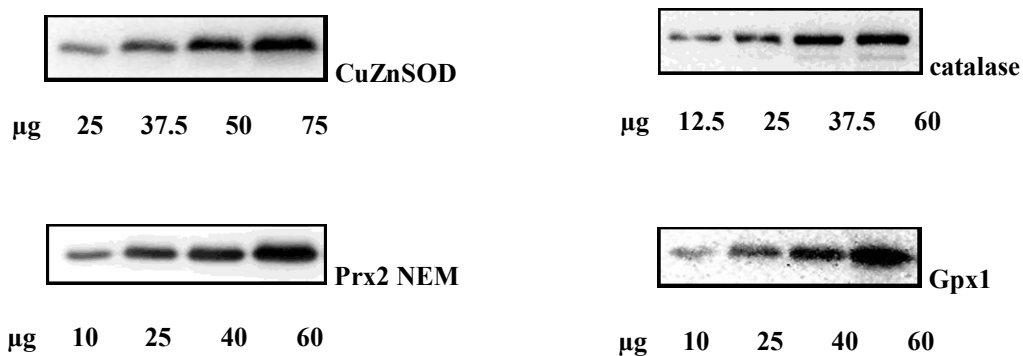


Fig 3.3 Four CuZnSOD, catalase, Prx2 and Gpx1 controls to be loaded on each gel for Western blotting. The signal strength varies linearly with each protein concentration loaded. The signal strength also varies with each antigen/antibody pair.

3.3 Sum of Coomassie bands as a loading control in Western blot analysis

Western blotting is a powerful and widely used technique for specifically measuring the content of single proteins in complex biological mixtures. Two factors that need to be controlled to ensure reliable comparisons of protein amounts in different samples are the total amount of protein loaded to each well in the electrophoretic separation and the efficiency of transfer in the blotting procedure. To address these possible sources of error, antibodies directed against housekeeping proteins are often used as loading controls, assuming these housekeeping proteins are constantly expressed. However, several problems are associated with this procedure. For example, when low abundant proteins are of interest, the gel might be overloaded with respect to the loading

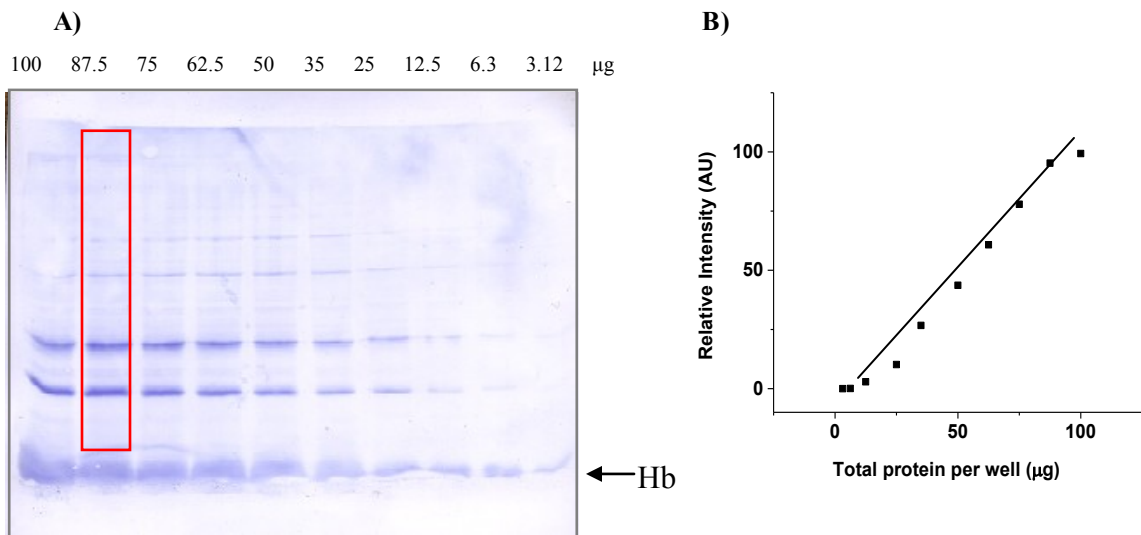


Fig 3.4 Plot of summed band intensities vs total protein per lane. A representative plot shown for RBC membrane proteins, $R^2=0.9842$ (A) After visualization by chemiluminescence, the PVDF membrane was stained with Coomassie, air-dried and scanned as described in Section 2.2.1.9. (B) The sum of the intensities of all the bands enclosed by the rectangle was recorded by densitometry as described in Section 2.2.1.8. Note that the Hb band intensity was excluded from the sum because of its irreproducible size and shape.

control (159). Also, there might be overlap in molecular weight between the sample and control.

Thus, to monitor protein loading and blotting efficiency, we used the Welinder method as a loading control (154) as described in Section 2.2.1.9. This method involves Coomassie staining of the PVDF membrane after the immunodetection step and provides superior linearity over antibody detection of housekeeping proteins. A representative plot of total protein per well (Fig 3.4A) vs relative intensity (Alpha Imager) is shown in Fig 3.4B. This method assesses the transfer efficiency of the entire lane, except Hb (because of its irreproducible size and shape) as opposed to one specific region, and was used as a loading control for all the Western blots reported here. Coomassie staining of PVDF membranes is performed after protein visualization and does not interfere with the chemiluminescence signal. The method works for PVDF but not for nitrocellulose membranes because the latter react with the Coomassie stain producing a dense background. PVDF membranes were scanned in a flatbed scanner (UMAX Powerlook III) at 600 dpi and the sum of the densities of all bands found in a lane was determined by densitometry.

3.4 Confocal controls for CDB3 and Hb localization in human RBCs

To characterize the localization of antioxidant proteins in RBCs under physiologically relevant conditions, we used a method developed by Low and coworkers in 2004 (157). Isolated fresh human RBCs were rapidly fixed as described in Section 2.2.2.2 and the localization of antioxidant enzymes in the intact cells was then examined by confocal microscopy as described in Sections 2.2.2.3 and 2.2.2.4. The working

conditions for cell fixing and staining were established by examining the localization of Hb and CDB3 in intact human RBCs.

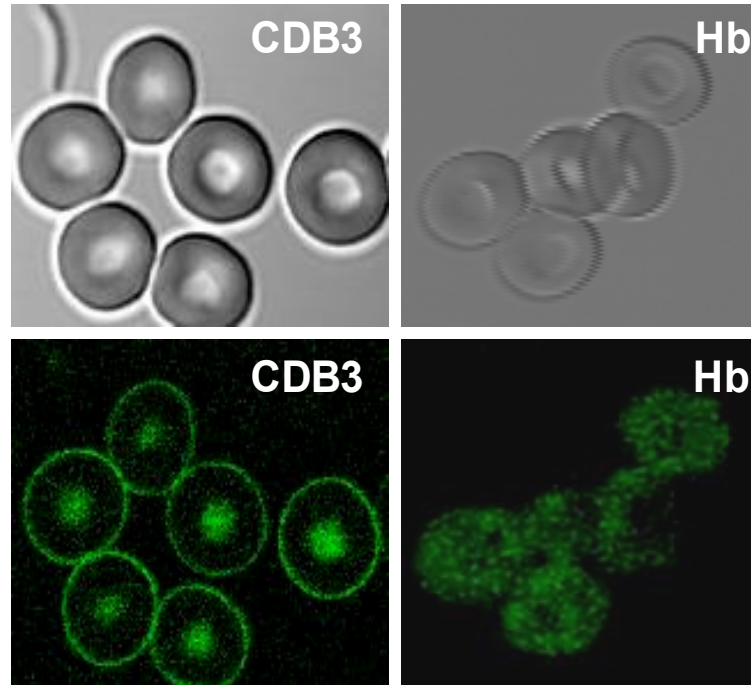


Fig 3.5 Confocal immunofluorescence and corresponding bright field images of Hb and CDB3 in fixed intact human RBCs. The bright filed images are shown in the upper panels and the corresponding immunofluorescence images in the lower panels. Hb was stained by sheep polyclonal anti-human Hb and FITC donkey anti-sheep IgG. CDB3 was stained by mouse monoclonal anti-human CDB3 and Cy2 donkey anti-mouse IgG. Filter settings were as follows: excitation 488 nm; emission 500-530 nm. The RBC pellet was fixed and stained as described in Section 2.2.2.2 and 2.2.2.3. Cells were exposed to air for <5 min, and fixed within 2 h of drawing blood.

Band-3 is an important structural component of the RBC membrane and each cell contains approximately 10^6 copies of Band-3 (160). Hb is the main protein in the RBC cytosol, being present at 5 mM or $\sim 270,000,000$ copies. Invariably, as expected, staining for CDB3 revealed that the protein was concentrated at the membrane and Hb staining showed that this protein was evenly dispersed throughout the cytosol (Fig 3.5). The

monoclonal anti-CDB3 antibody used in these studies specifically recognized an epitope within residues 1-136 of CDB3 (161). Hence, the membrane pattern of CDB3 staining in intact RBCs (Fig 3.5) confirmed that its antibody had access to the cytoplasmic side of the membrane after cell fixing and permeabilizing. CDB3, which comprises the first 403 amino acid residues of Band-3 (162), binds peripheral proteins and might play a role in the localization CuZnSOD, catalase, Prx2 and Gpx1. Also, the Hb distribution (Fig 3.5) demonstrated that the highly dense macromolecular network of crosslinked Hb expected after chemical fixation does not restrict access of anti-Hb antibody to the cell interior. Therefore, the staining patterns observed for other target proteins should reflect their actual localization (157).

3.5 Prx2 visualization in fixed human RBCs

To establish the response of key RBC antioxidant enzymes, CuZnSOD, catalase, Prx2 and Gpx1, to various oxidative-stress conditions, their localization under physiological conditions was first characterized. Freshly drawn human RBCs were fixed and stained immediately after washing. Fresh human RBCs were previously stained for CuZnSOD, catalase, and Gpx1 in our laboratory (163). To obtain confocal data for Prx2, human RBCs were fixed and stained for Prx2 as described in Section 2.2.2.2 and 2.2.2.3. Using the filter settings given in the figure legend, the confocal images reveal that Prx2 is evenly distributed in the cytosol of untreated human RBCs (Fig 3.6). Notably, the staining pattern resembles the staining of Hb (Fig 3.5) in these cells, which were exposed to air for <5 min and fixed within 2 h of drawing blood. Its high concentration (~240 μ M) in RBCs may mask membrane binding of Prx2 in control cells because we did not

attempt to distinguish cytosolic and membrane-bound Prx2 by confocal microscopy, although this can be achieved by the use of different focal planes.

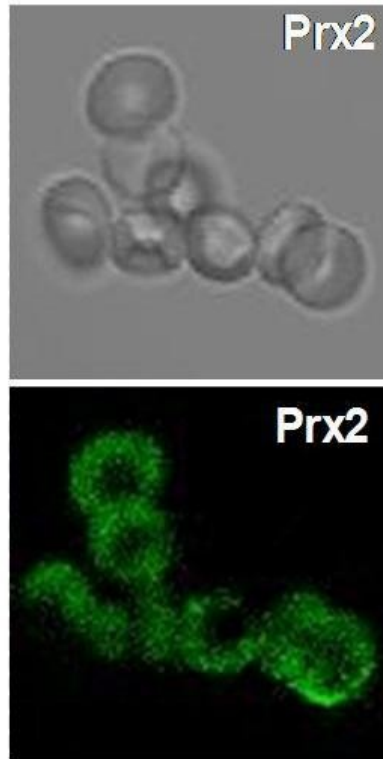


Fig 3.6 Confocal immunofluorescence and corresponding bright field images of Prx2 in fixed intact human RBCs. The bright field images are shown in the upper panels and the corresponding immunofluorescence images in the lower panels. Prx2 stained by rabbit anti-human Prx2 and Cy2 conjugated donkey anti-rabbit IgG. Filter settings for Cy2 were as follows: excitation 488 nm; emission 500-530 nm, 100x objective, Leica TCS SPII. The RBC pellet was fixed and stained as described in Sections 2.2.2.2 and 2.2.2.3. Cells were exposed to air for <5 min, and fixed within 2 h of drawing blood.

3.6 Determination of most appropriate hemolysis method

The RBC plasma membrane is a complex structure consisting of ~50% protein, ~40% lipid and ~10% carbohydrate (11). Gentle hemolysis of RBCs is necessary to minimize redistribution of membrane lipids and loss of membrane-associated proteins.

Ghosts, or post-hemolytic residues of RBCs, are widely used in studies of the composition, structure and function of RBC membranes. They are devoid of cellular structure and consist primarily of the plasma membrane.

Ghosts are prepared by the addition of hypertonic or hypotonic buffers to RBCs which either crenate (shrink) or lyse cells (164). Hypotonic hemolysis is most often used because such ghosts have membranes with a composition similar or identical to those of intact RBCs (164). Osmotic pressure difference between the RBC cytosol and the surrounding medium induces mechanical stress because water flows into the cells. At a certain critical level of membrane tension or stretch during swelling, holes form in the membrane and some Hb molecules escape after which the osmotic pressure difference between the cell cytoplasm and the surroundings vanishes and the holes close (164). The properties of the ghosts depend on the conditions at the instant of disruption of the plasma membrane (165). Two types of hypotonic ghosts can be prepared from RBCs: white ghosts and resealed ghosts. White ghosts are essentially devoid of Hb with no significant loss of membrane material. White ghosts are used for quantitative determination of various membrane structures, for studying RBC membrane properties, and investigation of enzyme activities at the membrane.

Resealed ghosts are generally used to study how variations in cell interior and extracellular medium might be involved in transport processes. The contents inside the resealed ghosts are replaced by solutions containing cations, such as Ca^{2+} or Mg^{2+} . Since it has been shown that cations affect membrane binding of some RBC proteins, resealed ghosts are not suitable for our investigation on the localization of antioxidant proteins. For example, when human RBCs are exposed to Ca^{2+} , catalase increases its membrane

binding (166). Thus, we used a modified protocol for white ghost preparation to investigate membrane association of the antioxidant proteins CuZnSOD, catalase, Gpx1 and Prx2.

Several methods for the hemolysis of human RBCs to obtain white ghosts have been described in the literature. Hillier & Hoffman first used stepwise hypotonic hemolysis in solutions of increasingly lower salt concentrations (167). Weed et al. showed that repeated hemolysis at decreasing salt concentrations is not necessary for obtaining Hb-free white ghosts (168). The most widespread hypotonic hemolysis method, developed by Dodge et al., is a single-step hemolysis for preparation of Hb-free white ghosts (169). This protocol represents a compromise between two conflicting requirements: the removal of the cytosolic contents while retaining the native organization of the plasma membrane without significant loss of membrane material.

Dodge et al. studied the effects of phosphate concentration and pH of the hemolysis buffer on Hb content and reorganization of the plasma membrane during white ghost preparation (169). The experiments were carried out at 4 °C because the rate of dissolution of membrane proteins in aqueous media is strongly dependent on the temperature and is greatly reduced at 4 °C. Dodge et al. reported that incubation of RBCs in 10 mM phosphate (pH 7.4) for 30 min removed most Hb from membrane when the membrane was subsequently washed with the same buffer. Hemolysis with 40 mM phosphate (pH 7.4) for 30 min left most Hb membrane-bound. Photomicrographs revealed that their white ghosts were approximately equal in diameter and similar in structure to intact RBCs with minimal reorganization of the membrane. The total amount and composition of lipids in these Hb-free ghosts were essentially comparable to those

found in intact RBCs (169). Nevertheless, in this work no biochemical analysis of membrane composition was performed and the authors relied on microscopy methods to analyze protein and lipid composition of the membrane.

Further published studies on the behaviour of membrane proteins after human RBC hemolysis lead us to conclude that hemolysis in 40 mM phosphate might be a more desirable condition for our investigation. Duchon et al. (148) reported that hemolysis in 15-40 mM phosphate yields intact white ghosts but with varying amounts of Hb at the membrane. They studied the recovery of enzyme activities after hemolysis at various phosphate concentrations and divided enzymes into two classes. The first class were loosely-bound and included the glycolytic enzymes triose-phosphate isomerase, lactate dehydrogenase, and also Gpx1. These proteins were lost from the membrane after exposure of white ghosts to low phosphate concentrations (10 mM) but were retained at 30 to 40 mM phosphate. Proteins in the second class were firmly-bound, including GAPDH and aldolase, which remained membrane-associated after hemolysis in 10 mM phosphate. Bramley et al. (170) observed less loss of membrane-associated proteins at 40 mM phosphate than at 15 mM phosphate.

From the above reports, it seems that human RBC hemolysis conditions critically determine the Hb content of ghosts and the preservation of native membrane structure with minimal protein loss. Thus, we further tested several hemolysis methods to optimize our hemolysis protocol. We lysed fresh human RBCs with 10 mM or 40 mM phosphate with or without N-ethylmaleimide (NEM) over 15 min, pH 7.4 at 4 °C to establish the effect on Hb content and antioxidant enzyme membrane localization. NEM is a thiol-

specific alkylating agent that prevents disulfide formation, including Prx2 dimerization which has been previously shown to occur as an artefact during hemolysis (117).

We investigated how phosphate concentration of the hemolysis buffer affects Hb membrane association by UV-Vis spectroscopy (Fig 3.7). Our spectroscopy data demonstrate that 40 mM phosphate in the lysis buffer results in more membrane-associated Hb than lysis with 10 mM phosphate (Fig 3.7) as observed by Dodge et al. (169). NEM had no effect on membrane-associated Hb but 30 min incubation following hemolysis in 10 mM phosphate decreased the association of Hb with the membrane (Fig 3.7). This indicates that 30 min incubation decreased Hb at the membrane and incubation periods should be minimized to avoid loss of other proteins that might interact with membrane-associated Hb.

Our investigation was further extended to investigate how hemolysis buffer osmolarity affects not only Hb-membrane association but also association of RBC antioxidant proteins with the membrane. We used non-reducing SDS-PAGE to observe the effect of NEM on Prx2 dimerization (Fig 3.8). SDS disrupts protein secondary, tertiary and quaternary structure and a reducing agent such as β -mercaptoethanol reduces any intramolecular bonds and cleaves any bonds formed during disulfide crosslinking. The only protein examined in the current work by non-reducing SDS-PAGE is Prx2 in Fig 3.8 since it has previously been reported to oligomerize in human RBCs (171). In Fig 3.8, lanes 1-6, Prx2 is mainly associated with the membrane as dimer in the absence of NEM, as previously reported by Low et al. (117). Since transfer of proteins from a non-reducing gel to a PVDF membrane is challenging and the amounts transferred differ significantly between experiments, we cannot make any quantitative conclusions

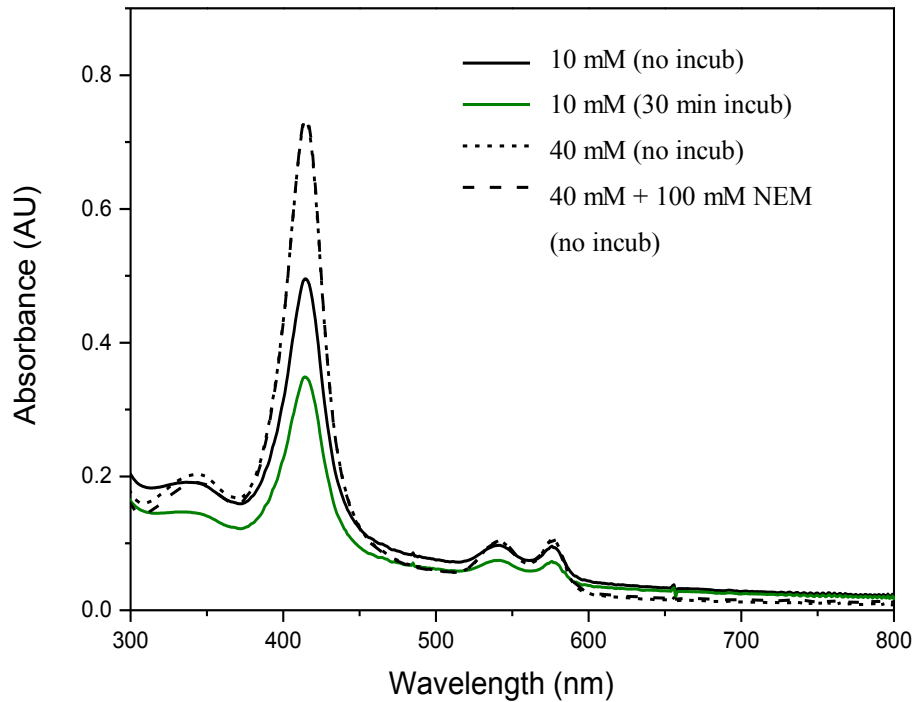


Fig 3.7 Hb content of membrane fractions from human RBCs varies with the phosphate concentration in the hemolysis buffer but not after NEM addition (n=3). Isolated membranes from human RBCs diluted in water to 0.138 $\mu\text{g}/\mu\text{L}$ total protein, pH 7.4. The supernatant was transferred to a cuvette with path length 1 cm; extinction coefficient at 415 nm is $128 \text{ mM}^{-1}\text{cm}^{-1}$ (per heme). Absorbances were read immediately after sample preparations on an Agilent UV-Vis spectrophotometer at 10 mM (black and green solid lines) or 40 mM phosphate (coarse and fine dashed lines). An incubation time of 30 min was in 10 mM phosphate concentration also was examined (solid green line). NEM (100 mM) addition to the 40 mM phosphate hemolysis buffer (coarse dashed line) had no effect on the Hb content. Note that the absorbance for Hb in 40 mM phosphate and 40 mM phosphate/100 mM NEM overlap. Hb is measured mostly as metHb (i.e. Fe^{III}).

regarding the relative amounts of dimer vs monomer in lanes 1-6. However, upon NEM addition to the hemolysis buffer, we conclude that at the membrane Prx2 is mainly monomeric (lanes 5, 6 vs lanes 7, 8) as previously reported (117). The faint band around

25 kD might be an overoxidized (-SO₂H or -SO₃H) form of the Prx2 monomer which would explain its altered migration. Phosphorylated proteins have also been detected as slower migrating species by electrophoresis and Western blotting so the faint band at 25 kD could be also the phosphorylated Prx2 monomer (172). A band at 25 kD has been reported by other groups investigating Prx2 properties (105, 117).

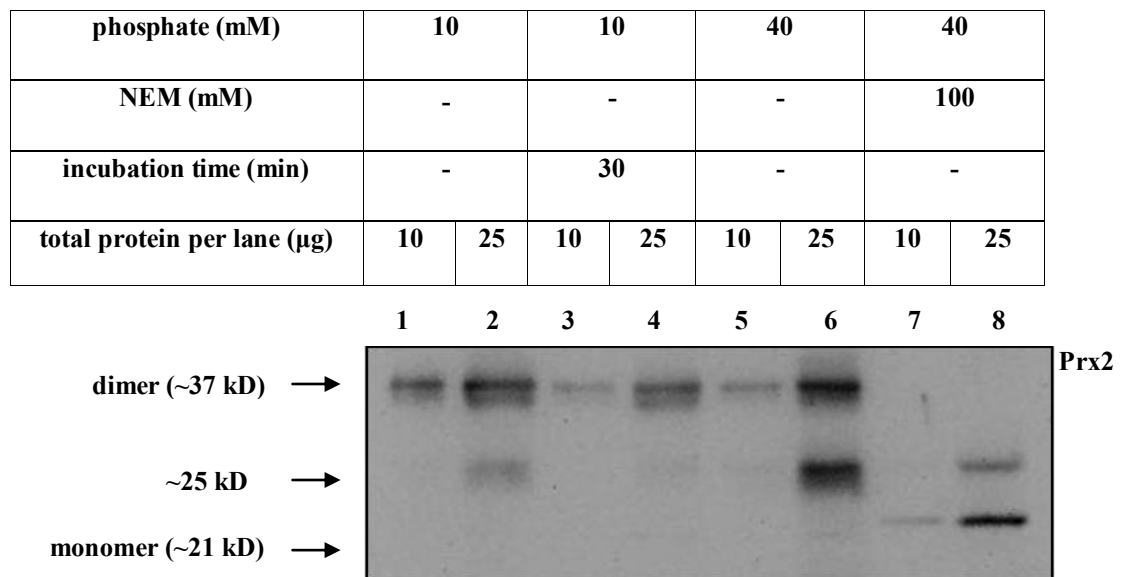


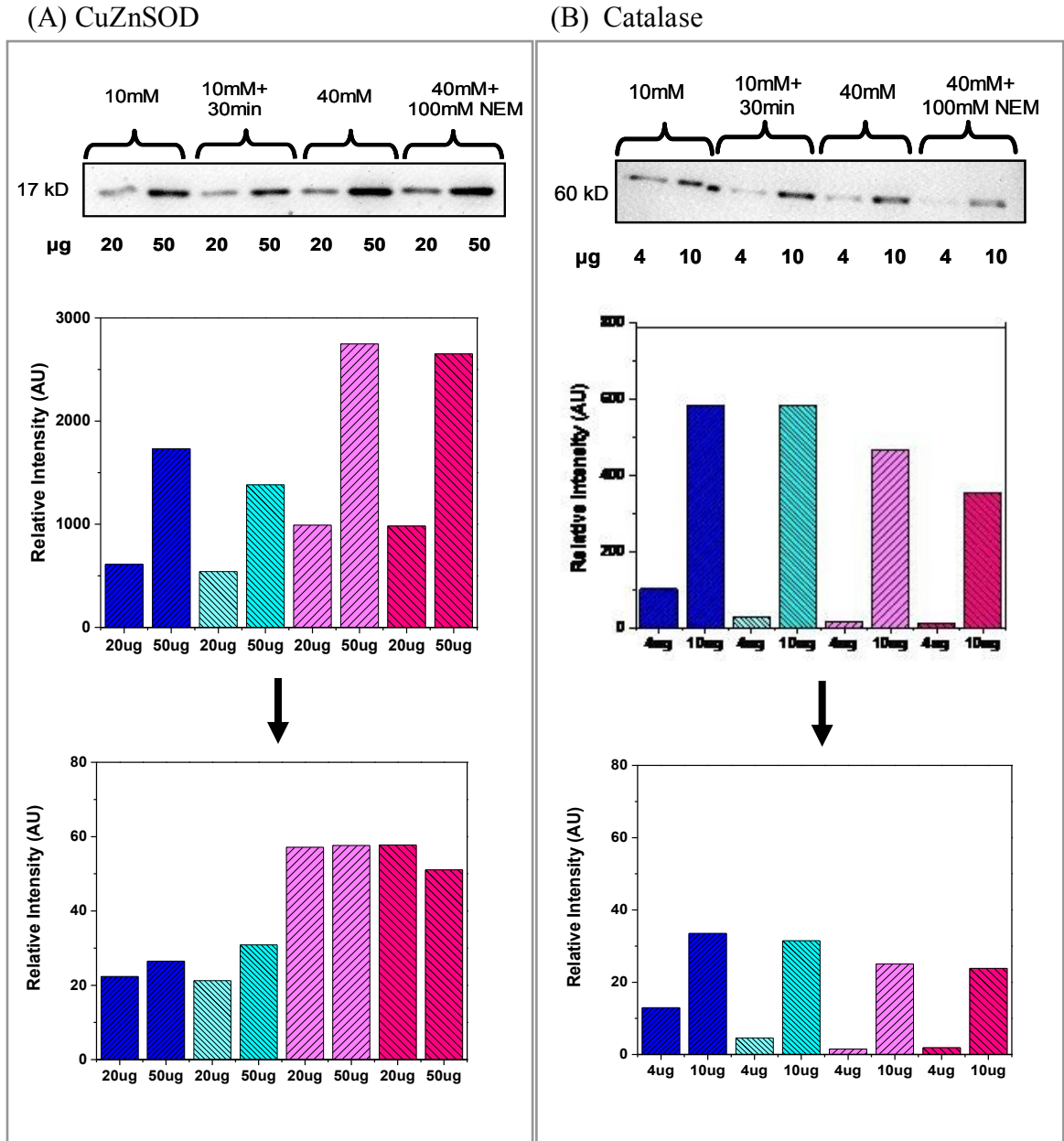
Fig 3.8 Western blot of Prx2 from a non-reducing SDS- PAGE (no β -mercaptoethanol) of membrane fractions of human RBCs lysed in 10 mM phosphate \pm 30 min incubation or 40 mM phosphate \pm 100 mM NEM. Human RBCs were collected and washed as described in Section 2.2.1.1. Membranes were isolated after hemolysis in 10 mM or 40 mM phosphate buffer \pm NEM as described in Section 2.2.1.4. A non-reducing SDS-PAGE (no β -mercaptoethanol) and Western blotting of the isolated membranes was performed as described in Section 2.2.1.7. Either 10 μ g or 25 μ g of total protein per lane was loaded per lane as shown in table above and lanes 7, 8 contain Prx2 that was NEM treated.

The concentration of phosphate in the hypotonic buffer influenced the amounts CuZnSOD, catalase and Prx2 (Fig 3.9) detected in isolated membrane fractions from human RBCs by reducing SDS-PAGE and Western blotting performed as described in

Section 2.2.1.7. The relative intensity of each band is shown before and after correction for loading as described in Section 3.3. CuZnSOD at the membrane increased with 40 mM phosphate in hemolysis buffer whereas less CuZnSOD was retained at the membrane when hemolysis was performed in 10 mM phosphate (Fig 3.9A). The phosphate concentration of hemolysis buffer had minimal effect on catalase localization (Fig 3.9B). However, the 4 μ g bands gave a weak signal, which as revealed by the corrected relative intensities for each set of conditions (Fig 3.9B). Notably, Prx2 is sensitive to both incubation time in the lysis buffer and to NEM addition since its localization at the membrane increased after 30 min incubation in 10 mM phosphate but decreased after NEM treatment in 40 mM phosphate (Fig 3.9C). These results suggest that Prx2 forms a time-dependent disulfide bridge with a membrane protein, which is prevented when NEM is present in the hemolysis buffer.

As discussed above, hemolysis in 40 mM phosphate (pH 7.4) keeps Hb at the membrane (Fig 3.7). Since 155 mM phosphate in hemolysis buffer is isotonic to the RBCs, using 40 mM phosphate (pH 7.4) is more physiologically relevant than using 10 mM phosphate. Therefore, 40 mM phosphate was chosen for human RBC hemolysis throughout this work. Since 30 min incubation at 4 °C seems to affect levels of membrane-associated Hb, such incubation was avoided in the present work. To prevent Prx2 dimerization during sample processing, 100 mM NEM was added to the hemolysis buffer of fractions to be probed for Prx2. Prx2 and catalase have been shown to interact with Hb in human RBC membranes (171) and washing away Hb from the membrane might lead to loss of crucial information pertaining to the localization of these antioxidant enzymes. Also, to minimize Hb removal from the membrane, no washing of ghosts was

performed. The detailed procedure for hemolysis of human RBCs is described in Section 2.2.1.4.



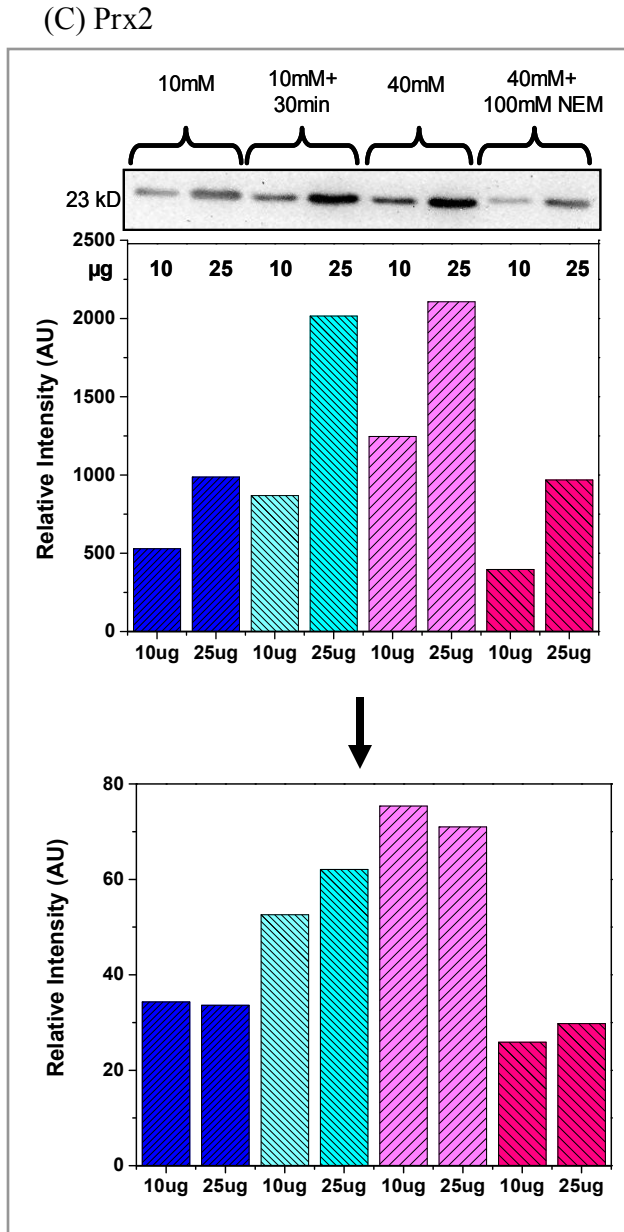


Fig 3.9 Effect of hemolysis method on CuZnSOD, catalase, and Prx2 membrane localization. RBCs were lysed with 10 mM phosphate \pm 30min incubation or 40 mM phosphate \pm 100 mM NEM. Semi-quantitative Western blots (n=1) for (A) CuZnSOD, (B) catalase, (C) Prx2 are shown. Proteins were separated by a reducing SDS-PAGE from membrane fractions isolated from human RBCs. The intensity of each band in the Western blots was recorded by densitometry as described in Section 2.2.1.8 and plotted after background subtraction. Relative intensities of bands are shown before and after correction for loading (Section 2.2.1.9). Gpx1 data are not available due to poor antibody binding. See appendix 3.1 for raw data of WB band intensity and Coomassie lane intensity (loading control).

For rat RBC hemolysis, 10 mM phosphate (pH 7.4, 4 °C) buffer was used followed by immediate centrifugation according to the Dodge method (169). The Dodge method is commonly used for rat RBC hemolysis (173) and was also used in our work before the realization that phosphate concentration in the hemolysis buffer might have an effect on membrane-associated proteins. Interestingly, a subsequent search of the

literature revealed that rat and human Hb have different properties. Rat Hb is found in a quazi-crystalline form inside rat RBCs and is more hydrophobic than human Hb, which is water soluble (174). Rat Hb has been shown to precipitate at pH 6.0 – 8.0 (175). Hydrophobicity might have an effect on Hb interaction with the RBC membrane. Also, species variability of transport ATP-ases among RBCs isolated from various mammals was reported (173) which implies that RBC membrane structure varies among species.

Appendix 3.1

Observed intensities for Fig 3.9. Effect of hemolysis method on (A) CuZnSOD, (B) catalase, and (C) Prx2 membrane localization in RBCs. Densitometry was performed on the Western blots shown in the figure and visualized on AlphaImager densitometer using FluorChem FC2 software and the background was subtracted. Western blots were visualized by chemiluminescence by ECL. The observed density readings of the WB bands and loading controls are shown below.

(A) CuZnSOD

	µg total protein per lane	WB band Intensity	Loading control (Coomassie lane intensity)	Corrected (WB/Coomassie)
10 mM P _i	20	610.73	27.34	22.34
10 mM P _i	50	1731.61	65.4	26.48
10 mM P _i / 30 min incubation	20	541	25.46	21.25
10 mM P _i / 30 min incubation	50	1382.18	44.79	30.86
40 mM P _i	20	990.79	17.34	57.14
40 mM P _i	50	2748.01	47.69	57.62
40 mM P _i + 100 mM NEM	20	982.55	17.01	57.76
40 mM P _i + 100 mM NEM	50	2650.96	51.91	51.07

(B) catalase

	µg total protein per lane	WB band Intensity	Loading control (Coomassie lane intensity)	Corrected (WB/Coomassie)
10 mM P _i	4	101.65	7.85	12.95
10 mM P _i	10	581.54	17.36	33.50
10 mM P _i / 30 min incubation	4	29.6	6.45	4.59
10 mM P _i / 30 min incubation	10	583.28	18.54	31.46
40 mM P _i	4	15.74	10.34	1.52
40 mM P _i	10	463.55	18.5	25.06
40 mM P _i + 100 mM NEM	4	10.63	5.68	1.87
40 mM P _i + 100 mM NEM	10	354.51	14.89	23.81

(C) Prx2

	μg total protein per lane	WB band Intensity	Loading control (Coomassie lane intensity)	Corrected (WB/Coomassie)
10 mM P_i	10	529.39	15.43	34.31
10 mM P_i	25	987.26	29.36	33.63
10 mM P_i / 30 min incubation	10	868.69	16.52	52.58
10 mM P_i / 30 min incubation	25	2015.75	32.48	62.06
40 mM P_i	10	1246.56	16.54	75.37
40 mM P_i	25	2106.83	29.67	71.01
40 mM P_i + 100 mM NEM	10	396.51	15.31	25.90
40 mM P_i + 100 mM NEM	25	968.65	32.53	29.78

Appendix 3.2

Observed intensities for Fig 3.2. Standard plots of (A) CuZnSOD, (B) catalase, (C) Prx2, and (D) Gpx1 in isolated membranes from human RBCs. Densitometry was performed on the Western blots shown in Fig 3.1 and visualized on AlphaImager densitometer using FluorChem FC2 software and the background was subtracted. Western blots were visualized by chemiluminescence by ECL. The observed density readings of the WB bands and loading controls are shown below.

(A) CuZnSOD

µg total protein per lane	WB band Intensity	Loading control (Coomassie lane intensity)	Corrected (WB/Coomassie)
100	6936.2	99.3	69.85
87.5	9196.33	95.25	96.55
75	6614.24	77.89	84.92
62.5	5850.26	60.79	96.24
50	4559.08	43.65	104.45
35	3365.42	26.69	126.09
25	2039.77	10.17	200.57
12.5	677.45	2.91	232.80
6.25	376.98	0.06	6283.00
3.13	1.61	0.00	1610000.00

(B) catalase

µg total protein per lane	WB band Intensity	Loading control (Coomassie lane intensity)	Corrected (WB/Coomassie)
100	2623.65		
75	2544.27	102.52	24.82
50	2141.74	73.03	29.33
37.5	1825.34	52.99	34.45
25	1466.79	42.99	34.12
12.5	1062.40	30.51	34.82
6.3	642.01	20.09	31.96
3.2	293.12	9.50	30.85
1.5	41.77	4.15	10.07
0.78	7.78	2.37	3.28

(C) Prx2

μg total protein per lane	WB band Intensity	Loading control (Coomassie lane intensity)	WB/Coomassie
100	2575.23	102.59	25.10
75	2437.94	85.59	28.48
50	1682.8	63.77	26.39
37.5	1460.65	54.24	26.93
25	1172.78	45.7	25.66
12.5	803.25	34.21	23.48
6.3	363.25	20.89	17.39
3.2	125.64	1.63	77.08
1.5	51.05	10.98	4.65
0.78	18.33	5.10	3.59

(D) Gpx1

μg total protein per lane	WB band Intensity	Loading control (Coomassie lane intensity)	Corrected (WB/Coomassie)
100	1801.63	104.59	17.23
75	1600.44	87.59	18.27
50	1463.24	72.77	20.11
37.5	1252.76	63.24	19.81
25	1102.79	53.71	20.53
12.5	704.91	36.97	19.07
6.3	359.58	20.88	17.22
3.2	88.39	13.86	6.38
1.5	105.43	6.76	15.60
0.78	43.24	3.18	13.60

Chapter 4: Effects of prolonged air exposure on membrane localization of CuZnSOD, catalase, Prx2 and Gpx1 in human RBCs

4.1 Introduction

Our interest in the effects of prolonged air exposure on RBC antioxidant enzymes was triggered by our observation by confocal microscopy that CuZnSOD concentrated at the RBC biconcave surface following 60 min air exposure (163). This surface is presumably the site of highly efficient gas transport in RBCs because the shorter distance between the two biconcave surfaces in the RBC might allow for more interactions between cytoplasmic proteins and Band-3. Also, there have been several reports of the effects of O₂ on RBC enzymes and properties. For example, prolonged exposure of humans to hyperbaric oxygen has been shown to decrease CuZnSOD and catalase activities in their RBCs, while Gpx1 activity was unaffected (176). Hyperbaric oxygen resulted in increased activity of lung CuZnSOD but decreased activity of lung catalase and Gpx1 (177). It was also shown that hyper-oxygenation leads to increased ROS formation in blood that causes cellular damage with lipid, protein and DNA oxidation (178). Notably, blood banks store blood for days to weeks in air-permeable bags, which causes RBC oxidation and irreversible changes in RBC proteins (77), collectively termed storage lesions.

Oxygen not only is transported by RBCs to meet the metabolic requirements of tissues, but it also determines the mechanical (179) and membrane properties of RBCs

(180). Oxygenation regulates binding of Hb and glycolytic enzymes to the RBC membrane and it was suggested that Hb may act as a transducer regulating cellular function in an O₂-dependent manner through its interaction with CDB3 (181). MetHb and deoxyHb can bind to CDB3, but not oxyHb, and this differential binding plays a role in the RBCs response to O₂ levels (179, 182). Stored RBCs accumulate ROS and surface-associated hemichromes, a partially denatured form of oxidized Hb (78). Interestingly, hemichromes have higher affinity for CDB3 than deoxyHb (37).

To investigate how hyper-oxygenation, a form of oxidative stress (178), affects localization of antioxidant enzymes at CDB3, prolonged air exposure was used as a method of hyper-oxygenation. In the lungs, RBCs are exposed to O₂ for only a few seconds so exposing them to ambient air for 30 or 60 min should mimic hyperbaric conditions with possible increased hemichrome formation.

4.2 Results

Western blots of CuZnSOD, catalase, Gpx1 and Prx2 in membranes isolated from human RBCs following air exposure for 30 min or 60 min are shown in Fig 4.1. The experimental procedure is described in Sections 2.2.1.2, 2.2.1.4 and 2.2.1.7. Densitometry was used to quantitate the intensity of the antibody-labelled bands from each Western blot as well as the intensity of the entire lane of the Coomassie-stained PVDF membranes (loading control) as shown in Fig 3.4. Once these values were determined, the intensity of the antibody band was divided by the intensity of the loading control yielding a corrected intensity in arbitrary units. These values were then

normalized by assigning the 0 min sample (control) value of 1, such that the fold-change from the control is reported.

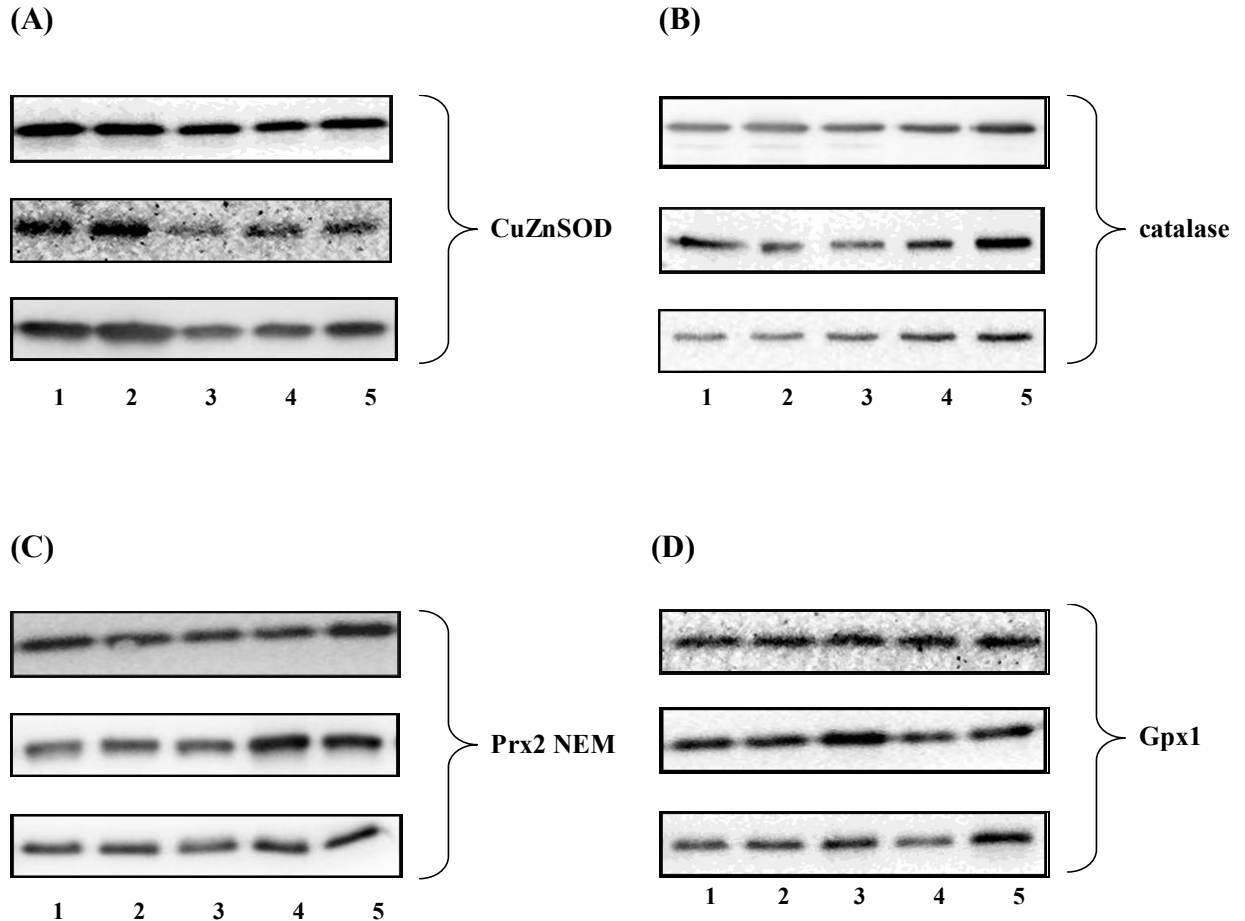


Fig 4.1 Western blots of CuZnSOD, catalase, Prx2 and Gpx1 in membrane fractions isolated from human RBC following air exposure for 0 min (control), 30 min and 60 min (n=3 individual donors). (A) CuZnSOD (B) Catalase (C) Prx2 (D) Gpx1. Washed RBCs (3×10^8 cells/mL) were exposed to air at 37 °C for 0 min, 30 min and 60 min by gently stirring (Sections 2.2.1.1 and 2.2.1.2) and hypotonic hemolysis in 40 mM sodium phosphate buffer, pH 7.4 (Section 2.2.1.4). 15 min incubations with 100 mM NEM for Prx2 samples were performed prior to hemolysis. Proteins were separated by a reducing SDS-PAGE [35 μ g total protein for CuZnSOD, 30 μ g total protein for catalase, Gpx1 and Prx2 (Table 3.1)] and Western blotted (Section 2.2.1.7). Western blots were visualized by chemiluminescence as described in Section 2.2.1.8 and analyzed data are shown in Fig 4.2. Lane 1: 0 min closed; Lane 2: 30 min closed; Lane 3: 60 min closed, Lane 4: 30 min open; Lane 5: 60 min open.

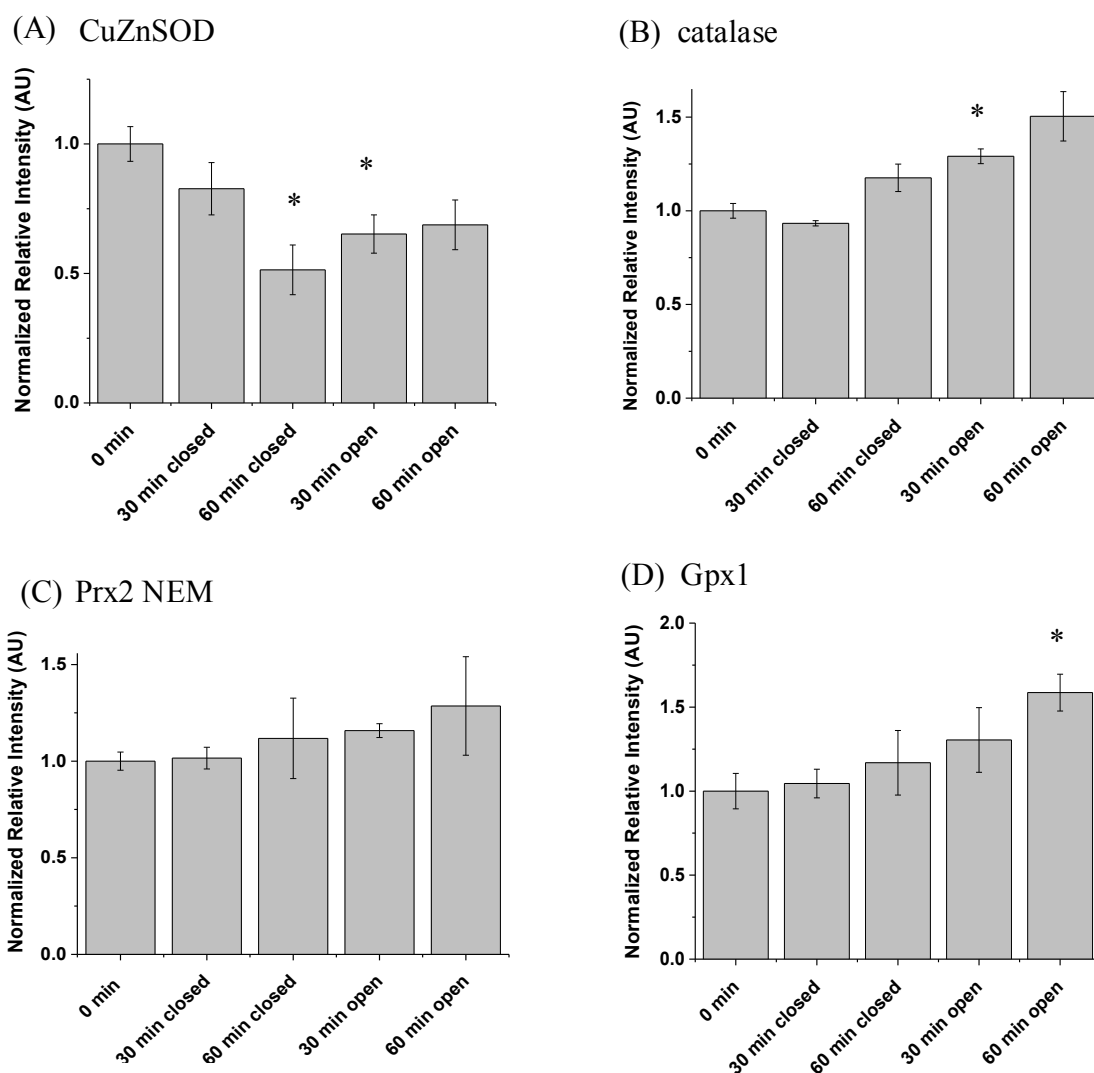


Fig 4.2 Relative amounts of CuZnSOD, catalase, Prx2 and Gpx1 in membrane fractions isolated from human RBC following air exposure for 0 min, 30 min and 60 min (n=3 individual donors). (A) CuZnSOD (B) Catalase (C) Prx2 (D) Gpx1. Densitometry was used to quantitate the intensity of each band in Fig 4.1. Then, Coomassie staining of PVDF membranes was performed as a loading control (Section 2.2.1.7) and the corrected chemiluminescence intensities were normalized to 0 min control. The normalized relative intensities are shown for each protein \pm S.E.M. Raw data are presented in Appendix 4. The statistical significance (*) of differences between the control (0 min) and treated RBCs was determined by Student's t-test (unpaired, 2-tailed), and p-values ≤ 0.05 were considered significant. The 2-tailed Student t-test is used when examining significant differences between control and treated RBCs without prior assumptions which group would be higher (or lower). An unpaired Student t-test is used when there is no need to control for a third confounding variable.

4.2.1. CuZnSOD localization after air exposure

Fig 4.1A reveals that a fraction of CuZnSOD is membrane-associated in all samples. Fig 4.2A indicated that there is a progressive loss of membrane CuZnSOD over 60 min incubation time (closed tubes). RBCs become more anaerobic in closed tubes and therefore levels of deoxyHb increase. DeoxyHb has high affinity for the RBC membrane (34) and may displace CuZnSOD from the membrane. Also, there was loss of CuZnSOD from the membrane on longer air exposure (open tubes). In highly aerobic RBCs, the oxyHb content is high and thus metHb formation increases. Hence, there is a possibility that metHb competes with CuZnSOD for the membrane in highly aerated cells.

4.2.2. Catalase localization after air exposure

A fraction of catalase is membrane-associated in all samples (Fig 4.1B). Since the levels do not decrease after 30 or 60 min incubation (closed tubes), it seems that membrane-associated catalase does not depend on the deoxyHb concentration in RBCs which is expected to be elevated in the closed tubes. Hence, it is possible that deoxyHb and catalase are not competing for the same binding site on CDB3. Sialic acid-modified catalase has been reported (183) and catalase has been shown to bind human RBC membranes reversibly via electrostatic interactions (184). Sialylation might be required to anchor catalase to the RBC membrane since sialic acid addition will modify its surface charge and thereby increase its electrostatic interaction with the membrane.

It has been shown that RBC catalase activity decreases after RBCs are hyperoxygenated (176) so we expected to see changes in catalase localization after prolonged air exposure. Catalase significantly increases at the membrane after 30 min air exposure

and this increase continues after 60 min air exposure (Fig 4.2B, open tubes). Prolonged air exposure generates more $O_2^{\bullet-}$ at the membrane, which is rapidly dismutated to H_2O_2 by CuZnSOD. Thus, increased H_2O_2 generation at the membrane may trigger catalase to migrate to the RBC membrane to protect it. Alternatively, catalase recruitment at the membrane after prolonged air exposure may be triggered by phosphorylation of Tyr8, Tyr21 and Tyr46 of CDB3 (26, 185). Phosphotyrosine phosphatase PTP1B has been proposed as the main membrane-associated PTPase that dephosphorylates Band-3 (186). Increased oxidative stress in aerated RBCs (80) leads to increased CDB3 phosphorylation due to PTP1B inactivation on oxidation of its active-site Cys215 (187). Such increased CDB3 phosphorylation in aerated RBCs should cause a loss of membrane-associated catalase. However, catalase levels at the RBC membrane increased after air exposure (Fig 4.2B) and we conclude that CDB3 phosphorylation does not regulate catalase membrane binding. Hemichrome formation might also act as a trigger for catalase to migrate to the RBC membrane. It was reported that catalase and Prx2 migrate together to the membrane of stored RBCs (171) and we speculate that Prx2 migrates to counteract the association of hemichromes with the membrane. Hemichrome formation is known to trigger Band-3 clustering, which marks altered RBCs for removal (17).

4.2.3. Prx2 localization after air exposure

Prx2 was maintained in its monomeric form by the addition of NEM following air exposure. A fraction of Prx2 is membrane-associated in all samples (Fig 4.1C), which is also confirmed by the confocal image in Fig 3.6. There is no obvious increase in Prx2 at the membrane after incubation (closed tubes) and air exposure (open tubes). Prx2 is a

highly abundant RBC protein (14×10^6 copies per RBC) (107) and is proposed to act as a chaperone for Hb (117), but the nature of its native oligomeric form inside the RBC is still a matter of considerable debate. It has been suggested that catalase and decameric Prx2 migrate to the RBC membrane in stored blood (171). The same group also reports dimers, trimers, pentamers, heptamers and decamers for cytosolic Prx2. Our experiment (Fig 4.1C) does not distinguish among various Prx2 oligomeric states at the RBC membrane. Moreover, we cannot distinguish how decameric Prx2 might bind to the membrane. If Prx2 binds via one subunit only, the other subunits might be lost in the processing of RBCs during isolation of membranes. Also, masking of the antigen during Prx2 oligomerization might limit antibody binding to Prx2.

4.2.4. Gpx1 localization after air exposure

Gpx1, an abundant RBC enzyme present at 4×10^5 copies, is an efficient lipid peroxidase (188). No change in membrane-associated Gpx1 was observed with incubation time in closed tubes (Fig 4.2D) and some Gpx1 is membrane-associated in all samples (Fig 4.1D) to protect the RBC membrane. Gpx1 increases at the membrane after 60 min air exposure (open tubes). What triggers Gpx1 recruitment to the membrane? Hyper-oxygenation has been associated with increased levels of lipid peroxidation (189), and oxidized lipids increase in volume (190). Thus, Gpx1 might be attracted to the changes in volume at the membrane. Gpx1 likely migrates specifically to areas rich in unsaturated lipids since these are more prone to oxidation than saturated lipids.

4.3 Discussion

Exposing RBCs to ambient air for 30 or 60 min alters the membrane localization of antioxidant enzymes (Fig 4.2). Our data demonstrate that CuZnSOD decreases at the RBC membrane after incubation for 30 and 60 min in closed tubes (Fig 4.2A). Also, we report that there is an overall decrease of CuZnSOD at the membrane after prolonged air exposure (Fig 4.2A, open tubes). Photomicrographs taken in our laboratory showed that 60 min air exposure caused relocation of CuZnSOD to the biconcave surface (Fig 4.3G) as compared to control cells (Fig 4.3A) (163). A rapid change in CuZnSOD localization is not unexpected since RBCs need to respond promptly to stress, such as hyper-oxygenation.

There are four Cys residues in each subunit of human CuZnSOD (Cys6, Cys57, Cys111, Cys146). Cys57 and Cys146 form an internal disulfide bond. Cys6 is buried and Cys111 is solvent exposed, near the dimer interface next to His110 and Asp109 (191). Because of its solvent exposure, it has been suggested that Cys modification of native CuZnSOD occurs exclusively at Cys111, which could be involved in a disulfide bond formation (191, 192). However, since all of the Cys residues are near the subunit interface and close to each other, any of the six residues in the homodimer could be involved in interactions with the RBC membrane. Decreased CuZnSOD activity in human RBCs following hyper-oxygenation was previously reported (176).

Catalase significantly increases at the membrane after 30 min air exposure and the increase continues after 60 min air exposure (Fig 4.2B, open tubes). This finding is consistent with confocal results recorded previously in our laboratory since photomicrographs revealed that catalase increased at the RBC membrane after 60 min air

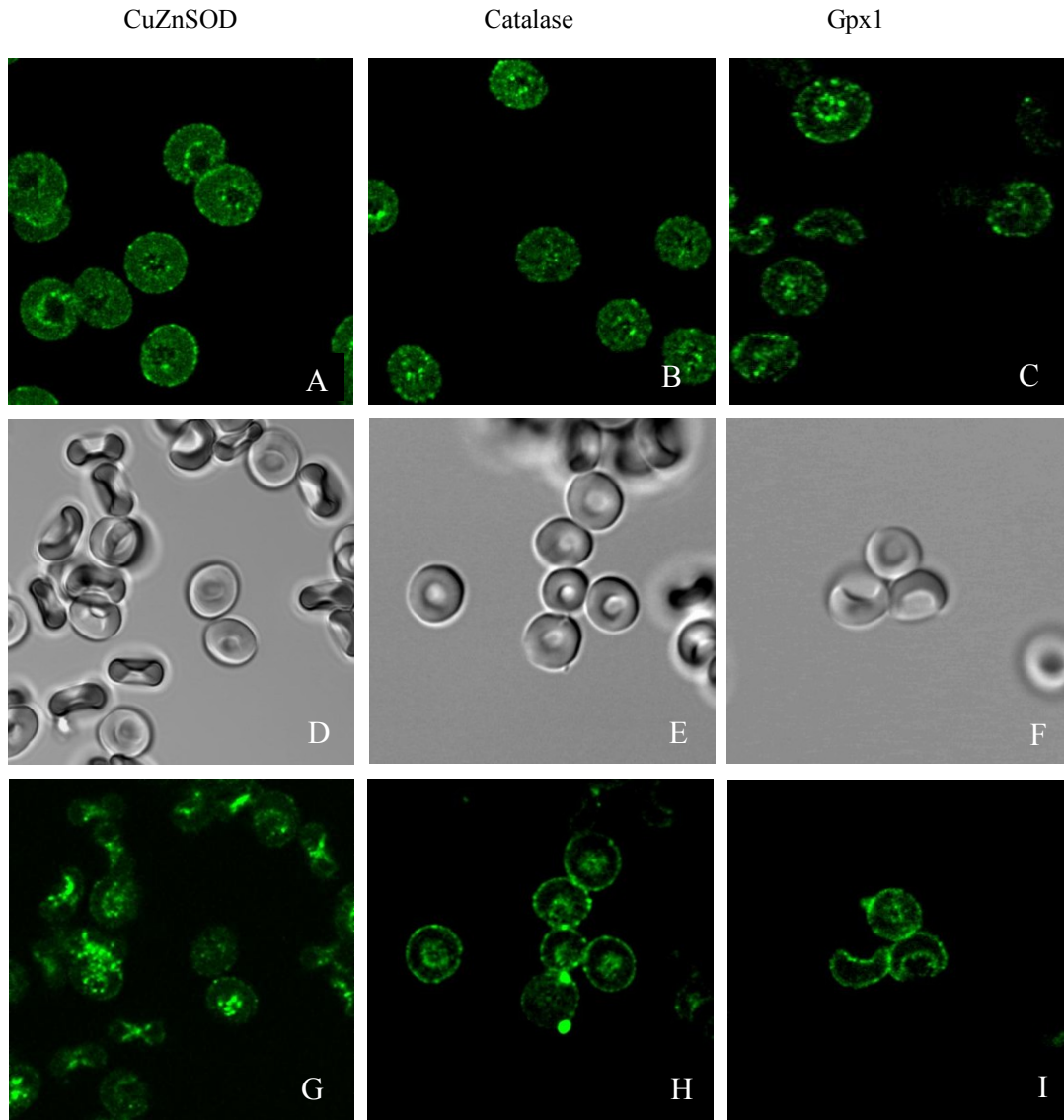


Fig 4.3 Confocal immunofluorescence and corresponding bright field images of CuZnSOD, catalase, and Gpx1 in fixed intact human RBCs – control (A, B, C) vs aerated (D, E, F, G, H, I), data previously obtained in our laboratory (163). Control RBCs were exposed to air for <5 min, and fixed within 2 h of drawing blood. Aerated RBCs were processed within 3 h of drawing blood and RBCs at 10% Ht in G-PBS were exposed to room air for 1 h at ambient temperature. The bright field images for the aerated RBCs are shown in panels D, E, F and the corresponding immunofluorescence images in panels G, H, I. RBCs were then stained as outlined in Section 2.2.2. CuZnSOD stained by rabbit polyclonal anti-human CuZnSOD and Cy2 conjugated anti-rabbit IgG. Catalase stained by sheep polyclonal anti-human catalase and Alexa conjugated anti-sheep IgG. Gpx1 stained by sheep anti-human GPx-1 and Alexa 488 conjugated anti-sheep IgG. Filter settings for both Cy2 and Alexa 488 were as follows: excitation 488 nm; emission 500-530 nm.

exposure (Fig 4.3H) as compared to control in Fig 4.3B (163). It has been reported that catalase competes with Hb for binding to the RBC membrane (184). Since oxyHb has a lower affinity for the membrane than deoxyHb, this would allow more catalase to bind to the membrane of RBCs exposed to air.

It was recently suggested that there is an association between catalase and Prx2 in human RBCs (171). Such an association might be important for RBC survival because these two proteins could act in synergy, with catalase acting as H₂O₂ scavenger while Prx2 acts as a chaperone for Hb. On the other hand, Prx2 has the ability to metabolize a wider range of peroxides than catalase, which only metabolizes H₂O₂ and very small peroxides, such as Me-OOH and Et-OOH (193). Hyper-oxygenation depresses the activity of Na⁺-K⁺ ATPase (194) and Prx2 and catalase might be required at the membrane to protect the function of this membrane-associated ATPase.

Lipid peroxidation products have been reported to accumulate in various tissues following hyper-oxygenation (195). Our Western blotting results suggest that Gpx1 increases at the human RBC membrane after 60 min air exposure. Previous photomicrographs recorded in our laboratory also suggest increased Gpx1 membrane localization after 60 min air exposure as compared to control (Fig 4.3C vs Fig 4.3I) (163). Overall, the combined data from our lab suggest rapid response of Gpx1 to prolonged air exposure. Given the critical importance of the RBC membrane, it is not surprising that Gpx1 migrates to the membrane to protect lipids and thus preserves the RBC intact.

Table A4.2

(B) catalase	Observed density					Observed density loading control					Corrected					
	0	30	60	30 open	60 open	0	30	60	30 open	60 open	0	30	60	30 open	60 open	
Exp 1	1357.9	1310.7	1365.8	1456.9	1581.9	37.0	41.6	31.0	34.1	34.1	36.7	31.5	44.0	42.7	46.5	
Exp 2	1478.7	1257.9	1372.3	1442.8	1980.4	43.4	40.3	33.4	30.8	32.7	34.1	31.3	41.1	46.9	60.5	
Exp 3	1258.7	1214.8	1239.9	1376.8	1485.9	39.4	37.1	35.0	32.0	31.1	32.0	32.8	35.5	43.0	47.8	
											Average	34.23	31.83	40.20	44.21	51.54
											Normalized	1	0.93	1.17	1.29	1.51
											SEM	0.040	0.014	0.073	0.039	0.132

Table A4.3

(C) Prx2 NEM	Observed density					Observed density loading control					Corrected					
	0	30	60	30 open	60 open	0	30	60	30 open	60 open	0	30	60	30 open	60 open	
Exp 1	1361.5	1147.7	1124.9	1114.6	1562.6	45.7	37.7	28.8	37.7	32.5	29.8	30.4	39.0	29.6	48.1	
Exp 2	1035.6	1027.8	1012.8	1399.3	1352.0	39.8	39.7	51.6	43.0	55.6	26.0	25.9	19.6	32.5	24.3	
Exp 3	1098.9	1120.5	1091.8	1194.5	1223.5	42.5	43.4	33.7	36.9	37.6	25.9	25.8	32.4	32.4	32.5	
											Average	27.23	27.38	30.36	31.49	34.96
											Normalized	1.00	1.01	1.11	1.16	1.28
											SEM	0.047	0.056	0.208	0.036	0.255

Table A4.4

(D) Gpx1	Observed density					Observed density loading control					Corrected					
	0	30	60	30 open	60 open	0	30	60	30 open	60 open	0	30	60	30 open	60 open	
Exp 1	1110.6	1145.4	1216.8	1134.8	1233.7	36.1	45.9	39.3	30.6	26.1	30.8	24.9	31.0	37.1	47.2	
Exp 2	1211.5	1146.7	1658.7	1129.6	1241.9	43.8	44.3	41.5	35.1	29.5	27.7	25.9	40.0	32.2	42.1	
Exp 3	1045.7	1061.6	1170.4	939.3	1299.7	49.2	33.0	52.5	27.0	35.0	21.3	32.2	22.3	34.8	37.1	
											Average	26.58	27.67	31.08	34.68	42.12
											Normalized	1	1.04	1.17	1.30	1.58
											SEM	0.105	0.085	0.192	0.054	0.110

Statistical significance (*) of differences between 0 min control and air-exposed RBCs shown in Fig 5.2 as determined by a Student t-test (unpaired, 2-tailed) with SPSS software, p-values ≤ 0.05 considered significant. Unpaired Student t-test is used when there is no need to control for a third confounding variable. The Student t-test was 2-tailed was used since we are examining differences between control and treated animals without initial assumptions that one of the groups would be higher (or lower) than the other group.

(A) CuZnSOD

30 min closed: $p = 0.4914$
60 min closed: $p = 0.0254^*$
30 min open: $p = 0.0297^*$
60 min open: $p = 0.0646$

(B) Catalase

30 min closed: $p = 0.2012$
60 min closed: $p = 0.2488$
30 min open: $p = 0.0217^*$
60 min open: $p = 0.0695$

(C) Prx2

30 min closed: $p = 0.7234$
60 min closed: $p = 0.7665$
30 min open: $p = 0.1505$
60 min open: $p = 0.4950$

(D) Gpx1

30 min closed: $p = 0.7630$
60 min closed: $p = 0.8003$
30 min open: $p = 0.0861$
60 min open: $p = 0.0467^*$

Chapter 5 Membrane localization of CuZnSOD, catalase, Prx2 and Gpx1 in human RBCs on exposure to H₂O₂ and CHP

5.1 Introduction

Our interest in the effects of peroxides on localization of antioxidant enzymes in RBCs was triggered by reports that CuZnSOD is inactivated by H₂O₂ (196). Catalase almost exclusively metabolizes H₂O₂ while Prx2 and Gpx1 can metabolize any ROOH where the R is hydrogen or an organic group. Prx2 metabolizes H₂O₂ and ROOH (123, 197) while Gpx1 has been reported to metabolize H₂O₂, ROOH, including lipid peroxides (123, 198, 199) (Table 1.2). The O-O bond easily breaks and forms RO[•] and OH[•] radicals which are highly reactive and damaging to membranes. Based on their substrate selectivity, we hypothesized that catalase, Prx2 and Gpx1 might change localization in RBCs in response to challenges with a bolus of H₂O₂ or ROOH. Thus, to investigate how enzyme localization correlates with function, we treated RBCs with a bolus of 50 μM H₂O₂ or 50 μM cumene hydroperoxide (CHP) and isolated the membranes after 30 min.

Various hydroperoxides have been used to initiate peroxidative mechanisms *in vitro*. CHP, the peroxide used in this study, shows a similar effect to other organic hydroperoxides and produces peroxy radicals, HCOO[•] (Fig 1.3). Hb is a powerful catalyst for the initiation of lipid peroxidation since its iron interacts with peroxides to produce reactive radical species via the Harber-Weiss cycle (Fig 1.3) (200). Since CHP is known to cause lipid peroxidation (201), we expect to see altered localization for the antioxidant enzymes involved in protecting the RBC membrane.

5.2 Results

The Western blots of CuZnSOD, catalase, Prx2 and Gpx1 after peroxide treatments are shown in Fig 5.1. The densitometric analysis of the bands from Fig 5.1 is shown in Fig 5.2.

5.2.1. CuZnSOD localization after peroxide treatment

Our data suggest that CuZnSOD association with the human RBC membrane is unaffected by a bolus of 50 μM H_2O_2 (Fig 5.2A). H_2O_2 is not a substrate for CuZnSOD which is inactivated by H_2O_2 (196). In human blood, neutrophils and macrophages release 149 μM H_2O_2 per hour (200) and RBCs are equipped with defences against H_2O_2 levels in the 50 μM used here (Section 2.2.1.3). Peroxides are the by-products of the oxidative destruction of foreign matter in these cells. CHP also has no effect on CuZnSOD association with the human RBC membrane (Fig 5.2A) although it was previously reported that CuZnSOD activity decreased after incubation with CHP *in vitro* (202).

5.2.2. Catalase localization after peroxide treatment

It was reported that catalase binds to the RBC membrane via CDB3 (203) and its activity decreased upon binding (184). Another group reported that the activity of membrane-bound catalase was increased in comparison to cytosolic catalase in human RBCs (204). Furthermore, reports of increased catalase activity after incubation of RBCs with CHP (202) suggested that catalase might alter its membrane localization after treatment with H_2O_2 or CHP. Surprisingly, the amount of catalase detected at the membrane did not change after H_2O_2 or CHP exposure (Fig 5.2B). This suggests that

there is a steady-state population of catalase at the RBC membrane that metabolizes H_2O_2 . CHP is not a substrate for catalase, since catalase cannot accommodate ROOH with bulky R groups (193).

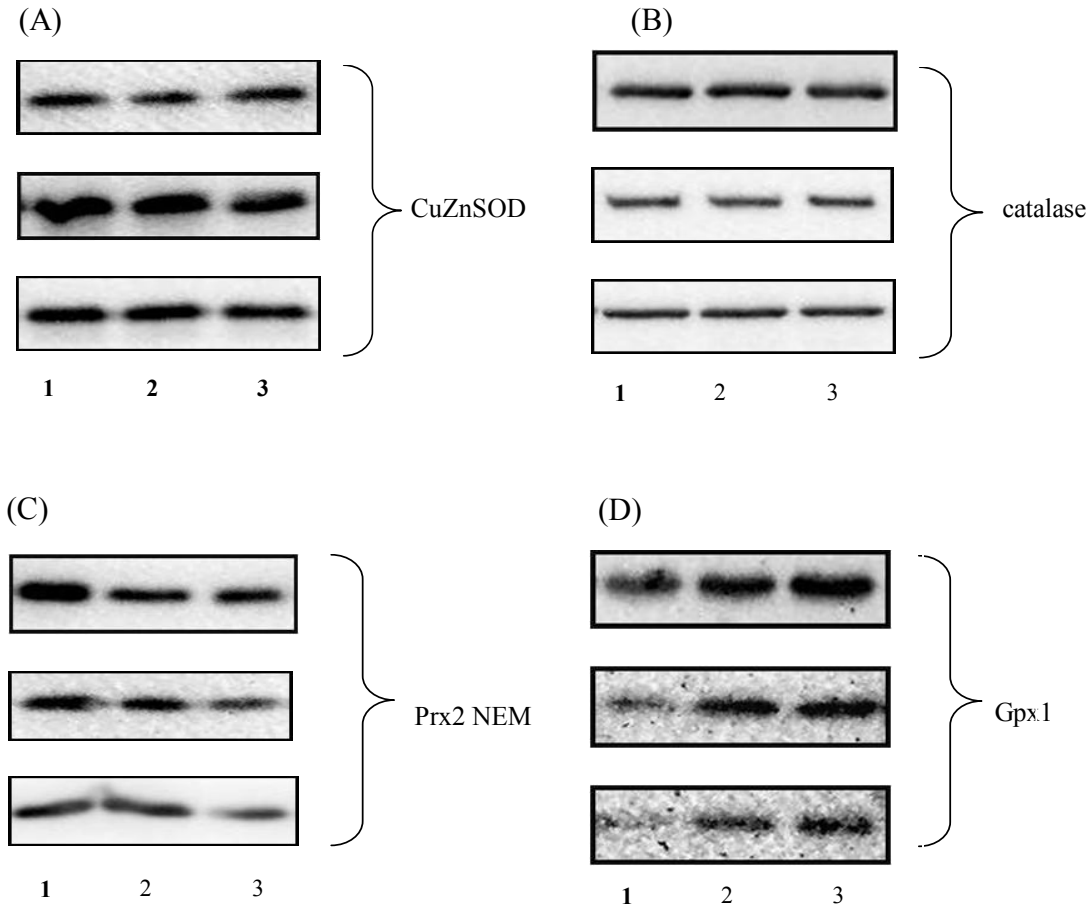


Fig 5.1 Western blots of CuZnSOD, catalase, Prx2 and Gpx1 in membranes isolated from human RBCs treated with H_2O_2 or cumene hydroperoxide (CHP), n=3 individual donors. (A) CuZnSOD (B) Catalase (C) Prx2 (D) Gpx1. Washed intact human RBCs ($500 \mu\text{L}$, 3×10^8 cells/mL) were treated with a bolus of $50 \mu\text{M}$ final concentration of H_2O_2 ($5 \mu\text{L}$ of $5 \text{ mM } H_2O_2$), $50 \mu\text{M}$ final concentration of CHP ($5 \mu\text{L}$ of 5 mM CHP) or G-PBS ($5 \mu\text{L}$, control) as described in Sections 2.2.1.1 and 2.2.1.3. Hypotonic hemolysis was performed with 40 mM sodium phosphate buffer, pH 7.4 (Section 2.2.1.4). All tubes were filled to top, closed, and gently stirred during incubation at $37 \text{ }^\circ\text{C}$ for 30 min. Samples containing $35 \mu\text{g}$ total protein for CuZnSOD, $30 \mu\text{g}$ total protein for catalase, Gpx1 and Prx2 (Table 3.1) were separated on a reducing SDS-PAGE. Western blots were visualized by chemiluminescence (Section 2.2.1.8). Lane 1: control; Lane 2: $50 \mu\text{M } H_2O_2$ (30 min); Lane 3: $50 \mu\text{M CHP}$ (30 min)

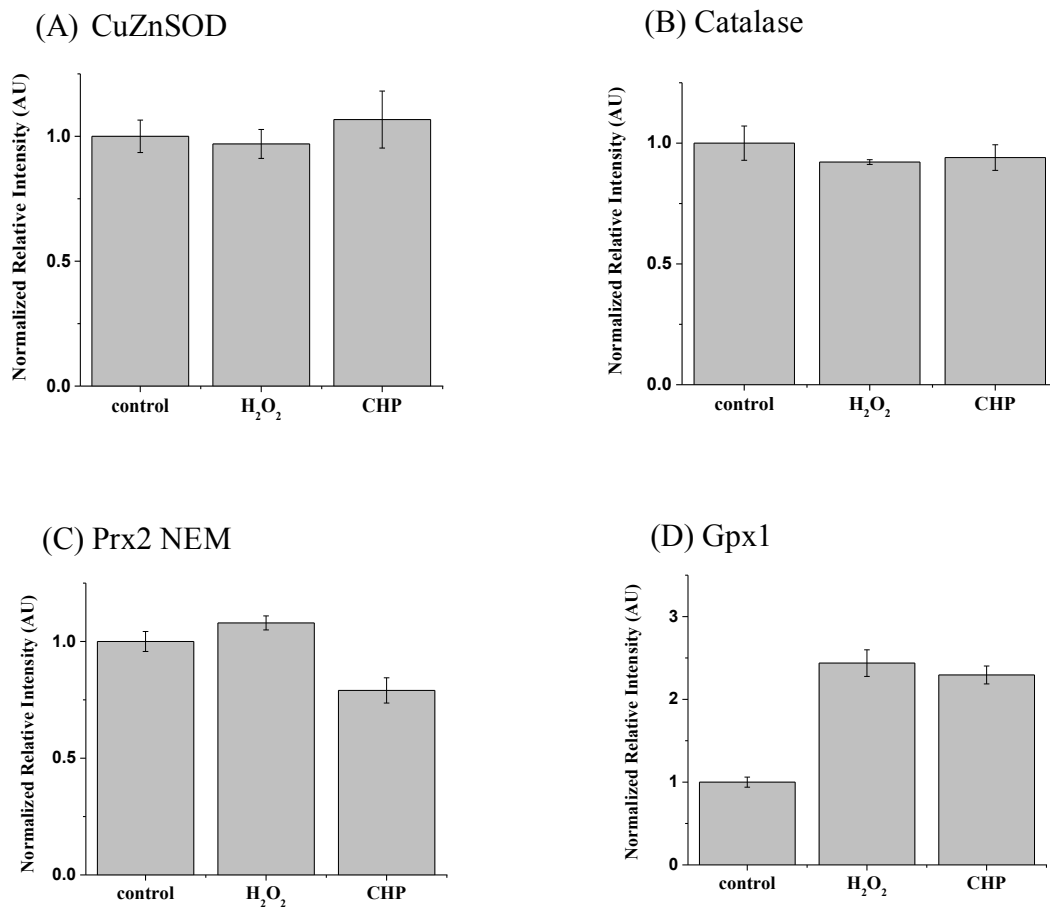


Fig 5.2 Relative amounts of CuZnSOD, catalase, Gpx1 and Prx2 in membranes isolated from human RBCs treated with H₂O₂ or cumene hydroperoxide (CHP), n=3 individual donors. (A) CuZnSOD (B) Catalase (C) Prx2 (D) Gpx1. The Western blots were visualized by chemiluminescence and densitometry was performed. Coomassie staining of PVDF membranes after visualization was used as loading control (Section 2.2.1.9) and chemiluminescence intensities were normalized by total protein loaded per lane. The normalized relative intensities (normalized to control) are shown for each protein \pm S.E.M.

5.2.3. Prx2 localization after peroxide treatment

Fig 5.1C demonstrates that a fraction of Prx2 is membrane-associated in all samples, which is also confirmed by our confocal images in Fig 3.6 and Western blots in Fig 4.2D. Adding a bolus of H₂O₂ to RBCs had no effect on the membrane localization of Prx2 (Fig

5.2C). Our experiment (Fig 5.2C) does not distinguish among various Prx2 oligomeric states at the RBC membrane, and if there is a change in oligomerization when Prx2 associates with the membrane, we cannot account for it. Prx2 decreased at the membrane after CHP treatment (Fig 5.2C). Since CHP is not a substrate for catalase, CHP may induce changes at the membrane that reduce the affinity of Prx2 for the membrane.

5.2.4. Gpx1 localization after peroxide treatment

In Fig 5.1D, a fraction of Gpx1 was membrane-associated in all samples. Furthermore, Gpx1 increased ~2.5 fold at the membrane after H₂O₂ or CHP treatment (Fig 5.2D). A bolus of H₂O₂ or CHP can cause lipid peroxidation, which is associated with an increase in membrane volume (192) and might recruit Gpx1 to the membrane. Thus, Gpx1 may respond to lipid oxidation and may be recruited to the RBC membrane because it is an efficient lipid peroxidase (190).

5.3 Discussion

As shown in Chapter 4, the antioxidant enzymes CuZnSOD, catalase, and Gpx1 change their localization in response to increased air exposure (Fig. 4.2A,B,D). This provides evidence for the response of these enzymes to ROS (178). In this chapter, we examined the response of RBC antioxidant enzymes to ROS as discussed in Section 4.1. RBCs have efficient enzymes for the decomposition of H₂O₂ and the best characterized ones are catalase, Gpx1 (135) and Prx2. However, CuZnSOD is the only known SOD in RBCs, and no change in CuZnSOD localization at the membrane after a bolus of H₂O₂ or CHP was observed here (Fig 5.2A). Catalase also did not change its membrane

localization after H₂O₂ or CHP treatment (Fig 5.2B), but Prx2 decreased after CHP treatment (Fig 5.2C) and Gpx1 membrane levels increased ~2.5 fold after H₂O₂ or CHP treatment (Fig 5.2D).

Western blotting results from Fig 5.1 and their analysis in Fig 5.2 are in agreement with previous confocal data obtained for CuZnSOD, catalase and Gpx1 in our laboratory and are shown in Fig 5.3 (163). The photomicrographs showing the effects of H₂O₂ on the localization of CuZnSOD, catalase, and Gpx1 in RBCs were obtained by generating H₂O₂ *in situ* using GOx plus 5 mM glucose which produced H₂O₂ at 8 μM/min (163). The results are summarized in Table 5.1.

Table 5.1 Localization of catalase, Gpx1 and CuZnSOD in human RBC after a steady-state generation of H₂O₂. Summary of confocal microscopy results as shown in Fig 5.3. Data was previously obtained in our laboratory (163).

Enzyme	G-PBS	glucose/GOx	glucose/GOx/catalase
catalase	Membrane and cytosol	Membrane and cytosol	Membrane and cytosol
Gpx1	Membrane and cytosol	Membrane	Membrane and cytosol
CuZnSOD	Membrane and cytosol	Membrane and cytosol	Membrane and cytosol

Confocal photomicrographs revealed that there is no catalase relocalization to the RBC membrane after the generation of H₂O₂ by GOx as compared to images from control cells (Fig 5.3B vs A,C) (163). Gpx1 increased its membrane localization after H₂O₂ exposure as compared to control cells (Fig 5.3E vs D,F). CuZnSOD also did not change its localization after H₂O₂ treatment as compared to control cells (Fig 5.3H vs G,I). Confocal results (Fig 5.3) agree with Western blotting data (Fig 5.2).

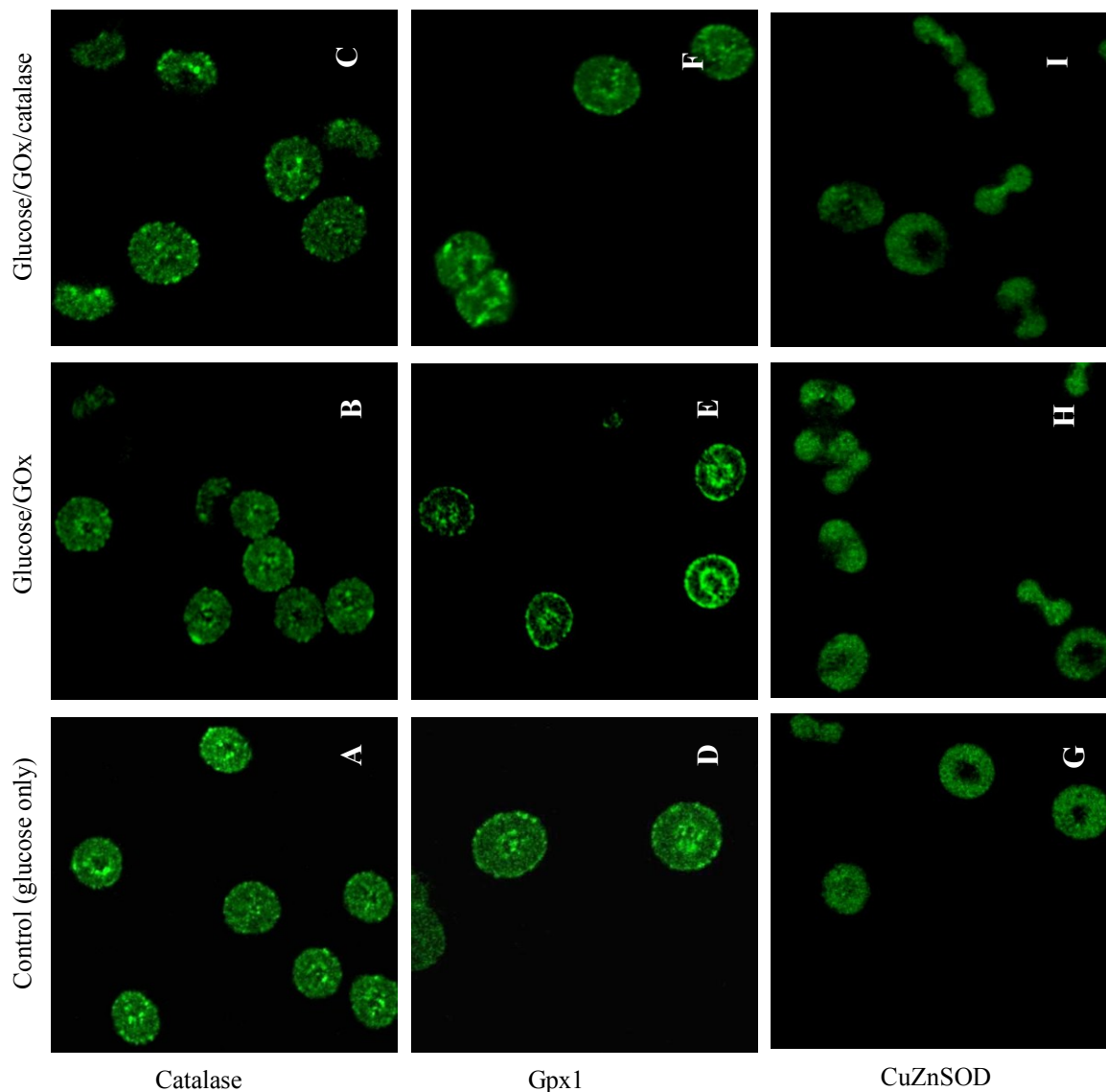


Fig 5.3 Confocal immunofluorescence images of CuZnSOD, catalase, and Gpx1 in fixed intact human RBCs under H₂O₂ flux. Data previously obtained in our laboratory (163). A-C. Catalase stained by sheep polyclonal anti-human catalase and Alexa conjugated anti-sheep IgG. D-F. Gpx1 stained by sheep anti-human Gpx1 and Alexa conjugated anti-sheep IgG. G-I. CuZnSOD stained by rabbit polyclonal anti-human CuZnSOD and Cy2 conjugated anti-rabbit IgG. Within 3 h of drawing blood, RBCs at 10% Ht in G-PBS at ambient temperature were exposed to 8 μ M/min exogenous H₂O₂ for 9 min. The cells were then stained as outlined in Section 2.2.2.2 and 2.2.2.3. Left column, control (5 mM glucose only). Middle column, 5 mM glucose plus 1.22 units GOx. Right column, 5 mM glucose plus 1.22 units GOx and 35 nM catalase. Filter settings were as follows: for both Cy2 and Alexa, excitation 488 nm; emission 500-530 nm.

In contrast, to obtain the Western blotting results, the RBCs were treated with a bolus H_2O_2 . Our results in Chapter 4 indicate that air exposure (30 or 60 min) affects some antioxidant enzymes (Fig 4.2). A bolus of H_2O_2 treatment was preferred in this thesis, rather than a steady-state H_2O_2 generation over 9 min, because our aim was to minimize RBC air exposure. Also, glucose oxidase (GOx) used for steady-state H_2O_2 generation consumes oxygen because the reaction was carried out in closed 2-mL tubes, filled to the top.

Appendix 5

Observed densities for Fig 5.2. Relative amounts of (A) CuZnSOD, (B) catalase, (C) Prx2, and (D) Gpx1 in membranes isolated from human RBCs treated with H₂O₂ or cumene hydroperoxide (CHP), n=3 individual donors. Proteins were separated by a reducing SDS-PAGE (35 µg total protein for CuZnSOD, 30 µg total protein for catalase, Prx2 and Gpx1) and Western blotted. The observed densities of WB bands and loading control are shown below.

Table A5.1

(A) CuZnSOD	Observed density			Observed density loading control			Corrected		
	control	H ₂ O ₂	CHP	control	H ₂ O ₂	CHP	control	H ₂ O ₂	CHP
Exp 1	2503.4	2426.7	2562.4	32.4	32.5	28.5	77.2	74.6	89.9
Exp 2	3234.4	3141.4	2804.5	52.5	48.5	42.4	61.6	64.8	66.1
Exp 3	2692.2	2452.6	2204.3	38.7	40.2	33.3	69.5	61.0	66.2
Average							69.46	66.83	74.08
Normalized							1.00	0.96	1.07
SEM							0.065	0.058	0.114

Table A5.2

(B) catalase	Observed density			Observed density loading control			Corrected		
	control	H ₂ O ₂	CHP	control	H ₂ O ₂	CHP	control	H ₂ O ₂	CHP
Exp 1	1456.3	1462.5	1398.6	52.5	50.5	52.5	27.7	28.9	26.6
Exp 2	1342.0	1299.6	1189.6	37.8	43.6	38.8	35.5	29.8	30.6
Exp 3	1438.5	1398.4	1405.7	45.5	48.6	43.4	31.6	28.8	32.4
Average							31.63	29.18	29.88
Normalized							1.00	0.92	0.94
SEM							0.071	0.010	0.053

Table A5.3

(C) Prx2 NEM	Observed density			Observed density loading control			Corrected		
	control	H ₂ O ₂	CHP	control	H ₂ O ₂	CHP	control	H ₂ O ₂	CHP
Exp 1	1606.4	1251.7	1178.9	59.4	37.4	48.6	27.0	33.5	24.3
Exp 2	1123.5	1064.5	893.0	36.9	33.6	34.9	30.4	31.7	25.6
Exp 3	1080.0	1089.3	702.4	34.6	35.8	34.6	31.2	30.4	20.3
Average							29.55	31.86	23.40
Normalized							1.00	1.08	0.79
SEM							0.043	0.030	0.054

Table A5.4

(D) Gpx1	Observed density			Observed density loading control			Corrected		
	control	H ₂ O ₂	CHP	control	H ₂ O ₂	CHP	control	H ₂ O ₂	CHP
Exp 1	1186.7	1296.8	1626.5	48.7	23.2	31.1	24.4	56.0	52.3
Exp 2	546.5	1095.5	1153.5	25.7	19.1	22.0	21.3	57.4	52.4
Exp 3	353.0	864.3	989.8	17.7	18.7	21.9	19.9	46.2	45.2
Average							21.86	53.19	49.97
Normalized							1.00	2.43	2.29
SEM							0.061	0.161	0.108

Chapter 6: Membrane localization of RBC antioxidant proteins in a diabetic rat model

6.1 Introduction

Diabetes is a disease associated with enhanced ROS generation in RBCs (80). Thus, we predicted a change in the recruitment of antioxidant enzymes to the diabetic RBC membrane to offset the effects of increased ROS. We induced diabetes in rats with streptozotocin (STZ) and monitored the levels of membrane-associated antioxidant enzymes in control and diabetic animals by Western blotting.

In Chapters 4 and 5, RBCs were treated with air, H₂O₂ and CHP for relatively short times (30 or 60 min). In this chapter we are investigating the long-term effects (4 weeks) of STZ-induced diabetes on the localization of antioxidant enzymes. Rat RBCs have a lifetime of ~60 days (205), while human RBCs have a lifetime of ~120 days (10). Thus, the diabetic RBCs used this study are not only aging (28 days) but are also subjected to dramatically increased glucose levels during their lifetime.

Western blotting and confocal data show that increased amounts of catalase and Gpx1 were recruited to the membrane whereas Prx2 remained unchanged in normal human RBCs exposed to air for 60 min (Fig 4.2B, C, D). CuZnSOD decreases at the membrane and re-localizes to the biconcave surface (Fig 4.2A). Based on such observations, we hypothesized that recruitment of different antioxidant enzymes is necessary to protect the membrane from various ROS. We speculated that loss of RBC membrane recruitment of antioxidant enzymes would make the membrane more

susceptible to damage. This damage would impair RBC function and likely contribute to the long-term vascular complications, such as those associated with diabetes (206).

Many proteins bind to CDB3 (15), and this binding can be controlled by CDB3 phosphorylation (186). When isolated RBC membranes were incubated in the presence of [γ -³²P]ATP, about 80% of the label was found in the N-terminal residues (1–56) (185). Thus, phosphorylation of the RBC membrane occurs mainly at CDB3 and 50-70% of the phosphorylation was observed at Tyr8 (26). Tyr21 and Tyr46 are also phosphorylated but to a lesser extent and the membrane-spanning fragment of Band-3 has no phosphorylation sites (185).

PTP1B is the main phosphatase at the RBC membrane (186). Changes in PTP1B activity were reported to occur in various tissues after 20-day STZ treatment. For example, PTP1B activity increased by 70% in the placenta, decreased by 40-50% in liver and skeletal muscle but remained unchanged in kidney and brain (207). There are no reports of PTP1B activity in diabetic RBCs, which undergo increased oxidative stress (80). This could lead to PTP1B inactivation by oxidation of its redox-sensitive catalytic Cys residue. Thus, we hypothesized that CDB3 phosphorylation may regulate binding of some antioxidant enzymes to the RBC membrane.

6.2 Results

6.2.1. CuZnSOD localization in diabetic RBCs

CuZnSOD increased at the RBC membrane of control animals in a 2-week period (no STZ treatment, Fig 6.2A). We also measured PTPase activity of the RBC membranes

(Fig 6.3) and found an increase over the same period (Fig 6.3). Increased PTPase activity likely results in decreased phosphorylation of CDB3, which we attribute to the increase of CuZnSOD at the RBC membrane of control animals.

There was a significant increase in CuZnSOD at the RBC membrane in STZ-treated animals, as compared to control, 2 weeks after the induction of diabetes (Fig 6.2A). However, no significant increase in PTP1B activity between STZ-treated and control RBCs was found 2 weeks after the induction of diabetes (Fig 6.3) raising the possibility that CuZnSOD is recruited to the membrane by altered CDB3 phosphorylation in diabetic RBCs. Also, non-specific binding of CuZnSOD to the membrane, via crosslinking for example, might be caused by increased oxidative stress associated with diabetes. There was a decrease in the levels of CuZnSOD at the membrane after 4 weeks of STZ treatment compared to 2 weeks of STZ treatment (Fig 6.2A), and we speculate that CuZnSOD might be competing with hemichromes or Prx2 for the RBC membrane in the 4-week diabetic RBCs.

6.2.2. Catalase localization in diabetic RBCs

RBCs from STZ-treated rats are expected to behave as cells from older animals because diabetes exacerbates RBC aging (208). The levels of membrane-associated catalase significantly decreased in the STZ-treated animals 4 weeks after the induction of diabetes as compared to RBCs exposed to elevated glucose for 2 weeks (Fig 6.2B). Elevated levels of methHb have been reported in diabetic RBCs (209). Since methHb is a precursor of hemichromes, catalase might compete with accumulation of irreversible hemichromes in diabetic RBCs 4 weeks after the induction of diabetes. Diabetes for 4

weeks likely induces more hemichrome formation, which would explain why the decrease observed between 2- and 4-weeks after treatment is more pronounced than the decrease in control RBCs.

6.2.3. Prx2 localization in diabetic RBCs

As discussed in Section 1.3 (Fig 1.3), hemichromes formation can be reversible or irreversible. Reversible hemichromes can be converted back to metHb, and eventually to reduced Hb. If irreversible hemichromes (bishistidine ferrihemochromes for e.g.) are formed, the Hb denaturation cannot be reversed and the RBCs are removed from circulation (61). In Fig 6.2C, there is an initial large increase in membrane-associated Prx2 2 weeks after STZ treatment as compared to the control. At this point, reversible hemichrome formation might be occurring and concomitant hemichrome association with the membrane. Thus, Prx2 would migrate to the RBC membrane to rescue the reversible hemichromes in the 2-week diabetic RBCs. However, after 4 weeks, membrane-associated Prx2 approaches control levels. At this point the RBCs probably contain an increased population of irreversible hemichromes at the membrane and Prx2 is unable to rescue them. Overall, the variation of catalase and Prx2 levels at the membrane suggests that Prx2 protects Hb from denaturation in diabetic RBCs and catalase likely associates with Prx2 as previously reported (171).

6.2.4. Gpx1 localization in diabetic RBCs

Gpx1 is an efficient lipid peroxidase (188). Thus, it is critical that its membrane levels are maintained to protect membrane lipids. Fig 6.2D shows only small diabetes-induced changes in Gpx1 membrane localization, indicating that the Gpx1 interaction

with the membrane is relatively robust. Such behaviour is expected since Gpx1 needs to stay at the membrane to protect lipids in older cells, as it is necessary to protect against Hb leakage and hemolysis. Lysis of old RBCs is as detrimental as lysis of young RBCs because Hb is released into plasma in both cases. Since lipids are found uniformly throughout the RBC membrane, we did not expect to see Gpx1 competing with phosphorylation at CDB3 or with other proteins that possess high affinity for CDB3.

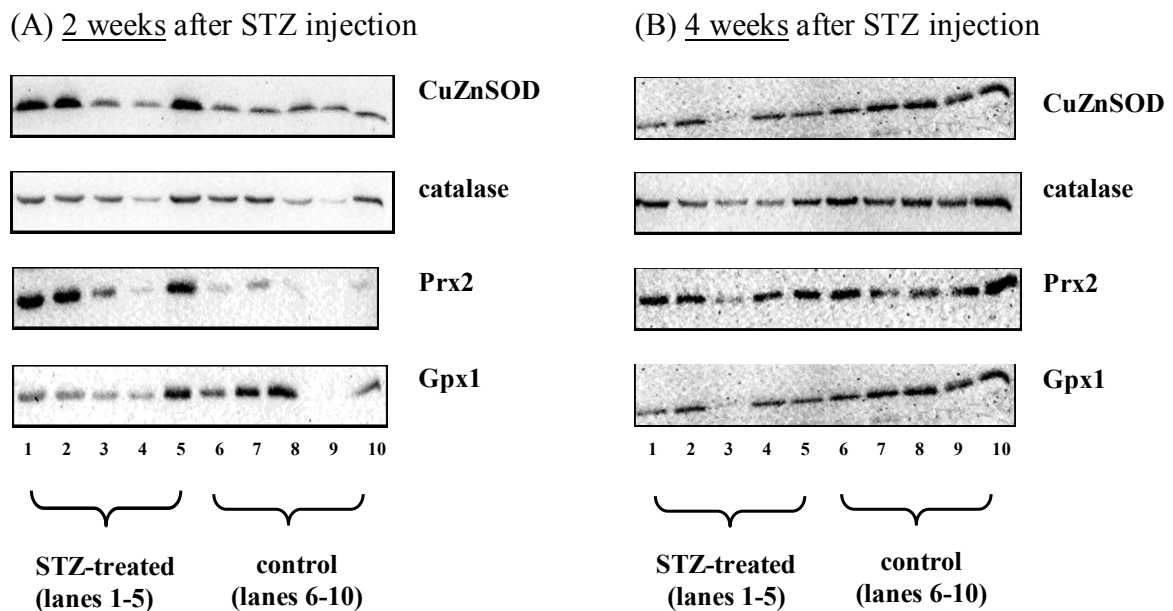


Fig 6.1 Western blots for CuZnSOD, catalase Prx2 and Gpx1 in isolated membranes from rat RBCs. (n = 5 animals). Rat membranes were prepared as described in Sections 2.2.1.5 and 2.2.1.6. Lanes 1 – 5 are STZ-treated animals and lanes 6 – 10 are control animals. RBCs were washed twice in isotonic physiological saline solution (PSS, pH 7.4), lysed and membranes were washed three times in 10 mM hypotonic sodium phosphate buffer, pH 7.4 (1:15 dilution) containing 0.1 mM PMSF at room temperature (Section 2.2.1.6). The non-ionic detergent 0.5% Triton-X was added to the pellet to solubilize the proteins. Proteins were separated by a reducing SDS-PAGE and immunoblotted (Section 2.2.1.7). 35 µg total protein per lane was loaded for CuZnSOD and Gpx1 and 30 µg total protein for catalase and Prx2. Densitometry results are shown in Fig 6.2 after correction with the loading control and normalization to 2-week control (Section 2.2.1.9).

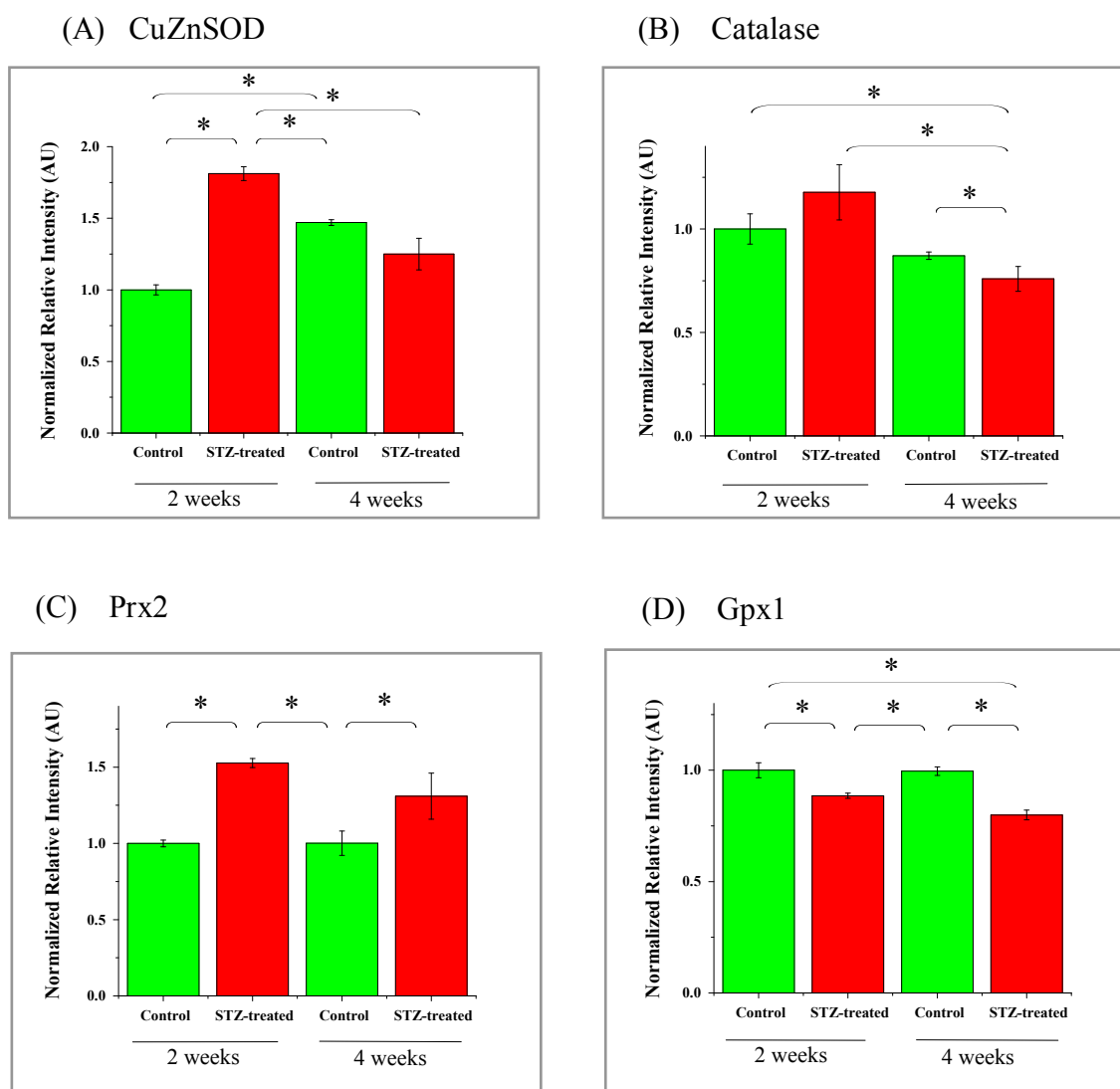


Fig 6.2 Densitometry of CuZnSOD, catalase, Prx2 and Gpx1 bands in Western blots from control and STZ-treated rat RBCs after removal of outliers. Densitometry was performed on the Western blots shown in Fig 6.1. (A) CuZnSOD (B) Catalase (C) Prx2 (D) Gpx1. Statistical significance (*) of differences among controls and STZ-treated animals was determined by Student t-test (unpaired, 2-tailed) using SPSS software and p-values ≤ 0.05 were considered significant. The 2-tailed t-test is used when examining significant differences between two groups without prior assumptions which group would be higher (or lower). Unpaired Student t-test is used when there is no need to control for a third confounding variable.

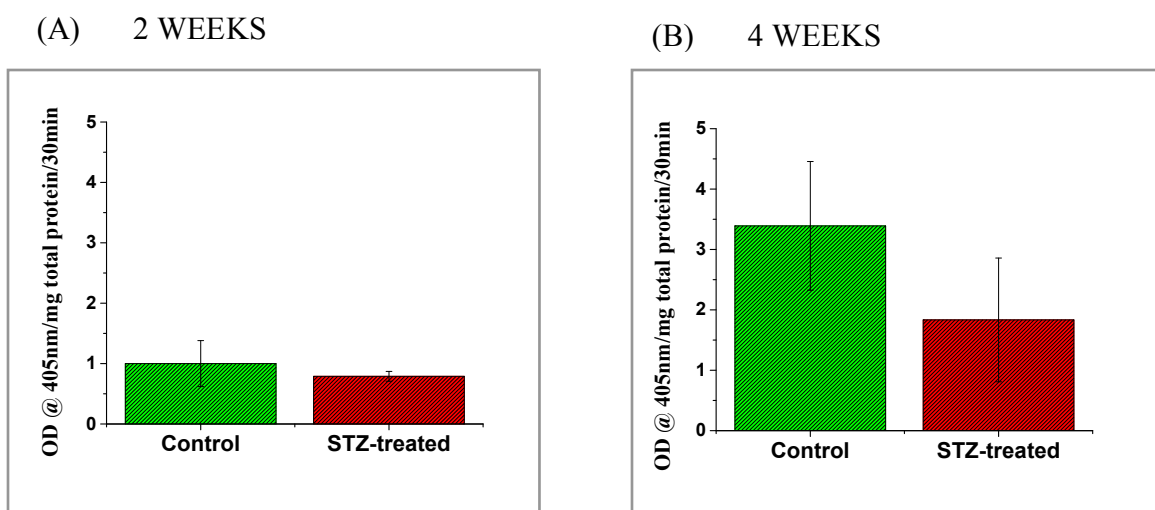


Fig 6.3 Comparison of PTP1B activity in membrane fractions from diabetic and normal rat RBCs. PTPase activity was determined using p-nitrophenyl phosphate (p-NPP) as substrate according to published procedures (210) with some modifications. The non-specific substrate p-NPP is used for determination of overall PTPase activity. Since PTP1B is the main phosphatase at the RBC membrane (186), we assume that PTP1B activity is being measured here. Membranes from rat RBCs were washed and isolated as described in Sections 2.2.1.5 and 2.2.1.6, diluted into 25 mM HEPES with 20 mM MgSO₄, pH 7.4 at room temperature, 1 mM DTT was added followed by 15 mM p-NPP (all concentrations are final), and the mixture was incubated for 30 min at 37 °C. The reaction was stopped with 0.1 mM NaOH, the samples were vortexed briefly and centrifuged at 8000 xg. Supernatants were collected and the OD at 405 nm was measured to determine the average PTP1B activity over 30 min. All data are normalized to the 2-week control. The average of n=5 animals + SEM shown for (A) 2-week STZ treatment and n=4 for (B) 4 weeks after STZ treatment.

6.3 Discussion

STZ treatment accelerates CuZnSOD, catalase, and Prx2 loss from the rat RBC membrane as revealed by their analysis at 2 vs 4 weeks after STZ treatment (Fig 6.2A,B,C). Elevated levels of methHb have been reported in diabetic RBCs (209) and

since metHb is a precursor of hemichromes, these three enzymes might be competing with increased hemichrome formation for CDB3 binding sites as the disease progresses.

Gpx1 membrane levels in the control and diabetic rat RBCs are the same during our observation period (Fig 6.2D). Since we anticipated that the increased oxidative stress induced by diabetes (80) would saturate the Gpx1 binding sites at the RBC membrane, it appears that these sites are also fully saturated in the control animals. This would imply that the lipid peroxidase activity of Gpx1 is of critical importance in maintaining the integrity of the RBC membrane.

Band-3 is a major substrate for kinases at the RBC membrane (211). Several PTPases have been detected in the RBC cytosol (212) but PTP1B is the main membrane-associated PTPase that dephosphorylates Band-3 (186). We hypothesized that increased oxidative stress in the RBCs of diabetic rats (80) would lead to increased CDB3 phosphorylation due to PTP1B inactivation on oxidation of its catalytic cysteine. Thus, to investigate a possible role for Band-3 Tyr phosphorylation in the localization of antioxidant enzymes, we measured the total PTPase activity, which largely reflects PTP1B activity, in ghost membranes from rat RBCs.

We observed no significant difference in PTPase activity between STZ-diabetic and control RBCs (Fig 6.3). However, in untreated animals, the PTPase activity increased significantly in a 2-week interval (Fig 6.3). Thus, we speculate that the 50% increase in CuZnSOD at the RBC membranes during this interval (Fig 6.2) may be due to less Tyr8, Tyr21, and/or Tyr46 phosphorylation at CDB3. The remarkable alteration in PTPase activity observed during a 2-week interval in 3-month-old untreated rats suggests that the

animals are responding to other factors in their environment separate from the STZ challenge.

Notably, the levels of catalase, Prx2 and Gpx1 associated with the membrane do not change with PTPase activity. This suggests that recruitment of these antioxidant proteins to CDB3 is independent of its phosphorylation status and, as mentioned above, may be controlled by the extent of hemichrome formation.

Appendix 6

Observed densities for Fig 6.2 Densitometry of CuZnSOD, catalase, Prx2 and Gpx1 bands in Western blots from control and STZ-treated rat RBCs (n=5). Proteins were separated by a reducing SDS-PAGE (35 µg total protein for CuZnSOD, 30 µg total protein for catalase, Prx2 and Gpx1) and Western blotted. The observed densities of WB bands and loading control are shown below. The shaded values are outliers and have been ignored when plotting the intensities.

Table A6.1
Before outlier removal

CuZnSOD (2 weeks)	Observed Intensity (WB)	Intensity Loading Control (Coomassie)	Corrected Intensity (WB/ Coomassie)	Average Corrected Intensity	SEM	
Standard 12.5 µg	234.83	9.63	24.39			
Standard 25 µg	437.28	18.45	23.70			
Standard 37.5 µg	787.98	29.50	26.71			
Standard 50 µg	2588.49	57.36	45.13			
Lane 1 (STZ)	2166.71	52.13	41.56	42.76	6.35	STZ-treated 2 weeks
Lane 2 (STZ)	2065.99	51.50	40.12	1.43	0.21	Normalized
Lane 3 (STZ)	755.11	37.42	20.18			
Lane 4 (STZ)	462.83	32.23	14.36			
Lane 5 (STZ)	2162.81	49.20	43.96			
Lane 6 (control)	681.07	28.38	24.00	29.94	3.82	Control 2 weeks
Lane 7 (control)	702.57	29.42	23.88	1.00	0.13	Normalized
Lane 8 (control)	835.66	23.43	35.67			
Lane 9 (control)	563.18	26.22	21.48			
Lane 10 (control)	673.97	12.60	53.49			

CuZnSOD (2 weeks)
After outlier removal

Average Corrected Intensity	SEM
41.87982	1.120659
1.811464	0.048474
23.11932	0.820849
1	0.035505

STZ-treated 2 weeks
Normalized (Fig 6.2A)
Control 2 weeks
Normalized (Fig 6.2A)

Table A6.2
Before outlier removal

CuZnSOD (4 weeks)	Observed Intensity (WB)	Intensity Loading Control (Coomassie)	Corrected Intensity (WB/ Coomassie)	Average Corrected Intensity	SEM	
Standard 12.5 µg	1382.70	26.43	52.32			
Standard 25 µg	2483.54	45.56	54.51			
Standard 37.5 µg	3616.54	56.75	63.73			
Standard 50 µg	4003.25	67.30	59.48			
Lane 1 (STZ)	1520.71	44.89	33.88	32.54	4.04	STZ-treated 4 weeks
Lane 2 (STZ)	1354.86	28.99	46.74	0.74	0.09	Normalized to 2 weeks control
Lane 3 (STZ)	810.45	32.12	25.23			
Lane 4 (STZ)	1208.24	49.89	24.22			
Lane 5 (STZ)	1200.68	36.76	32.66			
Lane 6 (control)	1397.87	22.89	61.07	43.69	5.99	Control 4 weeks
Lane 7 (control)	1597.55	45.69	34.96	1.00	0.14	Normalized to 2 weeks control
Lane 8 (control)	1662.69	50.26	33.08			
Lane 9 (control)	1822.79	32.98	55.27			
Lane 10 (control)	1738.07	51.03	34.06			

CuZnSOD (4 weeks)

After outlier removal, normalized to 2-week control

Average Corrected Intensity	SEM
29.00	2.49
1.25	0.11
34.04	0.54
1.47	0.02

STZ-treated
Normalized to 2 weeks
control (Fig 6.2A)

Control
Normalized to 2 weeks
control (Fig 6.2A)

Table A6.3
Before outlier removal

Catalase (2 weeks)	Observed Intensity (WB)	Intensity Loading Control (Coomassie)	Corrected Intensity (WB/ Coomassie)	Average Corrected Intensity	SEM	
Standard 12.5 µg	617.77	23.20	26.63			
Standard 25 µg	867.77	31.17	27.84			
Standard 37.5 µg	1309.21	41.65	31.43			
Standard 50 µg	1482.95	50.20	29.54			
Lane 1 (STZ)	1343.63	40.42	33.24	30.28	3.67	STZ-treated 2 weeks
Lane 2 (STZ)	1249.30	35.13	35.56	1.04	0.13	Normalized
Lane 3 (STZ)	1057.77	42.98	24.61			
Lane 4 (STZ)	524.61	23.78	22.06			
Lane 5 (STZ)	1756.39	39.42	44.56			
Lane 6 (control)	1286.52	33.43	38.48	29.07	3.36	Control 2 weeks
Lane 7 (control)	1443.14	38.45	37.53	1.00	0.10	Normalized
Lane 8 (control)	627.08	27.51	22.79			
Lane 9 (control)	282.77	12.47	22.68			
Lane 10 (control)	1312.90	46.73	28.10			

Catalase (2 weeks)
After outlier removal

Average Corrected Intensity	SEM	
28.87	3.27	STZ-treated 2 weeks
1.18	0.13	Normalized (Fig 6.2B)
24.52	1.79	Control 2 weeks
1.00	0.07	Normalized (Fig 6.2B)

Table A6.4

Catalase (4 weeks)	Observed Intensity (WB)	Intensity Loading Control (Coomassie)	Corrected Intensity (WB/ Coomassie)	Average Corrected Intensity	SEM	
Standard 12.5 µg	295.94	16.06	18.43			
Standard 25 µg	401.99	21.45	18.74			
Standard 37.5 µg	809.68	36.90	21.94			
Standard 50 µg	926.98	41.59	22.29			
Lane 1 (STZ)	453.88	24.39	18.61	18.61	1.4737	STZ-treated 4 weeks
Lane 2 (STZ)	283.42	20.96	13.52	0.87	0.07	Normalized to 2 weeks control
Lane 3 (STZ)	195.22	13.48	14.48			
Lane 4 (STZ)	220.62	18.73	11.78			
Lane 5 (STZ)	435.67	22.49	19.37			
Lane 6 (control)	656.67	32.49	20.21	21.35	0.4433	Control 4 weeks
Lane 7 (control)	589.22	27.92	21.10	1.00	0.02	Normalized to 2 weeks control
Lane 8 (control)	664.88	28.99	22.93			
Lane 9 (control)	594.15	27.76	21.40			
Lane 10 (control)	728.59	34.52	21.11			

Catalase (4 weeks)
normalized to 2-weeks control

Average Corrected Intensity	SEM
18.61	1.47
0.76	0.06
21.35	0.44
0.87	0.02

STZ-treated
Normalized to 2 weeks control
(Fig 6.2B)
Control
Normalized to 2 weeks control
(Fig 6.2B)

Table A6.5
Before outlier removal

Prx2/NEM (2 weeks)	Observed Intensity (WB)	Intensity Loading Control (Coomassie)	Corrected Intensity (WB/ Coomassie)	Average Corrected Intensity	SEM	
Standard 10 µg	161.26	10.36	15.566			
Standard 25 µg	419.39	24.4	17.188			
Standard 40 µg	904.46	46.14	19.603			
Standard 54 µg	1279.72	62.51	20.472			
Lane 1 (STZ)	841.59	45.23	18.607	19.139	1.6894	STZ-treated 2 weeks
Lane 2 (STZ)	781.59	39.27	19.903	1.51	0.08	Normalized
Lane 3 (STZ)	330.97	17.12	19.332			
Lane 4 (STZ)	133.45	9.47	14.092			
Lane 5 (STZ)	655.82	23.55	27.848			
Lane 6 (control)	141.63	11.52	12.294	12.633	0.3031	Control 2 weeks
Lane 7 (control)	197.78	14.54	13.602	1.00	0.02	Normalized
Lane 8 (control)	108.7	8.93	12.172			
Lane 9 (control)	74.41	6.12	12.158			
Lane 10 (control)	158.95	12.32	12.902			

Prx2 NEM (2 weeks)
After outlier removal

Average Corrected Intensity	SEM
19.28	0.38
1.53	0.03
12.63	0.28
1.00	0.02

STZ-treated 2 weeks
Normalized (Fig 6.2C)
Control 2 weeks
Normalized (Fig 6.2C)

Table A6.6
Before outlier removal

Prx2/NEM (4 weeks)	Observed Intensity (WB)	Intensity Loading Control (Coomassie)	Corrected Intensity (WB/ Coomassie)	Average Corrected Intensity	SEM	
Standard 10 µg	118.65	7.26	16.34			
Standard 25 µg	233.67	17.32	13.49			
Standard 40 µg	282.26	21.63	13.05			
Standard 54 µg	550.93	34.89	15.79			
Lane 1 (STZ)	301.91	16.64	18.14	13.58	2.14	STZ-treated 4 weeks
Lane 2 (STZ)	284.37	21.45	13.26	1.07	0.18	Normalized to 2 weeks control
Lane 3 (STZ)	128.64	17.45	7.37			
Lane 4 (STZ)	238.84	22.40	10.66			
Lane 5 (STZ)	305.73	16.56	18.46			
Lane 6 (control)	345.44	27.41	12.60	11.62	1.30	Control 4 weeks
Lane 7 (control)	199.05	18.70	10.64	0.92	0.10	Normalized to 2 weeks control
Lane 8 (control)	234.76	19.67	11.93			
Lane 9 (control)	273.35	36.56	7.48			
Lane 10 (control)	551.98	35.78	15.43			

Prx2 NEM (4 weeks)
After outlier removal, normalized to 2-week control

Average Corrected Intensity	SEM	
16.62	1.91	STZ-treated 2 weeks
1.31	0.15	Normalized to 2 weeks control (Fig 6.2C)
12.65	1.01	Control 2 weeks
1.00	0.08	Normalized to 2 weeks control (Fig 6.2C)

Table A6.7
Before outlier removal

Gpx1 (2 weeks)	Observed Intensity (WB)	Intensity Loading Control (Coomassie)	Corrected Intensity (WB/ Coomassie)	Average Corrected Intensity	SEM	
Standard 10 µg	400.84	19.45	20.61			
Standard 25 µg	736.39	33.21	22.17			
Standard 40 µg	1128.42	49.2	22.94			
Standard 54 µg	1690.52	74.56	22.67			
Lane 1 (STZ)	571.24	34.32	16.64	18.14	0.86	STZ-treated 2 weeks
Lane 2 (STZ)	420.58	27.26	15.43	0.81	0.04	Normalized
Lane 3 (STZ)	277.51	14.56	19.06			
Lane 4 (STZ)	268.74	13.52	19.88			
Lane 5 (STZ)	903.14	45.76	19.74			
Lane 6 (control)	532.49	25.68	20.74	22.09	0.74	Control 2 weeks
Lane 7 (control)	812.46	35.84	22.67	1.00	0.04	Normalized
Lane 8 (control)	1049.24	42.64	24.61			
Lane 9 (control)	51.21	2.34	21.88			
Lane 10 (control)	483.1	23.49	20.57			

Gpx1 (2 weeks)
After outlier removal

Average Corrected Intensity	SEM	
19.56	0.25	STZ-treated 2 weeks
0.89	0.01	Normalized (Fig 6.2D)
22.09	0.74	Control 2 weeks
1.00	0.03	Normalized (Fig 6.2D)

Table A6.8

Gpx1 (4 weeks)	Observed Intensity (WB)	Intensity Loading Control (Coomassie)	Corrected Intensity (WB/ Coomassie)	Average Corrected Intensity	SEM	
Standard 10 µg	259.69	12.89	20.15			
Standard 25 µg	664.87	29.56	22.49			
Standard 40 µg	723.22	32.51	22.25			
Standard 54 µg	752.02	33.86	22.21			
Lane 1 (STZ)	280.40	15.67	17.89	17.65	0.48	STZ-treated 4 weeks
Lane 2 (STZ)	420.97	24.74	17.02	0.80	0.02	Normalized to 2 weeks control
Lane 3 (STZ)	177.35	10.95	16.20			
Lane 4 (STZ)	396.94	20.93	18.97			
Lane 5 (STZ)	393.47	21.64	18.18			
Lane 6 (control)	493.88	21.56	22.91	22.00	0.43	Control 4 weeks
Lane 7 (control)	566.36	26.38	21.47	1.00	0.02	Normalized to 2 weeks control
Lane 8 (control)	573.18	25.71	22.29			
Lane 9 (control)	482.96	21.25	22.73			
Lane 10 (control)	504.88	24.51	20.60			

Gpx1 (4 weeks)

Normalized to 2-week control

Average Corrected Intensity	SEM
17.65	0.48
0.80	0.02
22.00	0.43
1.00	0.02

STZ-treated 2 weeks
Normalized to 2 weeks control
(Fig 6.2D)

Control 2 weeks
Normalized to 2 weeks control
(Fig 6.2D)

Statistical significance (*) of differences between samples shown in Fig 6.2 were determined by a Student t-test (unpaired, 2-tailed) with SPSS software, p-values ≤ 0.05 considered significant. Unpaired Student t-test is used when there is no need to control for a third confounding variable. The Student t-test was 2-tailed was used since we are examining differences between control and treated animals without initial assumptions which group would be higher (or lower).

(A) CuZnSOD

Control 2 wks vs STZ-treated 2 wks: p = 0.0002*
Control 4 wks vs STZ-treated 4 wks: p = 0.1148
Control 2 wks vs Control 4 wks: p = 0.002*
STZ-treated 2 wks vs STZ-treated 4 wks: p = 0.0229*
STZ treated 2 wks vs Control 4 wks: p = 0.0127*
Control 2 wks vs STZ-treated 4 wks: p = 0.2468

(B) Catalase

Control 2 wks vs STZ-treated 2 wks: p = 0.3431
Control 4 wks vs STZ-treated 4 wks: p = 0.0121*
Control 2 wks vs Control 4 wks: p = 0.0688
STZ-treated 2 wks vs STZ-treated 4 wks: p = 0.0126*
STZ treated 2 wks vs Control 4 wks: p = 0.0657
Control 2 wks vs STZ-treated 4 wks: p = 0.0073*

(C) Prx2

Control 2 wks vs STZ-treated 2 wks: p = 0.0001*
Control 4 wks vs STZ-treated 4 wks: p = 0.0512*
Control 2 wks vs Control 4 wks: p = 0.933
STZ-treated 2 wks vs STZ-treated 4 wks: p = 0.3618
STZ treated 2 wks vs Control 4 wks: p = 0.0114*
Control 2 wks vs STZ-treated 4 wks: p = 0.0766

(D) Gpx1

Control 2 wks vs STZ-treated 2 wks: p = 0.0429*
Control 4 wks vs STZ-treated 4 wks: p = 0.0001*
Control 2 wks vs Control 4 wks: p = 0.7783
STZ-treated 2 wks vs STZ-treated 4 wks: p = 0.0864
STZ treated 2 wks vs Control 4 wks: p = 0.0009*
Control 2 wks vs STZ-treated 4 wks: p = 0.0176*

Chapter 7: Overall discussion and conclusions

We examined the localization in RBCs of CuZnSOD, catalase, Prx2 and Gpx1 to gain insight into their function. We examined prompt RBC responses on oxidant challenge vs the effects of diabetes over 4 weeks.

In Chapters 4 and 5, we report on the prompt changes in human RBCs upon challenge with air, H₂O₂ and CHP. Exposure to air for 30 or 60 min should have similar effects on RBCs as hyperbaric challenge. As RBCs pass through the lungs, they are exposed to O₂ for only a few seconds so exposing RBCs to ambient air for an extended period of time (30 or 60 min) should mimic exposing RBCs to higher O₂ partial pressures in the vasculature. Exposure to peroxides was also short-term (30 min). Chapter 6 examines long-term changes occurring in rat RBCs exposed to increased plasma glucose levels over a 4-week period. Specifically, we investigated the association of CuZnSOD, catalase, Prx2, and Gpx1 with the RBC membrane. Based on the literature, we assume CDB3 to be their major binding site. Diabetes causes major changes in RBCs, including hemichrome formation (213) and decreased PTP1B activity (207, 214)

The data obtained on control rats suggest that CDB3 phosphorylation may regulate CuZnSOD membrane binding. CuZnSOD increased its membrane localization in rat RBCs during a 2-week interval (Fig 6.2A), which correlates with loss of PTPase activity (Fig 6.3). CuZnSOD also decreased its membrane localization after 60 min aeration (Fig 4.2A) but PTPase activity was not monitored under these conditions.

Catalase significantly increased at the membrane after 30 min air exposure and increased further after 60 min air exposure (Fig 4.2B, open tubes). Prolonged air

generates more $O_2^{\bullet-}$, which is rapidly dismutated to H_2O_2 . Possible increased H_2O_2 generation at the membrane may trigger catalase migration to protect the membrane. In contrast, membrane-associated catalase changed slightly over a 2-week period in control rat RBCs (Fig 6.2B) but STZ treatment accelerated loss of this enzyme from the membrane as revealed by the blots at 4 vs 2 weeks after induction of diabetes (Fig 6.2B). As mentioned in Section 6.3, we attribute this to the possible increase in hemichrome formation.

Prx2 is likely recruited to the membrane to act as a chaperone and rescue reversible hemichromes to prevent their conversion to irreversible forms. Prolonged air exposure does not alter Prx2 levels at the human RBC membrane (Fig 4.2C), presumably because hemichrome formation is a slow and gradual process (213). However, diabetes accelerates the aging process such that Prx2 membrane localization increased 2 weeks after STZ treatment but irreversible hemichrome formation as diabetes progresses likely results in a loss of Prx2 from the membrane (Fig 6.2C).

Gpx1 membrane levels in diabetic and control RBCs remain unchanged between 2 and 4 weeks (Fig 6.2D), but 60 min air exposure triggers increased Gpx1 recruitment to the RBC membrane (Fig 4.2D). We speculate that all Gpx1 binding sites at the membrane are saturated in rat RBCs due to the additional oxidative stress induced by diabetes. However, Gpx1 in human RBCs promptly responded to an acute stress such as 60 min air exposure (Fig 4.2D) by moving to the membrane to protect the lipids from oxidation. We speculate that oxidized lipids, which undergo an increase in volume (190), recruit Gpx1, which is a highly efficient lipid peroxidase.

Based on the results presented in this thesis, we suggest some possible studies of current blood storage practices, which cause “storage lesions” associated with oxidative stress (75). Storage of blood under hypobaric conditions should be investigated as should the use of low molecular weight SOD mimetics (215). Modulation of PTPase activity and hemichrome formation should be investigated as we speculate that they control recruitment of antioxidant enzymes to the RBC membrane.

Finally, we note that the results in this thesis were mainly acquired by semi-quantitative Western blotting. Confocal microscopy is a highly complementary technique for determining protein localization within cells. While low-affinity interactions can be disrupted during RBC handling and membrane isolation prior to Western blotting, such is not the case with confocal microscopy, which can be quantitative and also provides important spatial information depending on the image collection conditions (controls vs. experimental, number of z planes, detector control, laser intensity etc.).

Chapter 8: Future studies

Many interesting results reported in this work need further investigation. Below are some suggestions, separated into experiments to be performed by biochemical techniques and by confocal microscopy.

Biochemical techniques:

- 1) Measure PTPase activity in membrane fractions after 60 min air exposure. To confirm our hypothesis that PTP1B regulates CuZnSOD membrane-binding in RBCs, we expect to see a decrease in PTPase activity in membrane fractions after 60 min air exposure.
- 2) Also, measure PTPase activity in H₂O₂-treated and CHP-treated RBCs and correlate this with the drop in CuZnSOD at the membrane after prompt stress (H₂O₂, CHP).
- 3) Determine phosphorylation of CDB3 in RBCs by anti-phosphotyrosine antibody.
- 4) Measure the activity of CuZnSOD, catalase, Prx2, and Gpx1 in RBC membranes and cytosolic fractions to validate the data obtained by Western blotting and confocal microscopy. Differences in activities at the membrane and in the cytosol would provide further insight into the precise function of the antioxidant proteins. Prx2, catalase and Hb were reported to interact in cytosol of stored RBCs (171). No Prx2 peroxidase activity was found in association with both catalase and Hb (171), indicating that Prx2 is acting as a chaperone for Hb. However, when in association with catalase at the membrane, Prx2 was reported to exhibit peroxidase activity (171).

- 5) Investigate hemichrome formation in RBCs under oxidative stress by electron paramagnetic resonance (EPR).

Confocal microscopy:

- 1) Confocal micrographs have been obtained in our laboratory for CuZnSOD, catalase, and Gpx1 after 60 min air exposure. To obtain a complete dataset, confocal photomicrographs for Prx2 after 60 min air exposure should be obtained.
- 2) Confirm CDB3 binding sites by competition between anti-CDB3 antibody and antioxidant proteins. A monoclonal anti-CDB3 antibody, which recognizes an epitope within residues 1-136 of CDB3 was used (161). If two proteins colocalize or their locations are very close, their antibodies would have to compete for binding within a limited space. Hence, antibody binding to one protein should hinder antibody binding to the second protein. Competition between anti-CuZnSOD and anti-CDB3 was performed previously in our group and we found that CuZnSOD binds at or near the N-terminus of CDB3 (149, 163). Competition between anti-catalase (or anti-Gpx1, anti-Prx2) and anti-CDB3 binding needs to be performed to confirm the membrane binding sites of these antioxidant proteins. Also, the effect of treatment and aging on anti-CDB3 binding to CDB3 is of interest since hemichrome formation may compete with the antibody for its binding site.

References

1. Volpe EP (1993) *Blood and circulation. Biology and human concerns.* (Wm. C. Brown Publishers), pp 253-265.
2. Bunn HF (1991) *Pathophysiology of the anemias. Harrison's principles of internal medicine.* ed Wilson J, Braunwald E, Isselbacher K (McGraw-Hill, New York), pp 1514 - 1518.
3. Weed RI (1970) The importance of erythrocyte deformability. *Am J Med* 49(2): 147-150.
4. La Celle PL & Weed RI (1971) The contribution of normal and pathologic erythrocytes to blood rheology. *Prog Hematol* 7(0): 1-31.
5. Weiss L & Tavassoli M (1970) Anatomical hazards to the passage of erythrocytes through the spleen. *Semin Hematol* 7(4): 372-380.
6. Mohandas N, Phillips WM & Bessis M (1979) Red blood cell deformability and hemolytic anemias. *Semin Hematol* 16(2): 95-114.
7. Chien S (1987) Red cell deformability and its relevance to blood flow. *Annu Rev Physiol* 49: 177-192.
8. Borst JW, Visser NV, Kouptsova O & Visser AJ (2000) Oxidation of unsaturated phospholipids in membrane bilayer mixtures is accompanied by membrane fluidity changes. *Biochim Biophys Acta* 1487(1): 61-73.
9. Leblond PF, LaCelle PL & Weed RI (1971) Cellular deformability: a possible determinant of the normal release of maturing erythrocytes from the bone marrow. *Blood* 37(1): 40-46.
10. Vander A (2001) *Human Physiology: The Mechanism of Body Function, 8th ed.* (McGraw-Hill, Singapore), pp 377.
11. Telen MJ KR (1999) *The mature erythrocyte. Wintrobe's Clinical Hematology,* ed Greer JP FJ (Lippincott Williams & Wilkins, Philadelphia), pp 217-47.
12. Bruce LJ, Beckmann R, Ribeiro ML, Peters LL, Chasis JA, Delaunay J, Mohandas N, Anstee DJ, Tanner MJ (2003) A band 3-based macrocomplex of integral and peripheral proteins in the RBC membrane. *Blood* 101(10): 4180-4188.
13. Allenspach EJ, Cullinan P, Tong J, Tang Q, Tesciuba AG, Cannon JL, Takahashi SM, Morgan R, Burkhardt JK & Sperling AI (2001) ERM-dependent movement of CD43 defines a novel protein complex distal to the immunological synapse. *Immunity* 15(5): 739-750.

14. Yi SJ, Liu SC, Derick LH, Murray J, Barker JE, Cho MR, Palek J & Golan DE (1997) Red cell membranes of ankyrin-deficient nb/nb mice lack band 3 tetramers but contain normal membrane skeletons. *Biochemistry* 36(31): 9596-9604.
15. Salomao M, Zhang X, Yang Y, Lee S, Hartwig JH, Chasis JA, Mohandas N & An X. (2008) Protein 4.1R-dependent multiprotein complex: new insights into the structural organization of the red blood cell membrane. *Proc Natl Acad Sci U S A* 105(23): 8026-8031.
16. Tanner MJ (1997) The structure and function of band 3 (AE1): recent developments (review). *Mol Membr Biol* 14(4): 155-165.
17. Low PS, Waugh SM, Zinke K & Drenckhahn D (1985) The role of hemoglobin denaturation and band 3 clustering in red blood cell aging. *Science* 227(4686): 531-533.
18. Turrini F, Arese P, Yuan J & Low PS (1991) Clustering of integral membrane proteins of the human erythrocyte membrane stimulates autologous IgG binding, complement deposition, and phagocytosis. *J Biol Chem* 266(35): 23611-23617.
19. Kannan R, Yuan J & Low PS (1991) Isolation and partial characterization of antibody- and globin-enriched complexes from membranes of dense human erythrocytes. *Biochem J* 278(Pt 1): 57-62.
20. Reid ME LC (1997) in *The blood group antigen: facts book* (Academic Press, San Diego) pp 25.
21. Zhang D, Kiyatkin A, Bolin JT & Low PS (2000) Crystallographic structure and functional interpretation of the cytoplasmic domain of erythrocyte membrane band 3. *Blood* 96(9): 2925-2933.
22. Thevenin BJ, Periasamy N, Shohet SB & Verkman AS (1994) Segmental dynamics of the cytoplasmic domain of erythrocyte band 3 determined by time-resolved fluorescence anisotropy: sensitivity to pH and ligand binding. *Proc Natl Acad Sci U S A* 91(5): 1741-1745.
23. Low PS, Westfall MA, Allen DP & Appell KC (1984) Characterization of the reversible conformational equilibrium of the cytoplasmic domain of erythrocyte membrane band 3. *J Biol Chem* 259(21): 13070-13076.
24. Tanner MJ, Martin PG & High S (1988) The complete amino acid sequence of the human erythrocyte membrane anion-transport protein deduced from the cDNA sequence. *Biochem J* 256(3): 703-712.
25. Lux SE, John KM, Kopito RR & Lodish HF (1989) Cloning and characterization of band 3, the human erythrocyte anion-exchange protein (AE1). *Proc Natl Acad Sci U S A* 86(23): 9089-9093.

26. Dekowski SA, Rybicki A & Drickamer K (1983) A tyrosine kinase associated with the red cell membrane phosphorylates band 3. *J Biol Chem* 258(5): 2750-2753.
27. Bennett V & Stenbuck PJ (1980) Association between ankyrin and the cytoplasmic domain of band 3 isolated from the human erythrocyte membrane. *J Biol Chem* 255(13): 6424-6432.
28. Cohen CM, Dotimas E & Korsgren C (1993) Human erythrocyte membrane protein band 4.2 (pallidin). *Semin Hematol* 30(2): 119-137.
29. Rybicki AC, Schwartz RS, Hustedt EJ & Cobb CE (1996) Increased rotational mobility and extractability of band 3 from protein 4.2-deficient erythrocyte membranes: evidence of a role for protein 4.2 in strengthening the band 3-cytoskeleton linkage. *Blood* 88(7): 2745-2753.
30. An XL, Takakuwa Y, Nunomura W, Manno S & Mohandas N (1996) Modulation of band 3-ankyrin interaction by protein 4.1. Functional implications in regulation of erythrocyte membrane mechanical properties. *J Biol Chem* 271(52): 33187-33191.
31. Pasternack GR, Anderson RA, Leto TL & Marchesi VT (1985) Interactions between protein 4.1 and band 3. an alternative binding site for an element of the membrane skeleton. *J Biol Chem* 260(6): 3676-3683.
32. Rogalski AA, Steck TL & Waseem A (1989) Association of glyceraldehyde-3-phosphate dehydrogenase with the plasma membrane of the intact human red blood cell. *J Biol Chem* 264(11): 6438-6446.
33. Jenkins JD, Madden DP & Steck TL (1984) Association of phosphofructokinase and aldolase with the membrane of the intact erythrocyte. *J Biol Chem* 259(15): 9374-9378.
34. Murthy SN, Liu T, Kaul RK, Kohler H & Steck TL (1981) The aldolase-binding site of the human erythrocyte membrane is at the NH₂ terminus of band 3. *J Biol Chem* 256(21): 11203-11208.
35. Walder JA, *et al* (1984) The interaction of hemoglobin with the cytoplasmic domain of band 3 of the human erythrocyte membrane. *J Biol Chem* 259(16): 10238-10246.
36. Salhany JM & Cassoly R (1989) Kinetics of p-mercuribenzoate binding to sulfhydryl groups on the isolated cytoplasmic fragment of band 3 protein. Effect of hemoglobin binding on the conformation. *J Biol Chem* 264(3): 1399-1404.
37. Waugh SM & Low PS (1985) Hemichrome binding to band 3: nucleation of heinz bodies on the erythrocyte membrane. *Biochemistry* 24(1): 34-39.
38. Harrison ML, Isaacson CC, Burg DL, Geahlen RL & Low PS (1994) Phosphorylation of human erythrocyte band 3 by endogenous p72syk. *J Biol Chem* 269(2): 955-959.
39. Blacken M. (2009) Cysteine 93 of hemoglobin beta chain is the major target of oxidation during red blood cell storage, *51st Annual ASH Meeting and Exposition*.

40. Low PS, *et al* (1987) Tyrosine phosphorylation of band 3 inhibits peripheral protein binding. *J Biol Chem* 262(10): 4592-4596.
41. Low PS, Willardson BM, Mohandas N, Rossi M & Shohet S (1991) Contribution of the band 3-ankyrin interaction to erythrocyte membrane mechanical stability. *Blood* 77(7): 1581-1586.
42. Low PS, Rathinavelu P & Harrison ML (1993) Regulation of glycolysis via reversible enzyme binding to the membrane protein, band 3. *J Biol Chem* 268(20): 14627-14631.
43. Malik S, Sami M & Watts A (1993) A role for band 4.2 in human erythrocyte band 3 mediated anion transport. *Biochemistry* 32(38): 10078-10084.
44. Gerschman R, Gilbert DL, Nye SW, Dwyer P & Fenn WO (1954) Oxygen poisoning and x-irradiation: a mechanism in common. *Science* 119(3097): 623-626.
45. Yahya H (2007) *The Miracle of the Blood and Heart, 1st ed.* (Global Publishing, Istanbul), pp 25.
46. Branemark and Bagge (1977) Intravascular rheology of erythrocytes in man. *Blood Cells* 3: 11-24.
47. Turrens JF (2003) Mitochondrial formation of reactive oxygen species. *J Physiol* 552(Pt 2): 335-344.
48. Baynes JW (2005) *Oxygen and life. Medical biochemistry, 2nd ed.* (Elsevier Mosby, Philadelphia) pp 497-506.
49. Dumaswala UJ, Zhuo L, Jacobsen DW, Jain SK & Sukalski KA (1999) Protein and lipid oxidation of banked human erythrocytes: role of glutathione. *Free Radic Biol Med* 27(9-10): 1041-1049.
50. Ruch W, Cooper PH & Baggiolini M (1983) Assay of H₂O₂ production by macrophages and neutrophils with homovanillic acid and horse-radish peroxidase. *J Immunol Methods* 63(3): 347-357.
51. Chockalingam K, Luba J, Nick HS, Silverman DN & Zhao H (2006) Engineering and characterization of human manganese superoxide dismutase mutants with high activity and low product inhibition. *FEBS J* 273(21): 4853-4861.
52. Cimen MY (2008) Free radical metabolism in human erythrocytes. *Clin Chim Acta* 390(1-2): 1-11.
53. Hebbel RP, Eaton JW, Balasingam M & Steinberg MH (1982) Spontaneous oxygen radical generation by sickle erythrocytes. *J Clin Invest* 70(6): 1253-1259.
54. Claster S, Chiu DT, Quintanilha A & Lubin B (1984) Neutrophils mediate lipid peroxidation in human red cells. *Blood* 64(5): 1079-1084.

55. Al-Omar MA, Beedham C & Alsarra IA (2004) Pathological roles of reactive oxygen species and their defence mechanisms. *Saudi Pharm J* 12: 1-18.
56. Bienert GP, Schjoerring JK & Jahn TP (2006) Membrane transport of hydrogen peroxide. *Biochim Biophys Acta* 1758(8): 994-1003.
57. Chiu D, Kuypers F & Lubin B (1989) Lipid peroxidation in human red cells. *Semin Hematol* 26(4): 257-276.
58. Johnson RM, Goyette G, Jr, Ravindranath Y & Ho YS (2005) Hemoglobin autoxidation and regulation of endogenous H₂O₂ levels in erythrocytes. *Free Radic Biol Med* 39(11): 1407-1417.
59. Jacob HS (1970) Mechanisms of heinz body formation and attachment to red cell membrane. *Semin Hematol* 7(3): 341-354.
60. Peisach J, Blumberg WE & Rachmilewitz EA (1975) The demonstration of ferrihemochrome intermediates in heinz body formation following the reduction of oxyhemoglobin A by acetylphenylhydrazine. *Biochim Biophys Acta* 393(2): 404-418.
61. Kay MM (1975) Mechanism of removal of senescent cells by human macrophages in situ. *Proc Natl Acad Sci U S A* 72(9): 3521-3525.
62. Waugh SM, Willardson BM, Kannan R, Labotka RJ & Low PS (1986) Heinz bodies induce clustering of band 3, glycophorin, and ankyrin in sickle cell erythrocytes. *J Clin Invest* 78(5): 1155-1160.
63. Arese P, Gallo V, Pantaleo A & Turrini F (2012) Life and death of glucose-6-phosphate dehydrogenase (G6PD) deficient erythrocytes - role of redox stress and band 3 modifications. *Transfus Med Hemother* 39(5): 328-334.
64. Yoshida T & Shevkoplyas SS (2010) Anaerobic storage of red blood cells. *Blood Transfus* 8(4): 220-236.
65. Van Dort HM, Moriyama R & Low PS (1998) Effect of band 3 subunit equilibrium on the kinetics and affinity of ankyrin binding to erythrocyte membrane vesicles. *J Biol Chem* 273(24): 14819-14826.
66. Blackman SM, Piston DW & Beth AH (1998) Oligomeric state of human erythrocyte band 3 measured by fluorescence resonance energy homotransfer. *Biophys J* 75(2): 1117-1130.
67. Salhany JM, Cordes KA & Sloan RL (1997) Gel filtration chromatographic studies of the isolated membrane domain of band 3. *Mol Membr Biol* 14(2): 71-79.
68. Shalev O, Leida MN, Hebbel RP, Jacob HS & Eaton JW (1981) Abnormal erythrocyte calcium homeostasis in oxidant-induced hemolytic disease. *Blood* 58(6): 1232-1235.

69. Giulivi C & Davies KJ (2001) Mechanism of the formation and proteolytic release of H₂O₂-induced dityrosine and tyrosine oxidation products in hemoglobin and red blood cells. *J Biol Chem* 276(26): 24129-24136.
70. Caprari P, Scuteri A, Salvati AM, Bauco C, Cantafora A, Masella R, Modesti D, Tarzia A & Marigliano V (1999) Aging and red blood cell membrane: a study of centenarians. *Exp Gerontol* 34(1): 47-57.
71. Fujino T, Ando K, Beppu M & Kikugawa K (2000) Enzymatic removal of oxidized protein aggregates from erythrocyte membranes. *J Biochem* 127(6): 1081-1086.
72. Snyder LM, Fortier NL, Trainor J, Jacobs J, Leb L, Lubin B, Chiu D, Shohet S & Mohandas N (1985) Effect of hydrogen peroxide exposure on normal human erythrocyte deformability, morphology, surface characteristics, and spectrin-hemoglobin cross-linking. *J Clin Invest* 76(5): 1971-1977.
73. Lux SE (1983) *Disorders of the red cell membrane skeleton: hereditary spherocytosis and hereditary elliptocytosis. The Metabolic Basis of Inherited Disease*, ed Stanbury JB (McGraw Hill, New York), pp 1573-1605.
74. Wolfe LC, Byrne AM & Lux SE (1986) Molecular defect in the membrane skeleton of blood bank-stored red cells. abnormal spectrin-protein 4.1-actin complex formation. *J Clin Invest* 78(6): 1681-1686.
75. Tinmouth A, Fergusson D, Yee IC, Hébert PC; ABLE Investigators & Canadian Critical Care Trials Group (2006) Clinical consequences of red cell storage in the critically ill. *Transfusion* 46(11): 2014-2027.
76. Brechter ME (2002) Technical manual (14th ed). *American Association of Blood Banks, Bethesda, MD*.
77. Antonelou MH, Kriebardis AG, Stamoulis KE, Economou-Petersen E, Margaritis LH & Papassideri IS (2010) Red blood cell aging markers during storage in citrate-phosphate-dextrose-saline-adenine-glucose-mannitol. *Transfusion* 50(2): 376-389.
78. Kriebardis AG, Antonelou MH, Stamoulis KE, Economou-Petersen E, Margaritis LH, & Papassideri IS (2007) Progressive oxidation of cytoskeletal proteins and accumulation of denatured hemoglobin in stored red cells. *J Cell Mol Med* 11(1): 148-155.
79. Rinalducci S, D'Amici GM, Blasi B, Vaglio S, Grazzini G & Zolla L (2011) Peroxiredoxin-2 as a candidate biomarker to test oxidative stress levels of stored red blood cells under blood bank conditions. *Transfusion* 51(7): 1439-1449.
80. Moussa SA (2008) Oxidative stress in diabetes mellitus. *Rom J Biophys* 18(3): 225-236.
81. Bryszewska M & Szosland K (1988) Association between the glycation of erythrocyte membrane proteins and membrane fluidity. *Clin Biochem* 21(1): 49-51.

82. Miller JA, Gravallesse E & Bunn HF (1980) Nonenzymatic glycosylation of erythrocyte membrane proteins. Relevance to diabetes. *J Clin Invest* 65(4): 896-901.
83. Bucala R, Vlassara H & Cerami A (1992) *Post-Translation Modification of Proteins*, ed J.J. Harding MJCC (CRC Press Inc, Boca Raton, Florida), pp 53-79.
84. Durak I, Kacmaz M, Cimen MY, Buyukkocak U & Ozturk HS (2001) Blood oxidant/antioxidant status of atherosclerotic patients. *Int J Cardiol* 77(2-3): 293-297.
85. Bielski BH & Cabelli DE (1991) Highlights of current research involving superoxide and perhydroxyl radicals in aqueous solutions. *Int J Radiat Biol* 59(2): 291-319.
86. Kennett EC & Kuchel PW (2003) Redox reactions and electron transfer across the red cell membrane. *IUBMB Life* 55(7): 375-385.
87. Colleen M (2005) *Mark's Basic Medical Biochemistry, 2nd ed.* (Lippincott & Wilkins, Philadelphia), pp 57.
88. Altuntas I, Aksoy H, Coskun I, Caykoylu A & Akcay F (2000) Erythrocyte superoxide dismutase and glutathione peroxidase activities, and malondialdehyde and reduced glutathione levels in schizophrenic patients. *Clin Chem Lab Med* 38(12): 1277-1281.
89. Sailaja YR, Baskar R & Saralakumari D (2003) The antioxidant status during maturation of reticulocytes to erythrocytes in type 2 diabetics. *Free Radic Biol Med* 35(2): 133-139.
90. Valentine JS, Doucette PA & Zittin Potter S (2005) Copper-zinc superoxide dismutase and amyotrophic lateral sclerosis. *Annu Rev Biochem* 74: 563-593.
91. Hart PJ, Balbirnie MM, Ogihara NL, Nersissian AM, Weiss MS, Valentine JS, Eisenberg D (1999) A structure-based mechanism for copper-zinc superoxide dismutase. *Biochemistry* 38(7): 2167-2178.
92. Rakhit R & Chakrabartty A (2006) Structure, folding, and misfolding of Cu,Zn superoxide dismutase in amyotrophic lateral sclerosis. *Biochim Biophys Acta* 1762(11-12): 1025-1037.
93. Getzoff ED, Tainer JA, Weiner PK, Kollman PA, Richardson JS & Richardson DC (1983) Electrostatic recognition between superoxide and copper, zinc superoxide dismutase. *Nature* 306(5940): 287-290.
94. Zamocky M & Koller F (1999) Understanding the structure and function of catalases: clues from molecular evolution and in vitro mutagenesis. *Prog Biophys Mol Biol* 72(1): 19-66.
95. Loew O (1900) A new enzyme of general occurrence in organisms. *Science* 11(279): 701-702.

96. Schroeder WA, Shelton JR, Shelton JB, Robberson B & Apell G (1969) The amino acid sequence of bovine liver catalase: a preliminary report. *Arch Biochem Biophys* 131(2): 653-655.
97. Chelikani P, Fita I & Loewen PC (2004) Diversity of structures and properties among catalases. *Cell Mol Life Sci* 61(2): 192-208.
98. Nicholls P, Fita I & Loewen PC (2000) Enzymology and structure of catalases. *Advances in Inorganic Chemistry* 51: 51-106.
99. Putnam CD, Arvai AS, Bourne Y & Tainer JA (2000) Active and inhibited human catalase structures: ligand and NADPH binding and catalytic mechanism. *J Mol Biol* 296(1): 295-309.
100. Aebi H (1984) Catalase in vitro. *Methods Enzymol* 105: 121-126.
101. Deisseroth A & Dounce AL (1970) Catalase: physical and chemical properties, mechanism of catalysis, and physiological role. *Physiol Rev* 50(3): 319-375.
102. Wood ZA, Schroder E, Robin Harris J & Poole LB (2003) Structure, mechanism and regulation of peroxiredoxins. *Trends Biochem Sci* 28(1): 32-40.
103. Kang SW, Chae HZ, Seo MS, Kim K, Baines IC & Rhee SG (1998) Mammalian peroxiredoxin isoforms can reduce hydrogen peroxide generated in response to growth factors and tumor necrosis factor- α . *J Biol Chem* 273(11): 6297-6302.
104. Kang SW, Rhee SG, Chang TS, Jeong W & Choi MH (2005) 2-cys peroxiredoxin function in intracellular signal transduction: therapeutic implications. *Trends Mol Med* 11(12): 571-578.
105. O'Neill JS & Reddy AB (2011) Circadian clocks in human red blood cells. *Nature* 469(7331): 498-503.
106. Schroder E, Littlechild JA, Lebedev AA, Errington N, Vagin AA & Isupov MN (2000) Crystal structure of decameric 2-cys peroxiredoxin from human erythrocytes at 1.7 Å resolution. *Structure* 8(6): 605-615.
107. Moore RB, Mankad MV, Shriver SK, Mankad VN & Plishker GA (1991) Reconstitution of Ca²⁺-dependent K⁺ transport in erythrocyte membrane vesicles requires a cytoplasmic protein. *J Biol Chem* 266(28): 18964-18968.
108. Cohen G & Hochstein P (1963) Glutathione peroxidase: the primary agent for the elimination of hydrogen peroxide in erythrocytes. *Biochemistry* 2: 1420-1428.
109. Gaetani GF, Galiano S, Canepa L, Ferraris AM & Kirkman HN (1989) Catalase and glutathione peroxidase are equally active in detoxification of hydrogen peroxide in human erythrocytes. *Blood* 73(1): 334-339.

110. Scott MD, Lubin BH, Zuo L & Kuypers FA (1991) Erythrocyte defense against hydrogen peroxide: preeminent importance of catalase. *J Lab Clin Med* 118(1): 7-16.
111. Gaetani GF, Ferraris AM, Rolfo M, Mangerini R, Arena S & Kirkman HN (1996) Predominant role of catalase in the disposal of hydrogen peroxide within human erythrocytes. *Blood* 87(4): 1595-1599.
112. Johnson RM, Goyette G, Jr, Ravindranath Y & Ho YS (2000) Red cells from glutathione peroxidase-1-deficient mice have nearly normal defenses against exogenous peroxides. *Blood* 96(5): 1985-1988.
113. Ho YS, Xiong Y, Ma W, Spector A & Ho DS (2004) Mice lacking catalase develop normally but show differential sensitivity to oxidant tissue injury. *J Biol Chem* 279(31): 32804-32812.
114. Lim YS, Cha MK, Yun CH, Kim HK, Kim K & Kim IH (1994) Purification and characterization of thiol-specific antioxidant protein from human red blood cell: a new type of antioxidant protein. *Biochem Biophys Res Commun* 199(1): 199-206.
115. Cha MK, Yun CH & Kim IH (2000) Interaction of human thiol-specific antioxidant protein 1 with erythrocyte plasma membrane. *Biochemistry* 39(23): 6944-6950.
116. Chae HZ, Chung SJ & Rhee SG (1994) Thioredoxin-dependent peroxide reductase from yeast. *J Biol Chem* 269(44): 27670-27678.
117. Low FM, Hampton MB, Peskin AV & Winterbourn CC (2007) Peroxiredoxin 2 functions as a noncatalytic scavenger of low-level hydrogen peroxide in the erythrocyte. *Blood* 109(6): 2611-2617.
118. Yang KS, Kang SW, Woo HA, Hwang SC, Chae HZ, Kim K, Rhee SG (2002) Inactivation of human peroxiredoxin I during catalysis as the result of the oxidation of the catalytic site cysteine to cysteine-sulfinic acid. *J Biol Chem* 277(41): 38029-38036.
119. Biteau B, Labarre J & Toledano MB (2003) ATP-dependent reduction of cysteine-sulphinic acid by *S. cerevisiae* sulphiredoxin. *Nature* 425(6961): 980-984.
120. Hall A, Karplus PA & Poole LB (2009) Typical 2-cys peroxiredoxins-structures, mechanisms and functions. *FEBS J* 276(9): 2469-2477.
121. Mills GC (1957) Hemoglobin catabolism. I. glutathione peroxidase, an erythrocyte enzyme which protects hemoglobin from oxidative breakdown. *J Biol Chem* 229(1): 189-197.
122. Flohe L, Gunzler WA & Schock HH (1973) Glutathione peroxidase: a selenoenzyme. *FEBS Lett* 32(1): 132-134.
123. Toppo S, Flohe L, Ursini F, Vanin S & Maiorino M (2009) Catalytic mechanisms and specificities of glutathione peroxidases: variations of a basic scheme. *Biochim Biophys Acta* 1790(11): 1486-1500.

124. Rocher C, Lalanne JL & Chaudiere J (1992) Purification and properties of a recombinant sulfur analog of murine selenium-glutathione peroxidase. *Eur J Biochem* 205(3): 955-960.
125. Toppo S, Vanin S, Bosello V & Tosatto SC (2008) Evolutionary and structural insights into the multifaceted glutathione peroxidase (gpx) superfamily. *Antioxid Redox Signal* 10(9): 1501-1514.
126. Deponte M (2012) Glutathione catalysis and the reaction mechanisms of glutathione-dependent enzymes. *Biochim Biophys Acta*
127. Epp O, Ladenstein R & Wendel A (1983) The refined structure of the selenoenzyme glutathione peroxidase at 0.2-nm resolution. *Eur J Biochem* 133(1): 51-69.
128. Sunde R A. (1985) *Selenium: In Handbook of Nutritionally Essential Mineral Elements. vol 18*, ed O'Dell B. L., Sunde R. A. (Marcel Dekker, New York), pp 493 - 556.
129. Chu FF, Doroshov JH & Esworthy RS (1993) Expression, characterization, and tissue distribution of a new cellular selenium-dependent glutathione peroxidase, GSHPx-GI. *J Biol Chem* 268(4): 2571-2576.
130. Arthur JR (2000) The glutathione peroxidases. *Cell Mol Life Sci* 57(13-14): 1825-1835.
131. Takahashi K, Avissar N, Whitin J & Cohen H (1987) Purification and characterization of human plasma glutathione peroxidase: a selenoglycoprotein distinct from the known cellular enzyme. *Arch Biochem Biophys* 256(2): 677-686.
132. Takahashi K, Akasaka M, Yamamoto Y, Kobayashi C, Mizoguchi J & Koyama J. (1990) Primary structure of human plasma glutathione peroxidase deduced from cDNA sequences. *J Biochem* 108(2): 145-148.
133. Yamamoto Y, Nagata Y, Niki E, Watanabe K & Yoshimura S (1993) Plasma glutathione peroxidase reduces phosphatidylcholine hydroperoxide. *Biochem Biophys Res Commun* 193(1): 133-138.
134. Maiorino M, Thomas JP, Girotti AW & Ursini F (1991) Reactivity of phospholipid hydroperoxide glutathione peroxidase with membrane and lipoprotein lipid hydroperoxides. *Free Radic Res Commun* 12-13 Pt 1: 131-135.
135. Maiorino M, Ursini F, Bosello V, Toppo S, Tosatto SC, Mauri P, Becker K, Roveri A, Bulato C, Benazzi L, De Palma A & Flohé L (2007) The thioredoxin specificity of drosophila GPx: a paradigm for a peroxiredoxin-like mechanism of many glutathione peroxidases. *J Mol Biol* 365(4): 1033-1046.
136. Tanaka T, Izawa S & Inoue Y (2005) GPX2, encoding a phospholipid hydroperoxide glutathione peroxidase homologue, codes for an atypical 2-cys peroxiredoxin in *saccharomyces cerevisiae*. *J Biol Chem* 280(51): 42078-42087.

137. Schlecker T, Comini MA, Melchers J, Ruppert T & Krauth-Siegel RL (2007) Catalytic mechanism of the glutathione peroxidase-type tryparedoxin peroxidase of trypanosoma brucei. *Biochem J* 405(3): 445-454.
138. Low FM, Hampton MB & Winterbourn CC (2008) Peroxiredoxin 2 and peroxide metabolism in the erythrocyte. *Antioxid Redox Signal* 10(9): 1621-1630.
139. Hamann M, Zhang T, Hendrich S & Thomas JA (2002) Quantitation of protein sulfinic and sulfonic acid, irreversibly oxidized protein cysteine sites in cellular proteins. *Methods Enzymol* 348: 146-156.
140. Jeong W, Park SJ, Chang TS, Lee DY & Rhee SG (2006) Molecular mechanism of the reduction of cysteine sulfinic acid of peroxiredoxin to cysteine by mammalian sulfiredoxin. *J Biol Chem* 281(20): 14400-14407.
141. Woo HA, Jeong W, Chang TS, Park KJ, Park SJ, Yang JS & Rhee SG (2005) Reduction of cysteine sulfinic acid by sulfiredoxin is specific to 2-cys peroxiredoxins. *J Biol Chem* 280(5): 3125-3128.
142. Ren H, Ghebremeskel K, Okpala I, Lee A, Ibegbulam O, Crawford M (2008) Patients with sickle cell disease have reduced blood antioxidant protection. *Int J Vitam Nutr Res* 78(3): 139-147.
143. Cho CS, Kato GJ, Yang SH, Bae SW, Lee JS, Gladwin MT & Rhee SG (2010) Hydroxyurea-induced expression of glutathione peroxidase 1 in red blood cells of individuals with sickle cell anemia. *Antioxid Redox Signal* 13(1): 1-11.
144. Flohe L, Loschen G, Gunzler WA & Eichele E (1972) Glutathione peroxidase, V. The kinetic mechanism. *Hoppe Seylers Z Physiol Chem* 353(6): 987-999.
145. Byun BJ & Kang YK (2011) Conformational preferences and pK(a) value of selenocysteine residue. *Biopolymers* 95(5): 345-353.
146. Halliwell B & Gutteridge JMC (1999) *Free Radic Biol Med*, 3rd ed. (Oxford University Press Inc., New York), pp 143.
147. Kuldeep Mohanty, Swetasmita Mishra, Jhumur Pani, Tarannum Hasan, Abhishek Purohit, Subhadra Sharma, Rima Dada (2012) Heparin or EDTA: anticoagulant of choice in free radical estimation. *Oxid Antioxid Med Sci* 1(1): 21-24.
148. Duchon G & Collier H. B. (1971) Enzyme activities of human erythrocyte ghosts effects on various treatments. *J Membrane Biol* 6: 138-157.
149. Clarke A (2012) Externalized ATP in intact erythrocyte suspensions: Modulation and determination, MSc thesis, Concordia University
150. Jiang H (2008) Hydrolysis of cis- and trans-epoxyeicosatrienoic acids by rat red blood cells. *J Pharmacol Exp Ther* 326(1): 330-337.

151. Wang B & Sluyter R (2013) P2X7 receptor activation induces reactive oxygen species formation in erythroid cells. *Purinergic Signal* 9(1): 101-112.
152. Heidebrecht F, Heidebrecht A, Schulz I, Behrens SE & Bader A (2009) Improved semiquantitative western blot technique with increased quantification range. *J Immunol Methods* 345(1-2): 40-48.
153. Weaver R (2005) *Molecular Biology, 3rd ed.*, (McGraw Hill Companies, New York, NY), pp 59.
154. Welinder C & Ekblad L (2011) Coomassie staining as loading control in western blot analysis. *J Proteome Res* 10(3): 1416-1419.
155. Hayat MA (1989) *Chemical fixation in principles and techniques of electron microscopy: Biological applications, 3rd ed.*, (CRC press, Boca Raton), pp 6-80.
156. Kehrer JP & Biswal SS (2000) The molecular effects of acrolein. *Toxicol Sci* 57(1): 6-15.
157. Campanella ME, Chu H & Low PS (2005) Assembly and regulation of a glycolytic enzyme complex on the human erythrocyte membrane. *Proc Natl Acad Sci U S A* 102(7): 2402-2407.
158. Cai J, Bhatnagar A & Pierce WM (2009) Protein modification by acrolein: formation and stability of cysteine adducts. *Chem Res Toxicol* 22(4): 708-716.
159. Dittmer A & Dittmer J (2006) Beta-actin is not a reliable loading control in western blot analysis. *Electrophoresis* 27(14): 2844-2845.
160. Russo A, Tellone E, Ficarra S, Giardina B, Bellocco E, Lagana' G, Leuzzi U, Kotyk A & Galtieri A (2002) Band-3 protein function in human erythrocytes: effect of oxygenation-deoxygenation. *Biochim Biophys Acta* 1564(1): 214-218.
161. Anonymous, Band 3 antibody, <http://www.abcam.com/Band-3-antibody-BIII-136-ab11012.html>, accessed May 3, 2013
162. Yawata Y (2003) *Integral proteins in cell membrane: The red blood cell as a model* (Wiley-VCH, Darmstadt), pp 81.
163. Li B (2009) An antioxidant metabolon at the red blood cell membrane. *MSc Thesis, Concordia University*
164. Ponder E (1948) *Hemolysis and Related Phenomena*, (Grune & Stratton, New York), pp 46.
165. Schwoch G & Passow H (1973) Preparation and properties of human erythrocyte ghosts. *Mol Cell Biochem* 2(2): 197-218.

166. Allen DW, Cadman S, McCann SR & Finkel B (1977) Increased membrane binding of erythrocyte catalase in hereditary spherocytosis and in metabolically stressed normal cells. *Blood* 49(1): 113-123.
167. Hillier J & Hoffman JF (1953) On the ultrastructure of the plasma membrane as determined by the electron microscope. *J Cell Physiol* 42(2): 203-247.
168. Weed RI, Reed CF & Berg G (1963) Is hemoglobin an essential structural component of human erythrocyte membranes? *J Clin Invest* 42: 581-588.
169. Dodge JT, Mitchell C & Hanahan DJ (1963) The preparation and chemical characteristics of hemoglobin-free ghosts of human erythrocytes. *Arch Biochem Biophys* 100: 119-130.
170. Bramley TA, Coleman R & Finean JB (1971) Chemical, enzymological and permeability properties of human erythrocyte ghosts prepared by hypotonic lysis in media of different osmolarities. *Biochim Biophys Acta* 241(3): 752-769.
171. Rinalducci S, D'Amici GM, Blasi B & Zolla L (2011) Oxidative stress-dependent oligomeric status of erythrocyte peroxiredoxin II (PrxII) during storage under standard blood banking conditions. *Biochimie* 93(5): 845-853.
172. Kinoshita E, Kinoshita-Kikuta E, Ujihara H & Koike T (2009) Mobility shift detection of phosphorylation on large proteins using a phos-tag SDS-PAGE gel strengthened with agarose. *Proteomics* 9(16): 4098-4101.
173. Kazennov AM, Maslova MN, Matskevich Yu A, Rustamov FA & Shalabodov AD (1998) Species variability of erythrocyte transport ATPases in mammals. *Comp Biochem Physiol B Biochem Mol Biol* 119(1): 169-175.
174. Wiester MJ, Winsett DW, Richards JH, Doerfler DL & Costa DL (2002) Partitioning of benzene in blood: Influence of hemoglobin type in humans and animals. *Environ Health Perspect* 110(3): 255-261.
175. Elce J (2000) *Calpain Methods and Protocols, Vol. 144* (Humana Press, USA), pp 192.
176. Benedetti S, Lamorgese A, Piersantelli M, Pagliarani S, Benvenuti F & Canestrari F. (2004) Oxidative stress and antioxidant status in patients undergoing prolonged exposure to hyperbaric oxygen. *Clin Biochem* 37(4): 312-317.
177. Harabin AL, Braisted JC & Flynn ET (1990) Response of antioxidant enzymes to intermittent and continuous hyperbaric oxygen. *J Appl Physiol* 69(1): 328-335.
178. Narkowicz CK, Vial JH & McCartney PW (1993) Hyperbaric oxygen therapy increases free radical levels in the blood of humans. *Free Radic Res Commun* 19(2): 71-80.

179. Cicha I, Suzuki Y, Tateishi N & Maeda N (2003) Changes of RBC aggregation in oxygenation-deoxygenation: pH dependency and cell morphology. *Am J Physiol Heart Circ Physiol* 284(6): 2335-42.
180. Tuvia S, Levin S & Korenstein R (1992) Oxygenation-deoxygenation cycle of erythrocytes modulates submicron cell membrane fluctuations. *Biophys J* 63(2): 599-602.
181. Messana I, Orlando M, Cassiano L, Pennacchietti L, Zuppi C, Castagnola M & Giardina B (1996) Human erythrocyte metabolism is modulated by the O₂-linked transition of hemoglobin. *FEBS Lett* 390(1): 25-28.
182. Galtieri A, Tellone E, Romano L, Misiti F, Bellocco E, Ficarra S, Russo A, Di Rosa D, Castagnola M, Giardina B & Messana I (2002) Band-3 protein function in human erythrocytes: effect of oxygenation-deoxygenation. *Biochim Biophys Acta* 1564(1): 214-218.
183. Pegg M, Crane D & Masters C (1986) Confirmation that catalase is a glycoprotein. *Biochem Int* 12(6): 831-838.
184. Aviram I & Shaklai N (1981) The association of human erythrocyte catalase with the cell membrane. *Arch Biochem Biophys* 212(2): 329-337.
185. Yannoukakos D, Vasseur C, Piau JP, Wajcman H & Bursaux E (1991) Phosphorylation sites in human erythrocyte band 3 protein. *Biochim Biophys Acta* 1061(2): 253-266.
186. Zipser Y & Kosower NS (1996) Phosphotyrosine phosphatase associated with band 3 protein in the human erythrocyte membrane. *Biochem J* 314 (Pt 3): 881-887.
187. Salsman SJ, Hensley K & Floyd RA (2005) Sensitivity of protein tyrosine phosphatase activity to the redox environment, cytochrome C, and microperoxidase. *Antioxid Redox Signal* 7(7-8): 1078-1088.
188. Cheng W, Fu YX, Porres JM, Ross DA & Lei XG (1999) Selenium-dependent cellular glutathione peroxidase protects mice against a pro-oxidant-induced oxidation of NADPH, NADH, lipids, and protein. *FASEB J* 13(11): 1467-1475.
189. Staniszewska M (2004) The effect of hyperbaric air exposure on concentrations of malondialdehyde and some parameters of the antioxidant system in rat blood. *Ann Acad Med Stetin* 50(2): 105-114.
190. Jerome WG, Cash C, Webber R, Horton R & Yancey PG (1998) Lysosomal lipid accumulation from oxidized low density lipoprotein is correlated with hypertrophy of the golgi apparatus and trans-golgi network. *J Lipid Res* 39(7): 1362-1371.
191. Liu H, Zhu H, Eggers DK, Nersissian AM, Faull KF, Goto JJ, Ai J, Sanders-Loehr J, Gralla EB & Valentine JS (2000) Copper(2+) binding to the surface residue cysteine 111

of His46Arg human copper-zinc superoxide dismutase, a familial amyotrophic lateral sclerosis mutant. *Biochemistry* 39(28): 8125-8132.

192. Hallewell RA, Imlay KC, Lee P, Fong NM, Gallegos C, Getzoff ED, Tainer JA, Cabelli DE, Tekamp-Olson P & Mullenbach GT (1991) Thermostabilization of recombinant human and bovine CuZn superoxide dismutases by replacement of free cysteines. *Biochem Biophys Res Commun* 181(1): 474-480.

193. Palcic MM & Dunford HB (1980) The reaction of human erythrocyte catalase with hydroperoxides to form compound I. *J Biol Chem* 255(13): 6128-6132.

194. Kovachich GB, Mishra OP & Clark JM (1981) Depression of cortical Na⁺, K⁺-ATPase activity in rats exposed to hyperbaric oxygen. *Brain Res* 206(1): 229-232.

195. Noda Y, McGeer PL & McGeer EG (1983) Lipid peroxide distribution in brain and the effect of hyperbaric oxygen. *J Neurochem* 40(5): 1329-1332.

196. Tarhan L (2000) Some properties of cu, zn-superoxide dismutase from sheep erythrocyte. *24*: 109-116.

197. Dubuisson M, Vander Stricht D, Clippe A, Etienne F, Nauser T, Kissner R, Koppenol WH, Rees JF & Knoop B (2004) Human peroxiredoxin 5 is a peroxynitrite reductase. *FEBS Lett* 571(1-3): 161-165.

198. Christophersen BO (1969) Reduction of X-ray-induced DNA and thymine hydroperoxides by rat liver glutathione peroxidase. *Biochim Biophys Acta* 186(2): 387-389.

199. Little C & O'Brien PJ (1968) An intracellular GSH-peroxidase with a lipid peroxide substrate. *Biochem Biophys Res Commun* 31(2): 145-150.

200. Tsan MF, Douglass KH & McIntyre PA (1977) Hydrogen peroxide production and killing of staphylococcus aureus by human polymorphonuclear leukocytes. *Blood* 49(3): 437-444.

201. Stefek M, Masarykova M & Benes L (1992) Inhibition of cumene hydroperoxide-induced lipid peroxidation by a novel pyridoinole antioxidant in rat liver microsomes. *Pharmacol Toxicol* 70(6 Pt 1): 407-411.

202. Yesilkaya A, Yegin A, Ozdem S & Aksu TA (1998) The effect of bilirubin on lipid peroxidation and antioxidant enzymes in cumene hydroperoxide-treated erythrocytes. *Int J Clin Lab Res* 28(4): 230-234.

203. Lima PR, Gontijo JA, Lopes de Faria JB, Costa FF & Saad ST (1997) Band 3 campinas: a novel splicing mutation in the band 3 gene (AE1) associated with hereditary spherocytosis, hyperactivity of Na⁺/Li⁺ countertransport and an abnormal renal bicarbonate handling. *Blood* 90(7): 2810-2818.

204. Snyder LM, Liu SC, Palek J, Bulat P, Edelstein L, Srivastava SK & Fortier NL (1977) Partition of catalase and its peroxidase activities in human red cell membrane: effect of ATP depletion. *Biochim Biophys Acta* 470(2): 290-302.
205. Belcher EH & Harriss EB (1959) Studies of red cell life span in the rat. *J Physiol* 146(2): 217-234.
206. Giugliano D, Ceriello A & Paolisso G (1996) Oxidative stress and diabetic vascular complications. *Diabetes Care* 19(3): 257-267.
207. Hauguel-de Mouzon S, Peraldi P, Alengrin F & Van Obberghen E (1993) Alteration of phosphotyrosine phosphatase activity in tissues from diabetic and pregnant rats. *Endocrinology* 132(1): 67-74.
208. Mazzanti L, Rabini RA, Salvolini E, Tesei M, Martarelli D, Venerando B & Curatola G (1997) Sialic acid, diabetes, and aging: a study on the erythrocyte membrane. *Metabolism* 46(1): 59-61.
209. Moussa SA (2007) Biophysical changes in red blood cells and hemoglobin components of diabetic patients. *J Gen Engineer Biotech* 5(1): 27-32.
210. Clari G, Brunati AM & Moret V (1987) Membrane-bound phosphotyrosyl-protein phosphatase activity in human erythrocytes. Dephosphorylation of membrane band 3 protein. *Biochem Biophys Res Commun* 142(2): 587-594.
211. Phan-Dinh-Tuy F, Henry J & Kahn A (1985) Characterization of human red blood cell tyrosine kinase. *Biochem Biophys Res Commun* 126(1): 304-312.
212. Wo YY, McCormack AL, Shabanowitz J, Hunt DF, Davis JP, Mitchell GL & Van Etten RL (1992) Sequencing, cloning, and expression of human red cell-type acid phosphatase, a cytoplasmic phosphotyrosyl protein phosphatase. *J Biol Chem* 267(15): 10856-10865.
213. Rettig MP, Low PS, Gimm JA, Mohandas N, Wang J & Christian JA (1999) Evaluation of biochemical changes during in vivo erythrocyte senescence in the dog. *Blood* 93(1): 376-384.
214. Ciana A, Minetti G & Balduini C (2004) Phosphotyrosine phosphatases acting on band 3 in human erythrocytes of different age: PTP1B processing during cell ageing. *Bioelectrochemistry* 62(2): 169-173.
215. Salvemini D, Riley DP & Cuzzocrea S (2002) SOD mimetics are coming of age. *Nat Rev Drug Discov* 1(5): 367-374.